UNIVERSITA' DEGLI STUDI DI PADOVA

SEDE AMMINISTRATIVA: UNIVERSITA' DEGLI STUDI DI PADOVA

DIPARTIMENTO DI SCIENZE DEL FARMACO

SCUOLA DI DOTTORATO DI RICERCA IN BIOLOGIA E MEDICINA DELLA RIGENERAZIONE

INDIRIZZO IN BIOLOGIA DELL'INTEGRAZIONE INTERCELLULARE

CICLO XXV

STUDY OF NEW ANTIPROLIFERATIVE COMPOUNDS

DIRETTORE DELLA SCUOLA: CH.MA PROF.SSA MARIA TERESA CONCONI

COORDINATORE D'INDIRIZZO: CH.MA PROF.SSA LUISA DALLA VALLE

SUPERVISORE: CH.MA PROF.SSA LUISA DALLA VALLE

CORRELATORE: CH.MA PROF.SSA DANIELA ESTER VEDALDI

DOTTORANDA: SILVIA TISI

__Index__

Riassunto

L'attività di ricerca che ho svolto riguarda lo studio di nuovi composti a potenziale azione antineoplastica sintetizzati dal gruppo del prof. Cirrincione presso l'Università di Palermo.

Sono state valutate 104 molecole dotate di attività antiproliferativa, sia come tali sia in seguito ad attivazione con luce UVA (fotochemioterapici); in particolare, ho studiato due serie di pirrolochinazoline (BQ e LCQ) ed una serie di pirazolochinoline (PZQ).

Per tutti questi composti sono stati effettuati esperimenti di citotossicità in vitro volti a confermare la loro azione citotossica e/o fotocitotossica; alcune di queste molecole hanno dimostrato una discreta attività antiproliferativa, anche nell'ordine del sub-micromolare, mentre altre sono risultate inattive alle concentrazioni utilizzate.

Per i derivati più attivi sono poi stati effettuati ulteriori test citofluorimetrici per determinare il meccanismo di morte cellulare. Come risultato, queste sostanze sembrano indurre morte cellulare attraverso apoptosi, fenomeno che coinvolge alcuni organelli quali mitocondri e lisosomi; in particolare, sono state riscontrate variazioni del potenziale di membrana mitocondriale e produzione di specie reattive dell'ossigeno (ROS), fattori che indicano un importante coinvolgimento dei mitocondri. I lisosomi, invece, sembrano essere coinvolti nel fenomeno apoptotico solo in un secondo momento.

Per la serie BQ, poi, sono stati effettuati test volti a determinare il meccanismo d'azione. Inizialmente è stata valutata l'inibizione dell'EGFR, visto che questi composti erano stati sintetizzati allo scopo di ottenere degli inibitori di questo recettore tirosinchinasico; dai risultati ottenuti, tuttavia, questo non sembra essere il meccanismo d'azione della serie.

Dal momento che questi composti inducono un blocco nelle fasi G_2/M del ciclo cellulare, ho allora valutato una potenziale azione antimitotica; attraverso l'analisi dell'indice mitotico, della rete dei microtubuli e della polimerizzazione della tubulina in vitro questa ipotesi è stata confermata. Spesso, inoltre, gli antimitotici possiedono un'azione antivascolare che, in questo caso, è stata valutata mediante alcuni test preliminari in vitro; il trattamento con le pirrolochinazoline più attive sembra inibire la motilità cellulare e danneggiare la rete capillare neoformata da cellule HUVEC.

Per quel che riguarda, infine, i composti fotocitotossici, sono stati valutati i potenziali danni a carico di proteine e lipidi.

VI

Abstract

My research activity is based on the study of new potential anticancer compounds synthesised at Palermo University by prof. Cirrincione's group.

In this study, 104 new cytotoxic molecules were evaluated in the presence of UVA photoactivation or in the dark; particularly, some pyrroloquinazolines (BQ and LCQ series) and some pyrazoloquinolines (PZQ series) were assessed.

Cytotoxicity and photocytotoxicity assays were performed in vitro to confirm the antiproliferative activity of these derivatives; some molecules showed an interesting cytotoxicity, even in the sub-micromolar range, others were inactive at the employed concentrations.

The most cytotoxic compounds among these series were then further analysed by flow cytometric assays to find cell death mechanism. These molecules induce cell death by apoptosis with the involvement of mitochondria and lysosomes; particularly, the mitochondrial membrane potential and the production of reactive oxygen species (ROS) were tested: this is indicative of an important involvement of mitochondria. Instead, lysosomes are involved later compared to mitochondria.

Furthermore, the most active BQ derivatives were investigated to find out their mechanism of action. At first, because of their structural analogy with some EGFR inhibitors, these compounds were tested for this mechanism of action; nevertheless, they do not seem to be EGFR inhibitors.

Since these derivatives provoke a block in G_2-M phase in cell cycle, I evaluated their potential antimitotic activity; this hypothesis was confirmed by further studies as mitotic index, microtubule network perturbation and tubulin polymerisation in vitro.

Many antimitotic drugs can also have an effect on tumour immature and neo-formed vessel network, and this feature was assessed by some preliminary tests in vitro; the most active pyrroloquinazolines showed to inhibit cell motility and disrupt a neo-formed HUVEC vessel network.

Finally, a possible damage against lipids and proteins induced by the most photocytotoxic compounds was evaluated.

1. Introduction

In the developed world, roughly one in three people contracts cancer and around one in four of those dies from the disease [1].

Over the period 1980–2000, total cancer mortality for men was 166/100 000 in the EU, including lung and other tobacco-related neoplasms, but also stomach, intestines and liver, and a few neoplasms such as testis, Hodgkin's disease and leukaemias. Overall cancer mortality for women was 95/100 000 in the EU.

Most of the unfavourable patterns and trends in cancer mortality are due to recognised, and hence largely avoidable, causes of cancer. These include the exceedingly high rates of lung and other tobacco-related cancers but also the high rates of gastric and intestinal cancer, related to poorer and unfavourable dietary patterns. Alcohol drinking is also responsible for the gross excess and the consequent unfavourable trends in oral cavity, oesophageal and laryngeal cancers. The elevated liver cancer rates were largely due to high hepatitis B and C prevalence. Furthermore, there are high mortality rates for neoplasms related to inadequate screening, diagnosis and treatment, mainly for uterine cervical cancer, with the lack of adoption of effective screening programs, but also for breast and ovarian cancers, as well as testicular cancer, Hodgkin's disease and leukaemias [2].

Advances in treatment, with surgery, radiotherapy and conventional cytotoxic chemotherapy, have made only a modest overall impact on mortality. Cures can be achieved in childhood cancers, testicular cancer and lymphoma, and improvements in survival rates have been made as a result of adjuvant drug treatment of breast and colorectal cancer. However, the majority of human cancers is difficult to treat, especially in their advanced, metastatic forms. There is thus a pressing need for novel and effective forms of systemic therapy [3].

1.1 The hallmarks of cancer

In cancer, the particular challenge is to discover the series of molecular abnormalities that arise in the genomes of all types of cancer in precise detail, to use that information to understand the

process of malignancy, and then to develop more rational and effective strategies for diagnosis and treatment.

Complex cellular functions are generated by the dynamic interactions of a large number of molecular components (DNA, RNA, proteins and small molecules) modulated by internal and external cues. Thus the function is not determined by a single component or a single level of organization, but is found distributed as an emergent (or system-level) property over many levels and components. Accordingly, a cell can be viewed as a system composed of many interconnected modules coordinately performing specific biological functions (metabolism, signalling, transcription, growth, cycle, autophagy, apoptosis, differentiation, etc.), each module being characterized by a network of interacting molecules [4].

Tumourigenesis in humans is a multistep process; these steps reflect genetic alterations that drive the progressive transformation of normal human cells into highly malignant derivatives.

Cancer cells have defects in regulatory circuits that govern normal cell proliferation and homeostasis. The vast catalogue of cancer cell genotypes is a manifestation of six essential alterations in cell physiology that collectively dictate malignant growth.

- *Self-sufficiency in growth signals*: tumour cells show a greatly reduced dependence on exogenous growth stimulation and they generate many of their own growth signals, thereby reducing their dependence on stimulation from their normal tissue microenvironment.

- *Insensitivity to growth-inhibitory (antigrowth) signals*: within a normal tissue, multiple antiproliferative signals operate to maintain cellular quiescence and tissue homeostasis; incipient cancer cells must evade these antiproliferative signals if they are to prosper.

- *Evasion of programmed cell death (apoptosis)*: the ability of tumour cell population to expand in number is determined not only by the rate of cell proliferation, but also by the rate of cell attrition; programmed cell death represents a major source of this attrition and acquired resistance toward apoptosis is a hallmark of most and perhaps all types of cancer.

- *Limitless replicative potential*: three acquired capabilities – growth signal autonomy, insensitivity to antigrowth signals, and resistance to apoptosis – all lead to an uncoupling of a cellular growth program from signals in its environment. In principle, the resulting deregulated proliferation program should suffice to enable the generation of the vast cell populations that constitute macroscopic tumours; however, research performed over the past 30 years indicates that this acquired disruption of cell-to-cell signalling, on its own, does not ensure expansive tumour growth.

- *Sustained angiogenesis*: the oxygen and nutrients supplied by the vasculature are crucial for cell function and survival, obligating virtually all cells in a tissue to reside within 100 μm of

a capillary blood vessel. During organogenesis, this closeness is ensured by coordinated growth of vessels and parenchyma. The cells within aberrant proliferative lesions initially lack angiogenic ability, curtailing their capability for expansion. In order to progress to a larger size, incipient neoplasias must develop angiogenic ability.

- *Tissue invasion and metastasis*: sooner or later during the development of most types of human cancer, primary tumour masses spawn pioneer cells that move out, invade adjacent tissues, and thence travel to distant sites where they may succeed in founding new colonies; these distant settlements of tumour cells – metastases – are the cause of 90% of human cancer deaths. The capability for invasion and metastasis enables cancer cells to escape the primary tumour mass and colonize new terrain in the body where, at least initially, nutrients and space are not limiting. The newly formed metastases arise as amalgams of cancer cells and normal supporting cells conscripted from the host tissue. Successful invasion and metastasis depend upon all of the other five acquired hallmark capabilities.

Each of these physiologic changes – novel capabilities acquired during tumour development – represents the successful breaching of an anticancer defence mechanism hardwired into cells and tissues [5].

1.2 <u>Chemotherapy</u>

The word "chemotherapy" was created by Herlich at the beginning of the 20th century and it meant a medical therapy which uses synthetic chemical compounds as antimicrobials [6]. Now, this word indicates drugs for anticancer therapy with the aim of slowing or blocking neoplastic cellular proliferation through cytotoxic mechanisms.

The success possibility for a chemotherapeutic agent is as greater as the differences between target cells and healthy ones. If these differences are few, as in the case of a neoplastic cellular population and the original healthy cellular population, an anticancer agent cannot eliminate tumour cells without giving toxic effects to the patient. In fact, tissues or organs with a high proliferative index, such as bone marrow, epithelia of the gastro-intestinal tract and skin, are chemotherapy target like cancerous cells; this unwanted damage causes hair loss, nausea, infections and much other side effects.

Moreover, the efficacy of all chemotherapeutic agents is limited by the occurrence of drug resistance [7]. Multidrug resistance (MDR) is characterized clinically as a broad cross-resistance to

chemotherapeutic drugs and is the main reason for the failure of chemotherapy. Whereas MDR is inherently expressed in some cancers, in others it develops in response to treatment. Overexpression of the mdr1 gene product, P-glycoprotein, produces an MDR phenotype characterised by decreased accumulation of drug and cross-resistance to lipophilic natural-product drugs. P-glycoprotein is primarily located in the plasma membrane of drug-resistant cells, and it is believed that the decreased drug accumulation is the result of the adenosine triphosphate (ATP)-dependent drug-effluxing activity of P-glycoprotein. Similarly, increased expression of the MDR-associated protein (MRP) causes resistance to a range of lipophilic natural product drugs.

The molecular mechanism of MRP-mediated resistance has not yet been clearly defined. It is thought that MRP acts similarly to P-glycoprotein and causes drug efflux since MRP has several features in common with P-glycoprotein, such as its sequence homology with mdr1, its location primarily in the plasma membrane and its association with decreased intracellular drug accumulation [8].

1.2.1 <u>Chemotherapeutics and cell cycle</u>

Chemotherapeutics are antiproliferative agents, so there is often a connection between cell cycle and cytotoxicity. The cell cycle is commonly deregulated in cancer. This frequently occurs in a variety of ways at the level of cyclin-dependent kinases (CDKs) and their regulatory molecules [3].
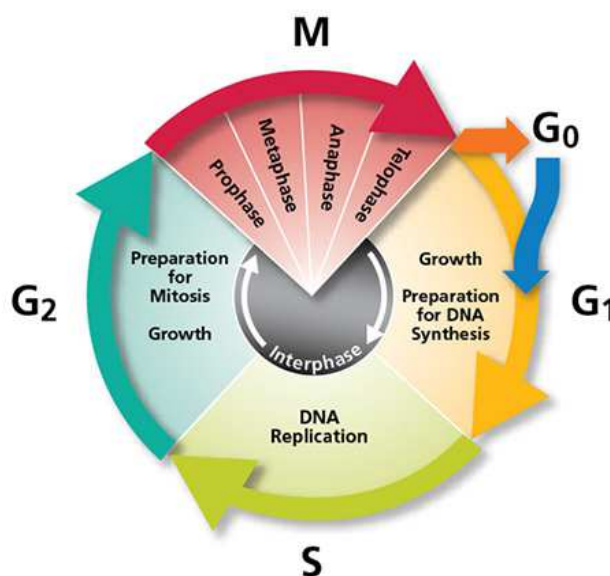

Fig. 1.1 Cell cycle phases.

Cell cycle can be divided into four phases:
- G_1 *phase*, in which the synthesis of enzymes for the functioning and production of new DNA occurs.
- *S phase*, with the synthesis of DNA and the duplication of genome.
- G_2 *phase*, associated with the metabolic activity for the production of all needed components for mitosis.
- *M phase (mitosis)*, marked by the generation of bipolar mitotic spindles, the segregation of sister chromatids and cell division.

There are also cells in G_0 phase or in quiescence state. External stimuli (mitogens or growth factors) induce them to move out of G_0 and through the early part of G_1 [9]. These external stimuli are communicated through a cascade of intracellular phosphorylations, by upregulating expression of the cyclins, which associate with the CDKs.

Anticancer drugs can be divided into three categories considering their relationship with cell cycle:
- *Cycle non-specific*, which demonstrate their antiproliferative activity independently of the presence of cells in cycle, that is also for cells in G_0 phase;
- *Phase-specific*, which kill cells when they are in a specific phase of the cycle;
- *Phase non-specific*, which are active towards proliferating cells but independently of cell cycle phase.

This classification is important for the operative meaning. For example, in a big tumour mass, there are often a lot of quiescent cells and so the therapeutic approach should begin with radiotherapy, surgery but also with the use of cycle non-specific drugs [10].

1.2.2 <u>Classification of chemotherapeutic agents</u>

Chemotherapeutic agents can be classified by their different mechanism of action:
- *Antimetabolites:* these drugs prevent the reproduction of tumour cells altering metabolic pathway such as the synthesis of folate, purines, pyrimidines and nucleosides, and so the synthesis of nucleic acids. These compounds present similar structures to endogenous metabolites, and this structural analogy causes the block of an enzymatic system or the synthesis of an inactive product. In this group, we can find methotrexate, which inhibits the formation of tetrahydrofolic acid, a coenzyme of DNA synthesis, acting as an anti-folic; purine analogues, such as 6-mercaptopurine or 6-thioguanine, which are able not only to inhibit purine synthesis but also to incorporate into DNA or RNA, damaging them;

pyrimidine analogues, such as ara-c, which inhibits DNA-polymerase, or 5-fluorouracile, which blocks DNA synthesis through the binding to timidilate synthetase and, when incorporated into RNA, causes errors during transcription [11]. Antimetabolites are phase-specific drugs as they inhibit DNA synthesis during S phase [10].

- *Alkylators:* they show the ability to alkylate nucleophilic sites in cellular macromolecules. Although these agents damage virtually all components of the cell, their biological effects are attributable to their direct interaction with DNA through the formation of a covalent bond between the activated form of the drug (electrophilic carbocation) and the nucleophilic nitrogen bases. Alkylating agents react with DNA either directly or via intermediaries, which are formed by metabolic activation or spontaneous chemical degradation [12]. Damage to base residues can result in further chemical modifications such as loss of a base and interstrand or intrastrand DNA crosslinking. Nitrogen mustards, nitrosoureas, mitomycins, tetrazines, platinum coordination complex belong to this group of drugs. Alkylators are cytotoxic in cells independently of cell cycle and so also in quiescent cells; however, they are more efficacious towards highly proliferating tissues, in which G_1 and S phases are very vulnerable. After DNA alkylation, cells accumulate and die in G_2 phase [10].

- *Topoisomerase inhibitors:* topoisomerases are enzymes that can change the topological state of DNA through the breaking and rejoining of DNA strands. Cells encode two classes of topoisomerases that are distinguished by their catalytic mechanisms. Type I topoisomerases act by generating a transient single-stranded break in the double helix, followed by either a single-stranded DNA passage event or controlled rotation about the break. As a result, these enzymes are able to alleviate torsional stress (i.e., remove superhelical twists) in duplex DNA [13]. Type II topoisomerases act by generating a transient double-stranded DNA break, followed by a double-stranded DNA passage event. Consequently, these enzymes are able to remove superhelical twists from DNA and resolve knotted or tangled duplex molecules [14]. Topoisomerases are valuable targets for cancer chemotherapeutic agents. Several classes of topo inhibitors have been introduced into cancer clinics as potent anticancer drugs, including camptothecins (Irinotecan, Topotecan) inhibiting topo I and anthracyclines (Doxorubicin, Daunorubicin), epipodophyllotoxins (etoposide, teniposide), aminoacridines (amsacrine) and ellipticines, targeting topo II. The activity of these agents is thought to derive from stabilization of DNA/topo cleavable complex, an intermediate in the catalytic cycle of the enzymes, resulting ultimately in apoptosis. As cells in S and G_2 phase

present the highest levels of topoisomerase, inhibitors are more cytotoxic during these phases [10].

- *Antimitotic agents:* these agents interfere with microtubules, which are essential components of the cytoskeleton that help regulate diverse processes such as cell migration, cell growth, organelle transport and correct segregation of chromosomes during mitosis [15]. Microtubule system is a high dynamic structure, constantly growing and shortening, and antimitotic drugs affect this dynamics by interacting with tubulin. The most clinically useful classes of antimitotic drugs are the Vinca alkaloids and the taxanes [16]. The strategy of using tubulin as a target for cancer chemotherapy is based on the increased growth and division of cancer cells and the fact that drugs that interfere with mitosis such as the Vinca alkaloids, which shift the equilibrium to the depolymerised form of tubulin, have proven effective in the treatment of cancer. Taxanes target tubulin but, unlike the Vinca alkaloids and colchicine, shift the equilibrium to the polymerized form, thus stabilizing microtubules. Antimitotic agents prevent the normal formation and above all the dynamics of mitotic spindle, stopping cellular division in metaphase. Nevertheless, as microtubules take part in many cellular functions (intracellular transport, signal transduction, receptor mechanisms), antimitotic agents can damage cells not only in mitosis but also during interphase [17].

- *Hormones or their antagonists:* tumours originated by hormone-sensitive tissues can retain their hormone-dependency, which can be used for the inhibition of their growth. Hormones with opposite activity to the ones that induce tumour development or hormone antagonists can be used. For example antiestrogens, such as tamoxifene, or antiandrogens, such as cyproterone, can be implied for hormone-dependent breast or prostate carcinoma, respectively [10].

A new generation of cancer drugs (*'targeted therapy'*) was designed to interfere with a specific molecular target (typically a protein) that is believed to have a critical role in tumour growth or progression. The identification of appropriate targets is based on a detailed understanding of the molecular changes underlying cancer [18]. This approach presents some advantages, such as the reduction of side effects thanks to the improvement of tumour specificity and the choice of the therapy after the identification of the molecular target alteration in the specific neoplasm. Among these new drugs, we can find inhibitors of kinases, which have so far proved to be a promising class of targets for cancer therapy. Kinases play key roles in cancer as they are directly or indirectly involved in most signalling pathway.
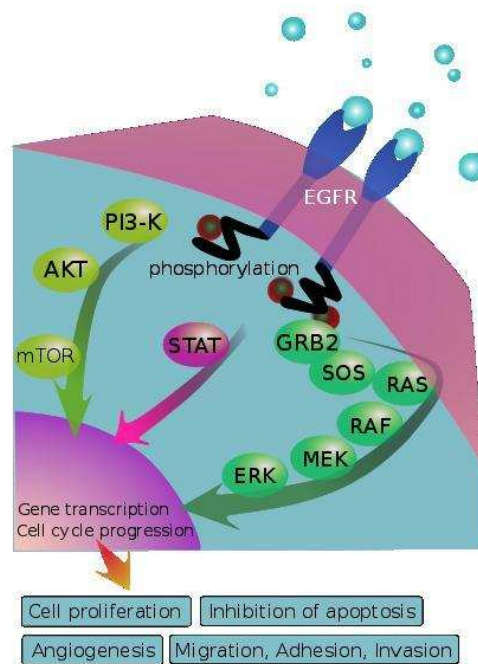
Fig. 1.2 EGFR pathway.

All these enzymes make use of ATP for phosphorylation of a specific Ser/Thr/Tyr residue on protein substrates. The success of small-molecule ATP-competitive inhibitors, such as imatinib (Gleevec) for the treatment of chronic myeloid leukaemia (CML) and gastrointestinal stromal tumours (GIST), and gefitinib (Iressa) and erlotinib (Tarceva) for the treatment of non-small-cell lung cancer (NSCLC), confirms that this strategy is indeed effective [19]. However, classical chemotherapy and radiotherapy approaches remain the mainstay of cancer treatment for tumours that cannot be cured solely by surgical excision. For example these conventional cancer therapies may be combined with targeted agents that disrupt the DNA-repair response; hopefully a more catastrophic cell kill in tumours will result [18].

1.3 <u>Cell death mechanisms</u>

Cell death occurs frequently in complex, multicellular organisms to maintain tissue homeostasis. For example, cells die during embryonic development. Also, the killing of infected cells by cytolytic effector cells of the immune system is an example of cell death in tissue maintenance.

Cell death is discriminated into two main forms: apoptosis and necrosis. In contrast to necrosis, apoptosis is a regulated, energy-dependent form of cell death leading to phagocytosis of cellular

remnants by neighbouring cells. Characteristic morphological features of these two forms of cell death will be discussed and correlated to underlying molecular mechanisms [20].
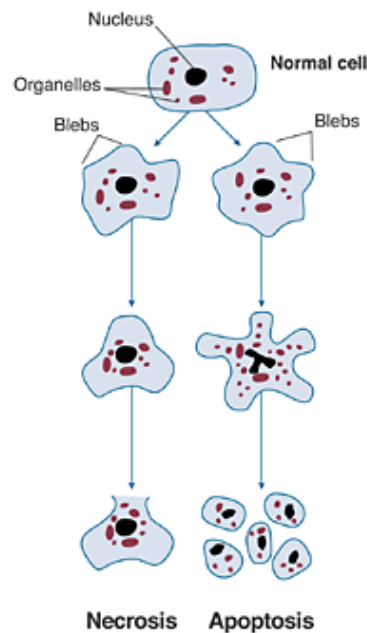

Fig. 1.3 Apoptosis and necrosis.

1.3.1 <u>Necrosis</u>

The term necrosis is used for a type of cell death that is not programmed but rather accidental. In contrast to apoptosis, necrosis is a passive form of cell death without the intricate regulatory mechanisms that are characteristic of apoptosis.

The causes of necrotic cell death, such as heat stress or toxic agents, can also induce apoptotic cell death in many cases. The intensity of the insult but also the energy level of a cell often decide the outcome as either apoptosis or necrosis. It could be shown that low ATP concentration or impaired ATP generation pushes the morphology of cell death toward necrosis.

The morphology of cells dying by necrosis is fairly diverse. The cell membrane becomes permeable early during the death process. Organelles may dilate, and ribosomes may dissociate from the endoplasmic reticulum. The nucleus disintegrates later, and in some cases chromatin condensation occurs. However, pyknotic and fragmented nuclei are not a common feature in necrotic cell death. Due to early leakage of cellular contents, a massive inflammation in the tissue is triggered.

Depending on the morphology and the involvement of lysosomes, two different types of necrotic cell death have been distinguished: autophagic and nonlysosomal disintegration. The autophagic

cell death is characterized by numerous vacuoles in the cytoplasm filled with cellular remnants. The nonlysosomal cell death shows that a pronounced dilation of organelles and empty spaces are formed and the degeneration proceeds without any detectable involvement of lysosomes [20].

1.3.2 <u>Apoptosis</u>

The ability of tumour cell populations to expand in number is determined not only by the rate of cell proliferation but also by the rate of cell attrition. Programmed cell death – apoptosis – represents a major source of this attrition and acquired resistance towards apoptosis is a hallmark of many types of cancer. The possibility that apoptosis serves as a barrier to cancer was first raised in 1972, when Kerr, Wyllie, and Currie described massive apoptosis in the cells populating rapidly growing, hormone-dependent tumours following hormone withdrawal.

The apoptotic program is present in latent form in virtually all cell types throughout the body. Once triggered by a variety of physiologic signals, this program unfolds in a precisely choreographed series of steps. Cellular membranes are disrupted, the cytoplasmic and nuclear skeletons are broken down, the cytosol is extruded, the chromosomes are degraded, and the nucleus is fragmented, all in a span of 30–120 min. In the end, the shrivelled cell corpse is engulfed by nearby cells in a tissue and disappears, typically within 24 hr.

The apoptotic machinery can be broadly divided into two classes of components – sensors and effectors. The sensors are responsible for monitoring the extracellular and intracellular environment for conditions of normality or abnormality that influence whether a cell should live or die. These signals regulate the second class of components, which function as effectors of apoptotic death. The sentinels include cell surface receptors that bind survival or death factors. Intracellular sensors monitor the cellular well-being and activate the death pathway after detecting abnormalities, including DNA damage, signalling imbalance provoked by oncogene action, survival factor insufficiency, or hypoxia. Further, the life of most cells is in part maintained by cell–matrix and cell–cell adherence-based survival signals whose abrogation elicits apoptosis [5].

One of the earliest signals of apoptosis is the externalisation of phosphatidylserine, providing an "eat-me" signal for phagocytosing cells. This can be employed in vitro as marker for the detection of apoptosis.

Morphological hallmarks of apoptosis in the nucleus are chromatin condensation and nuclear fragmentation. The condensation starts peripherally along the nuclear membrane, forming a crescent or ring-like structure. During later stages of apoptosis the nucleus further condenses, and

finally it breaks up inside a cell with an intact cell membrane. These morphological features can be initiated by the cleavage of various proteins by caspases. A major hallmark of apoptosis in the nucleus is the internucleosomal fragmentation of double-stranded DNA into fragments of 180- to 200-bp length. A number of caspase substrates that are involved in DNA repair and replication is responsible for this fragmentation of DNA.

Early during the initiation of apoptosis, cells lose contact with neighbouring cells. Membranes and organelles including mitochondria are well preserved during early apoptotic cell death. Subsequently, microvilli are lost and the cells start to show protrusions of the plasma membrane commonly referred to as *blebs*. The cells shrink, and finally the blebs separate, forming apoptotic bodies densely packed with cellular organelles and nuclear fragments that are engulfed by phagocytosis of surrounding cells [20].

The ultimate effectors of apoptosis include an array of intracellular proteases termed caspases. Two "gatekeeper" caspases, -8 and -9, are activated by death receptors such as FAS or by the cytochrome c released from mitochondria, respectively. These proximal caspases trigger the activation of effector caspases that execute the death program through selective destruction of subcellular structures and organelles, and of the genome [5].

The activation of caspase proteases is fundamental to apoptotic cell death, although their mode of action in promoting death is not fully understood. In vertebrate cells, inhibition of caspases does not necessarily prevent cell death but profoundly delays and alters the process [21].

Apoptosis occurs without associated inflammation due to the containment of the cellular constituents by an intact membrane and the subsequent engulfment of apoptotic bodies. However, if the remnants of apoptotic cells are not phagocytised, they will undergo degradation that resembles necrosis and is called *secondary necrosis* [20].

1.3.2.1   <u>Mitochondria role in apoptosis</u>

Mitochondria are semi-autonomous organelles that change in shape, size and association in different tissues or physio- pathological conditions. Morphological, biochemical, and genetic mitochondrial dysfunction has been reported to occur in several cancer cells.

Mitochondria play a key role in cellular bioenergetics, ion homeostasis, carbohydrate, and fatty acids metabolism and cell signalling. They are at the centre of several inter-connected important metabolic pathways, which are further connected to other important cellular functions. Consequently, any local mitochondrial dysfunction can potentially have direct or indirect effects on intra or extra mitochondrial metabolic pathways [4].

During apoptosis, mitochondria suffer specific damages that result in the loss of their function. For example, release of cytochrome c, the sole water soluble component of the electron transfer chain, can potentially halt the electron transfer, leading to failure in maintaining the mitochondrial membrane potential and ATP synthesis. Moreover, because cytochrome c carries electrons from cytochrome c reductase (complex III) to cytochrome c oxidase (complex IV), by which oxygen molecules are reduced to water, a blockade at this step would increase the production of reactive oxygen species with subsequent lipid peroxidation [21].

The central role of mitochondria in the process of apoptosis has been a focus of cell death research since the observations that the antiapoptotic Bcl-2 protein localizes to the outer membrane of this organelle, a mitochondria-rich fraction is required for the induction of apoptotic changes in a cell-free system, and mitochondrial transmembrane potential is lost during an early stage of apoptosis [22].

Members of the Bcl-2 family of proteins, which have either proapoptotic (Bax, Bak, Bid, Bim) or antiapoptotic (Bcl-2, Bcl-XL, Bcl-W) function, act in part by governing mitochondrial death signalling through cytochrome c release [5].

Over the past several years, it has become clear that a major event during apoptosis is the permeabilization of the mitochondrial outer membrane to release proteins from the intermembrane space. Several of these, including cytochrome c, AIF, Smac/DIABLO, Omi/Htra2, and EndoG, have roles in subsequent cell death. In particular, the release of cytochrome c induces the activation of caspase proteases through the induction of apoptosome formation.

Mitochondrial functions including protein import, ATP generation, and lipid biogenesis depend on the maintenance of transmembrane potential, and loss of transmembrane potential during apoptosis is likely to contribute to the death of the cell through loss of these functions. In addition, mitochondrial production of reactive oxygen species (ROS) also appears to play a role in cell death. The relationships between these events, release of mitochondrial proteins, and caspase activation remain controversial. This rapid effect of caspases on the function of the electron transport chain is therefore likely to be a major contributing factor to the process of caspase-dependent cell death [22].

1.3.2.2   <u>Lysosomes role in apoptosis</u>

Under oxidative stress, iron-catalysed oxidation within the lysosomal compartment leads to lysosomal leak and rupture. Minor lysosomal destabilization of this sort will trigger reparative autophagocytosis and restoration of normal cellular function. However, more marked lysosomal

leakage and rupture are associated with apoptotic and, in extremis, necrotic cell death. Interestingly, early and minor lysosomal leak induced by oxidative stress will cause further lysosomal destabilization and, ultimately, apoptosis, which occurs long after removal of the oxidant stress.

The intimate involvement of lysosomal leakage in apoptosis is emphasized by the finding that the release of mitochondrial cytochrome c can occur secondary to this lysosomal destabilization. Therefore, the release of lysosomal hydrolytic enzymes into the cytosol may be a key event, leading to proteolytic activation of pro-caspases and/or other cytosolic lytic pro-enzymes.

These early events then might lead to further lysosomal destabilization and direct attack on mitochondria, with consequent cytochrome c release. This scenario would be consistent with the aforementioned progressive lysosomal rupture occurring long after removal of the oxidant stress. Bcl-2 might somehow act to interrupt this sequence of events: Bcl-2 over-expression effectively prevents the later lysosomal destabilization and, expectably, apoptosis. These findings raise the possibility that Bcl-2 somehow blocks downstream events that result in the later phase of lysosomal rupture, and that this activity may be involved in the still mysterious mode of action of this anti-apoptotic protein [23].

1.4 <u>**Photomedicine**</u>

Photomedicine is employed to cure various cutaneous and neoplastic diseases and includes phototherapy and photochemotherapy [24]. Phototherapy and photochemotherapy are treatments in which the light with an appropriate wavelength is used to induce a therapeutic response, in the absence or in presence of a photosensitizer drug, respectively. To be effective, light has to be adsorbed by an endogenous chromophore (phototherapy) or by a photosensitizer agent (photochemotherapy), which can be administered by topical or systemic way.

The electromagnetic spectrum can be divided into subgroups on the basis of the biological effects of each wavelength. We limit our discussion to radiation within the ultraviolet range (10-400 nm).
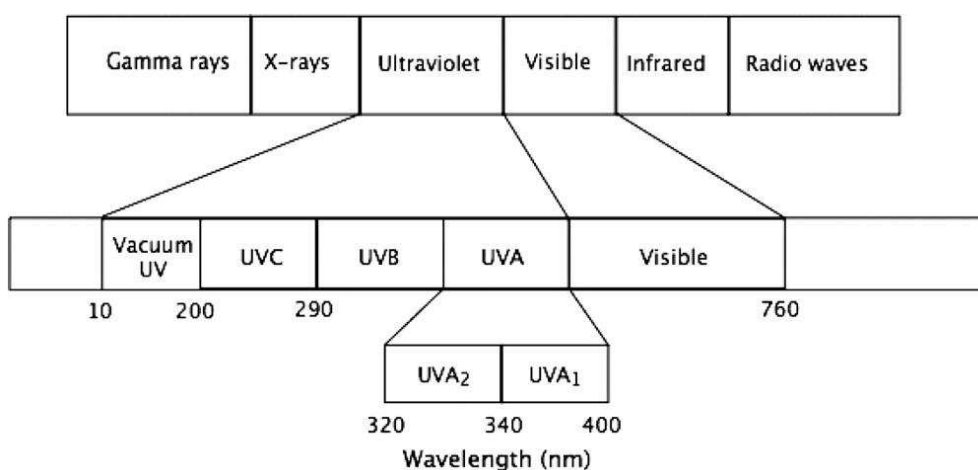
Fig. 1.4 Electromagnetic spectrum.

Ultraviolet radiation (UVR) can be divided into several subtypes, which are, from shortest to longest wavelengths, UVC (200-290 nm), UVB (290-320 nm), and UVA (320-400 nm). UVA can be further divided into UVA2 (320-340 nm) and UVA1 (340-400 nm).

Broadband (BB) UVB was one of the first phototherapy modalities used in the treatment of psoriasis. Today, however, the more commonly used form of UVB is narrowband (NB) UVB, which has a peak emission at 311 nm. A series of clinical trials have demonstrated its superiority in the treatment of psoriasis and other conditions when compared with BB UVB. Today, it has become a first-line therapy in the treatment of psoriasis and other nonpsoriatic conditions because of its many advantages. In addition, NB UVB treatment may be home or office based.

Unlike UVB radiation, UVA has the ability to penetrate to the deep dermis and subcutis. UVA1, because of its proximity to visible light on the far end of the UVA spectrum, does not induce erythema effectively, whereas UVA2, which resides at the lower wavelengths of UVA, may be

associated with effects similar to UVB, including acute sunburn. The therapeutic potential of UVA1 first emerged in 1992 in the treatment of atopic dermatitis and then in 1995 for the treatment of localized scleroderma. UVA1 has been reported to have efficacy in a growing number of skin disorders.

UV radiation exerts a multitude of biological effects in the skin from mutagenic to immunologic ones. The depth of penetration of the different light sources used for medical therapy dictates in which part of the skin they exert their greatest effect. UVB has more energy than UVA, but has less capability to penetrate beyond the superficial layers of the skin. Thus, UVB primarily affects Langerhans cells and epidermal keratinocytes. UVA radiation, particularly UVA1, reaches the deep dermis and potentially the subcutis, thereby impacting dermal fibroblasts, dendritic cells, lymphocytes, mast cells, and granulocytes.

The ability to induce lymphocyte apoptosis is an important immunomodulatory effect of UVA and UVB phototherapy. T cells are highly susceptible to the effects of UV irradiation.

The apoptotic effect of UVB is modulated via multiple mechanisms, including the Fas/Fas ligand system, p53, and apoptotic proteases. The apoptotic effects of UVA1 are different from those associated with UVB and include 2 independent caspase systems and an immediate apoptotic effect that may target specific types of cells preferentially [25].

Photochemotherapy can be divided into two main types: photodynamic therapy (PDT) and PUVA therapy.

PDT is a rapidly growing modality for the treatment of light-accessible tumours [26]. It involves two individually non-toxic components that are combined to induce cellular and tissue effects in an oxygen-dependent manner. The first component of PDT is photosensitizer – a porphyrine derivative that localizes to a target cell and/or tissue. The second component involves the administration of visible light that activate the sensitizer. The photosensitizer transfers energy from light to molecular oxygen to generate singlet oxygen.

PUVA therapy combines the effects of Psoralens and UVA light [27]. Oral administration of psoralens followed by irradiation of the cutaneous area by UVA radiation has been successfully used for the treatment of numerous autoimmune and/or hyperproliferative skin diseases, such as psoriasis, mycosis fungoides, lichen planus and vitiligo [28]. The most common PUVA regimen in the United States uses 8-methoxypsoralen (8-MOP), which is administered orally 2 hours before UVA irradiation. Bath PUVA is application of a topical psoralen before UVA irradiation, either to the entire body or limited areas (hands and feet). Advantages of bath PUVA include shorter irradiation times and a lack of gastrointestinal side effects associated with oral psoralens, but its use is limited by need for special facilities, patient inconvenience, and unpredictability (although this is

minimal for localized topical PUVA). Consequently, PUVA is usually administered via the use of oral psoralen [25].

1.4.1 <u>Psoralens and PUVA therapy</u>

Psoralens are planar, tricyclic compounds, consisting of a furan ring fused to a coumarin moiety.
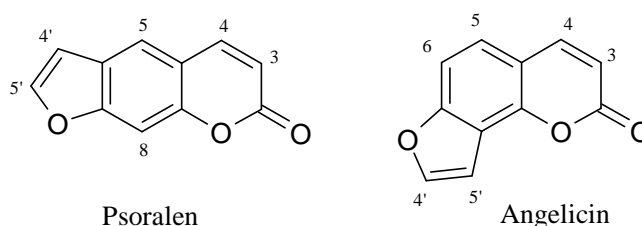

Fig. 1.5 Furocoumarins.

Most psoralens have strong absorption bands in the range 200–350 nm, with lower absorbance towards the visible region of the spectrum.

After the absorption of a photon by a molecule in the ground state, an electron is promoted to an excited singlet state. From here, it may return to the ground state, by the emission of a photon (fluorescence), or by the release of energy in the form of heat (radiationless collisional deactivation). Relatively infrequently, the electron in the singlet state can undergo intersystem crossing to the triplet state. Until there is some interaction with another molecule – be it another psoralen molecule, or more interestingly, something like DNA – all of the foregoing processes represent reversible photophysical processes. The excited state forms of the molecule can undergo several different photoreactions: photoaddition, photodimerization and/or photo-oxidation of nearby moieties (components of nucleic acids, proteins, membranes). Alternatively, energy transfer from the triplet state to molecular oxygen (normally in the triplet ground state) can lead to highly reactive singlet oxygen. Electron transfer from the sensitised molecule to a target molecule, leading to radical formation, is a type I photodynamic reaction.

The photochemical reactions of psoralens with DNA are the best characterized, having been studied for nearly 40 years. Their planar aromatic structure and hydrophobic nature facilitate their intercalation with DNA bases. Upon photoactivation of the intercalated psoralen molecule, different adducts may be formed: in particular a [2+2]-photocycloaddition can occur between one of the photoreactive sites in the psoralen moiety (i.e. the double bonds in 3,4 of the pyrone ring and in 4',5' of furan ring) and a double bond in a DNA base. From in vitro DNA photochemistry it has

16

been shown that the most frequently occurring adducts are those with thymine, followed by cytosine–psoralen adducts (10–20 times less efficiently). A psoralen–adenine photoadduct has also been characterized after in vitro photoreactions with adenine, but it has not yet been shown to occur in DNA isolated from cells irradiated in the presence of psoralens. The crosslinking process depends on the structure of the psoralen. Linear furocoumarins form crosslinks efficiently (up to 50% of total adducts formed). Angular furocoumarins, or angelicins, were long thought to be unable to form crosslinks because of their geometry. Thus, the extent and nature of adduct-formation and the distribution between monoadducts and crosslinks depend on the psoralen derivative, the nucleic acid sequence of the DNA and the dose and wavelength of radiation used for photoactivation.

Although DNA psoralen photochemistry has attracted the most attention, psoralens also react with proteins as well as other cell constituents. In studies of the subcellular fractions of rat epidermis after treatment with 8-MOP and UVA, it was found that 17% of the 8-MOP was bound to DNA, while a substantial amount was bound to proteins (57%) and lipids (26%). Several studies have demonstrated the ability of 8-MOP and TMP to react in an oxygen-independent way with unsaturated fatty acids. Proteins and lipids appear to form adducts with the pyrone ring in 8-MOP whereas DNA reacts with the furan moiety [29].

The combination of 8-methoxypsoralen and UVA irradiation is widely used for the treatment of various disorders mediated by T-cell (T-cell lymphomas, psoriasis). Special application of PUVA has been developed and named extracorporeal therapy according to its practical performance. Mononuclear cells (2–5% total volume of peripheral blood) are withdrawn from the patient's blood, submitted to UVA-activated 8-MOP and finally returned into the body.

A special immunomodulation response to this therapy is being developed in the organism and it is based on T-cell apoptosis and monocyte activation. UVA excitation of 8- MOP can lead to reactive oxygen species production playing an important role in oxidative damage of DNA, proteins and unsaturated lipids [30]. Although 8-MOP is biologically inert in the absence of UVA, the combination of 8-MOP and UVA causes the formation of monoadducts and covalent crosslinks of DNA [31]. Planar structure of 8-MOP enables its intercalation into double strand space of DNA. Following UVA-activation the 8-MOP molecule binds covalently to thymines of the opposite DNA strands and forms cross-links which hamper DNA replication. This results in decreased cell proliferation and cell death by apoptosis.

Apoptosis induction by PUVA treatment has been described in a number of experimental systems. However, the apoptosis is only triggered if the alteration is irreparable. If it is not the case the G_2/M checkpoint prevents cells from entering mitosis until the damage is repaired [30].

1.4.1.1   <u>Side effects and contraindications of PUVA</u>

Patients treated with UVA1 most commonly report no side effects other than tanning and, less commonly, erythema and pruritus. UVA1 has been reported to cause a polymorphic light eruption and activation of herpes simplex infection [25].

Nevertheless, PUVA therapy shows various toxic effects, such as severe skin erythema, and genotoxicity, with induction of point mutations and chromosomal aberrations. In addition, PUVA therapy is associated to a certain risk of skin cancer. Various authors attributed these dangerous effects to the severe damage induced into DNA by furocoumarin sensitisation. In fact psoralens form covalent monoadducts with pyrimidine bases, or diadducts: covalent inter-strands cross-links with two pyrimidine bases on the opposite DNA strands, and covalent DNA-protein cross-links [32]. The side effects of the psoralen, 8-MOP, used in PUVA therapy, include nausea and gastrointestinal upset. One strategy for reducing the side effects of 8-MOP–induced nausea is to decrease the dose and compensate by increasing the dose of UVA by the same percentage. 8-MOP may also be substituted with 5-MOP, which is relatively equivalent in efficacy and produces fewer side effects.

As mentioned previously, bath PUVA carries some inconveniences as compared with oral psoralen therapy. Despite these inconveniences, bath PUVA is preferential in patients with limited treatment areas, such as the hands and feet, and may also be considered in patients who would otherwise have difficulty in tolerating oral psoralen (when facilities are available). In addition, some patients treated with PUVA complain of a painful, burning itch that may persist for months after treatment.

Currently, PUVA is the only phototherapeutic modality definitively linked with the development of melanoma and nonmelanoma skin cancer in white patients. Various factors modulate the risk of carcinogenesis in each patient before any exposure to phototherapy. These factors include Fitzpatrick skin type, preexisting actinic damage, age, and personal habits and behaviour (extensive outdoor exposure, tanning bed use). These elevate the baseline risk for carcinogenesis for each patient and therefore, additional exposure to further risk is clearly contraindicated [25].

2. Aim of the project

This project is focused on studying new antiproliferative compounds synthesized by prof. Cirrincione's group in the Department of Molecular and Biomolecular Sciences and Technologies at Palermo University. Particularly, three series of compounds were analysed:

- BQ series
- LCQ series
- PZQ series

For every compound at first chemical and physical properties were analysed and then its antiproliferative activity in many cell lines was evaluated; the most active molecules, moreover, were further investigated.

2.1 BQ and LCQ series

These compounds were synthesized to identify new potential inhibitors of tyrosine kinase activity.

Receptor tyrosine kinases (RTKs) have been shown to be important mediators of signal transduction in cells. These transmembrane molecules characteristically consist of an extracellular ligand-binding domain connected through a segment in the plasma membrane to an intracellular tyrosine kinase domain. Binding of the ligand to the receptor results in receptor dimerization and stimulation of the receptor-associated tyrosine kinase activity, which leads to phosphorylation of tyrosine residues on both the receptor and other intracellular molecules. These changes in tyrosine phosphorylation initiate a signalling cascade leading to a variety of cellular responses [33].

RTKs, particularly, are associated to various growth factor receptors, for example EGFR (Epidermal Growth Factor Receptor), VEGFR (Vascular Endothelial Growth Factor Receptor) and PDGFR (Platelet Derived Growth Factor Receptor).

The epidermal growth factor receptor is known to be overexpressed in a large percentage of clinical cancers of various types and to be associated with poor prognosis. Compounds which inhibit the

ability of EGFR to transmit a phosphorylation signal following binding of EGF are therefore of potential interest as anticancer drugs [34].

VEGF is an important stimulator of both normal and pathological angiogenesis. VEGF has been shown to be secreted by human tumour cell lines in culture (e.g. glioma and melanoma). Moreover, VEGF protein as well as mRNA for the VEGF receptors Flk-1/KDR have been identified in primary tumours of breast, colon, and renal origin. Blockade of VEGF signal transduction has been shown to prevent tumour growth. VEGF RTKs must, therefore, be viewed as attractive therapeutic targets for the development of novel agents to treat angioproliferative diseases such as cancer [33].
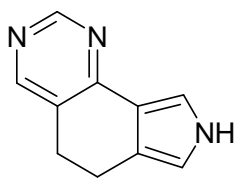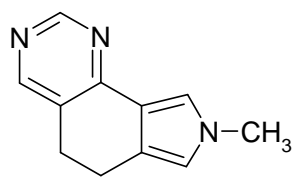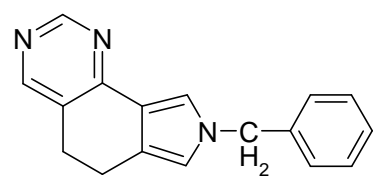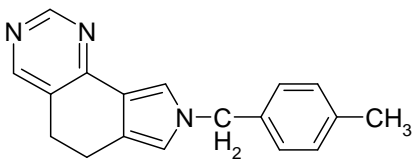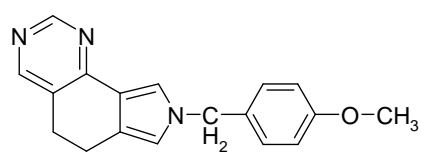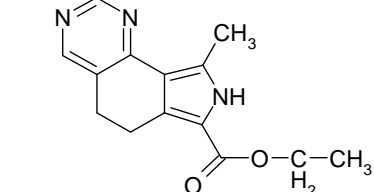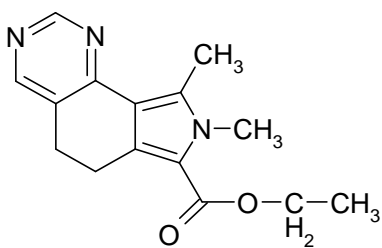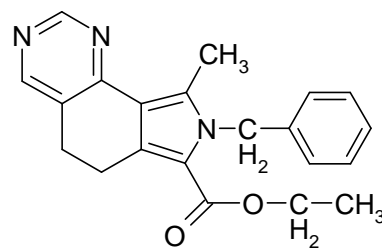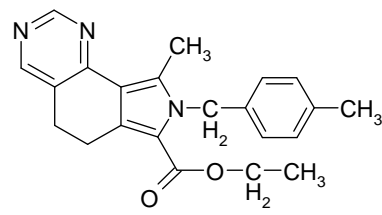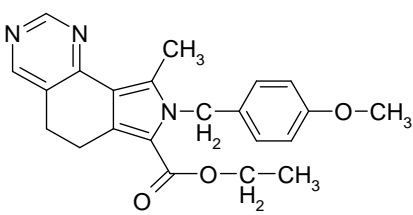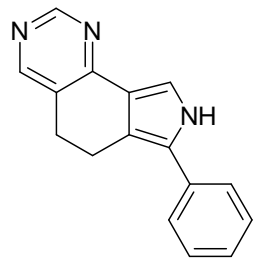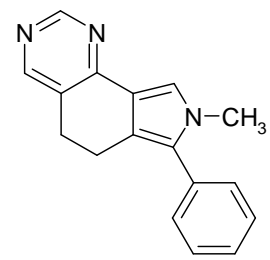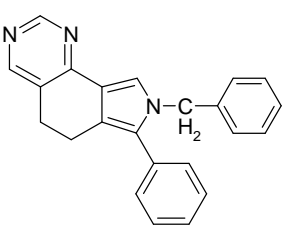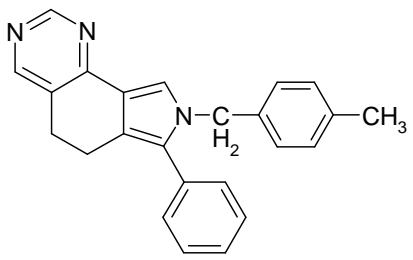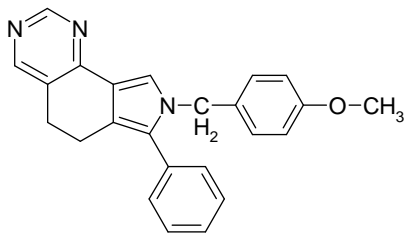
Platelet derived growth factor (PDGF) is known to act as a potent mitogen and chemotactic factor for various cells such as fibroblasts, smooth muscle cells, mesenchymal cells, and brain glial cells. Abnormal PDGF-induced cell proliferation has been proposed to lead to proliferative disorders such as atherosclerosis, restenosis following percutaneous transluminal coronary angioplasty, glomerulonephritis, glomerulosclerosis, liver cirrhosis, pulmonary fibrosis, and cancer. Additionally, PDGF and its receptor (PDGFR) are also upregulated in these proliferative disorders. Therefore, an inhibitor of PDGFR phosphorylation would be expected to possess a therapeutic potential in the treatment of these proliferative disorders [35].

In the past decade, efforts aimed at the discovery of therapeutically useful inhibitors of protein kinases have intensified. These efforts have resulted in the identification of a variety of templates which, depending upon the nature of attached substituents, provide selective inhibition both within and across different protein kinase families. One of these privileged scaffolds is the quinazoline nucleus, which has served as the core template for a variety of ATP-competitive kinase inhibitors.
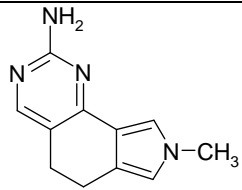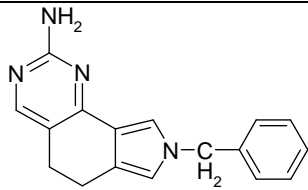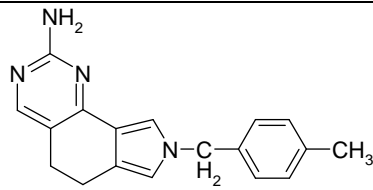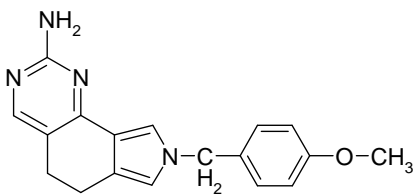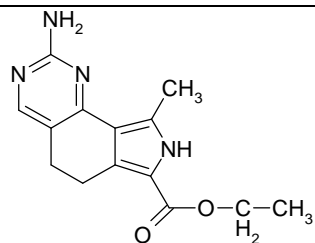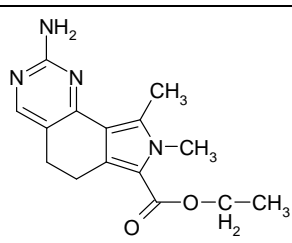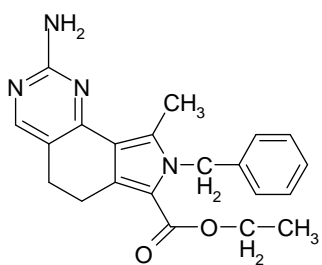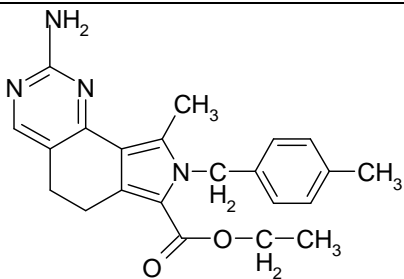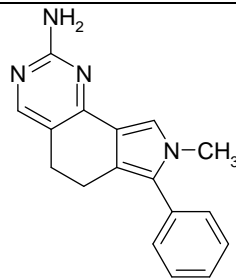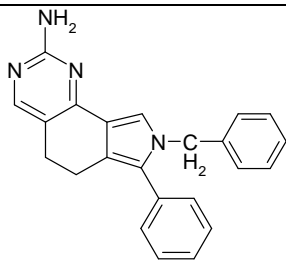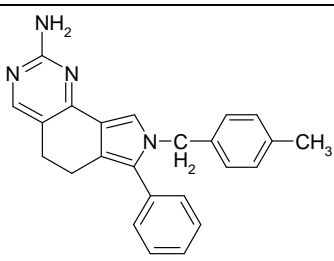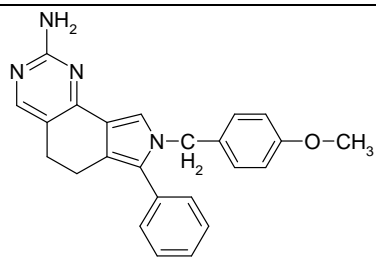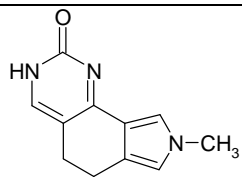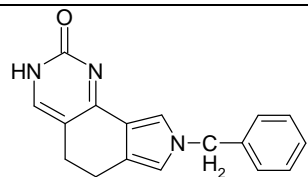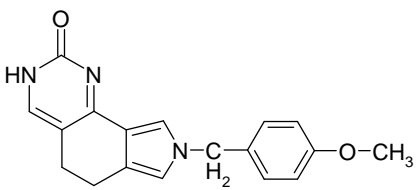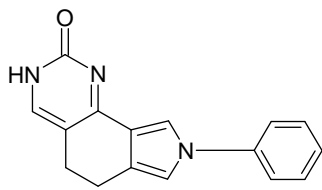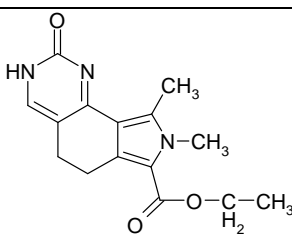
The leading examples of reversible quinazoline-based inhibitors are the clinically approved anticancer agents gefitinib (Iressa) and erlotinib (Tarceva). Both compounds are inhibitors of the receptor tyrosine kinase activity of the epidermal growth factor receptor (EGFR/HER1). There are also quinazoline-based compounds which target both EGFR and the related RTK HER2, for example the reversible inhibitor lapatinib or the irreversible inhibitor afatinib, which is undergoing clinical trials. Outside of the HER family, clinical compounds based on the quinazoline scaffold which target vascular endothelial growth factor receptor-2 (VEGFR-2/KDR) have been approved. Additionally, there are reports of other quinazoline-based RTK inhibitors, including compounds which target the tyrosine kinase activity of the platelet-derived growth factor receptor (PDGFR).
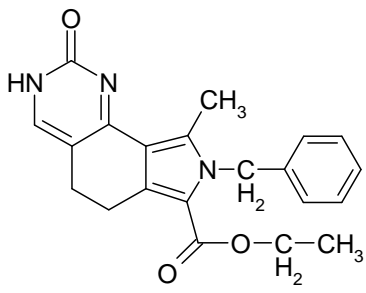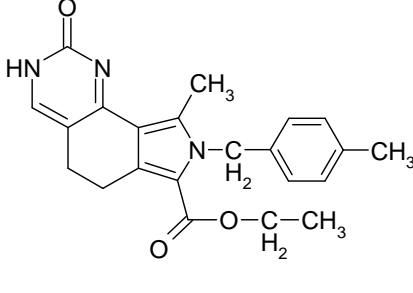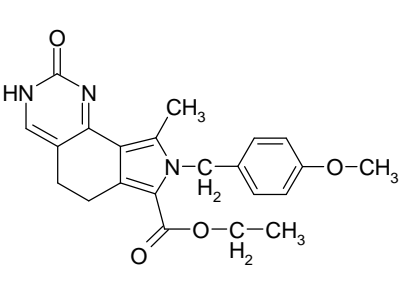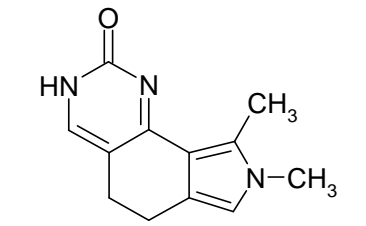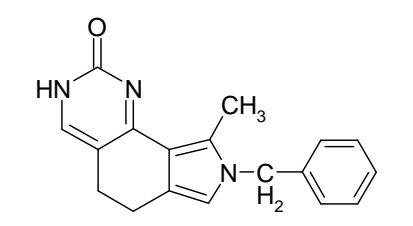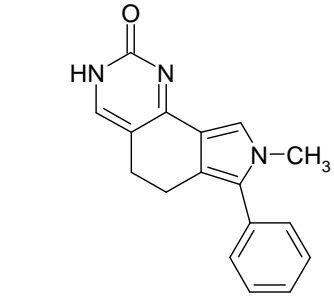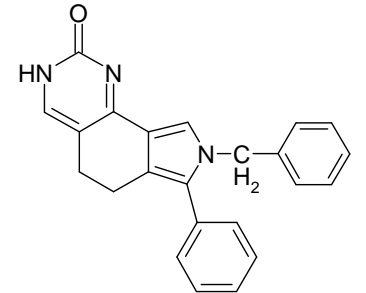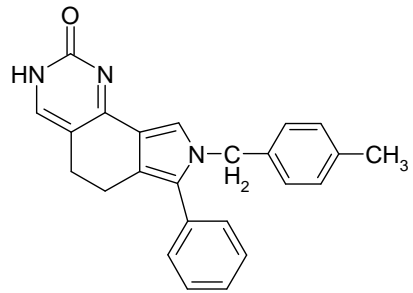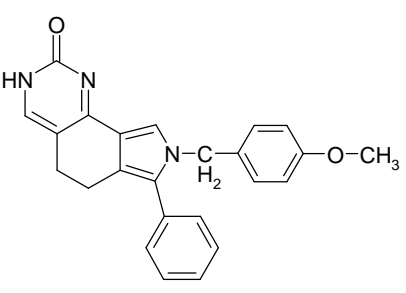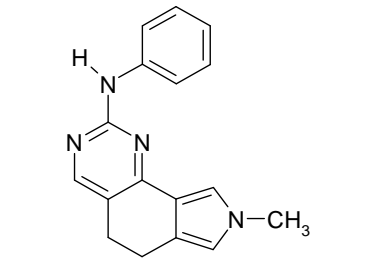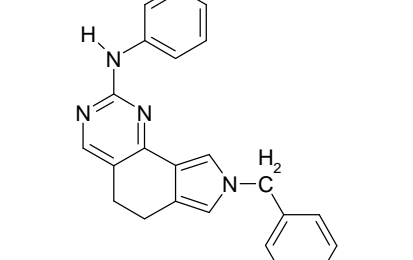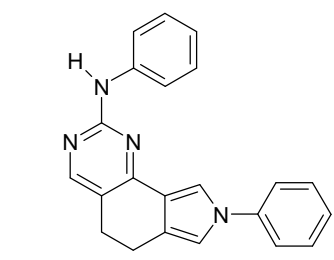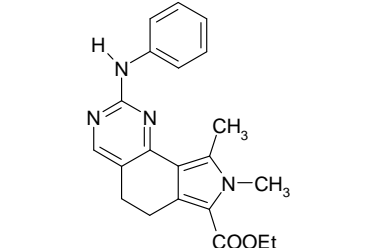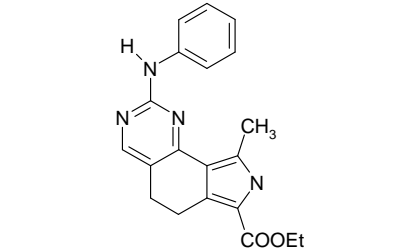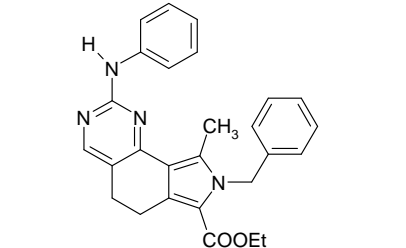
The search for novel analogues of the quinazoline template has generated kinase inhibitors containing a variety of carbon-fused heterocycles [36]; prof. Cirrincione's group synth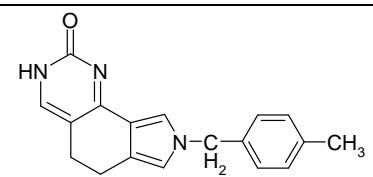esized these news compounds through the condensation of the quinazoline structure to a pyrrolic group: pyrrolo, in fact, is also present in some tyrosine kinase inhibitors [34,36].

The BQ series is composed by 49 pyrrolo[3,4-h]quinazoline derivatives:
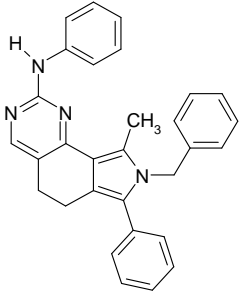
BQ1	BQ2	BQ3
BQ4	BQ5	BQ6
BQ7	BQ8	BQ9
BQ10	BQ11	BQ12
BQ13	BQ14	BQ15

BQ16	BQ17	BQ18
BQ19	BQ20	BQ21
BQ22	BQ23	BQ25
BQ26	BQ27	BQ28
BQ29	BQ30	BQ31
BQ32	BQ33	BQ34
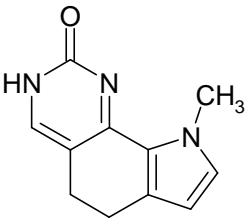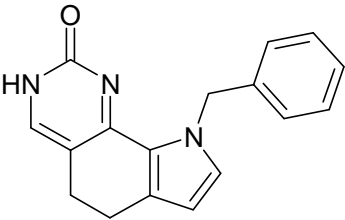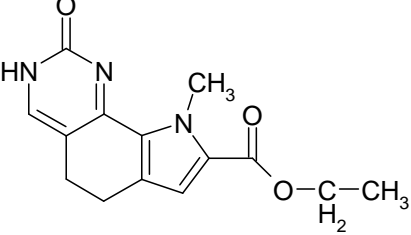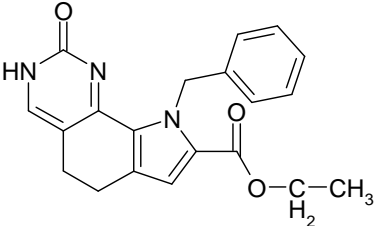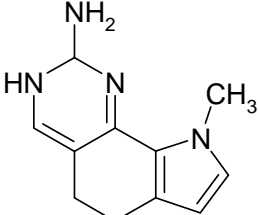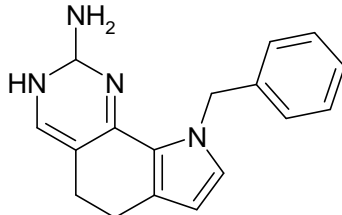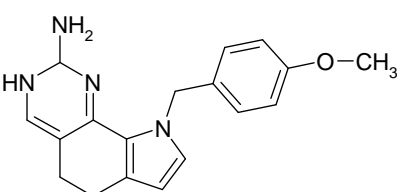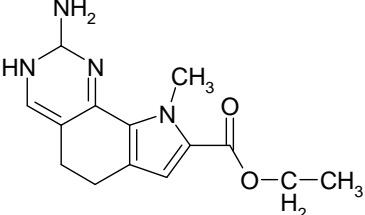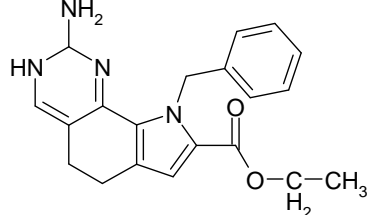
BQ35	BQ36	BQ37
BQ38	BQ39	BQ40
BQ41	BQ42	BQ43
BQ44	BQ45	BQ46
BQ47	BQ48	BQ49
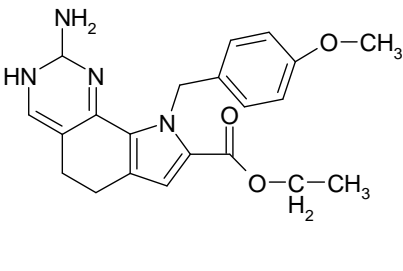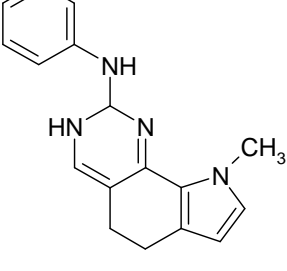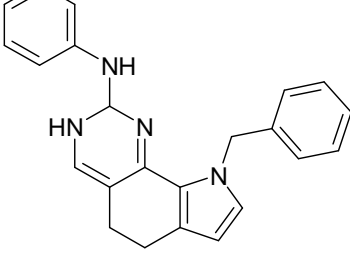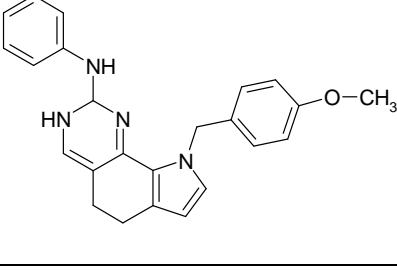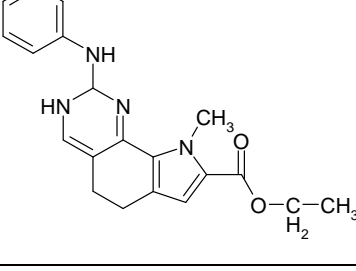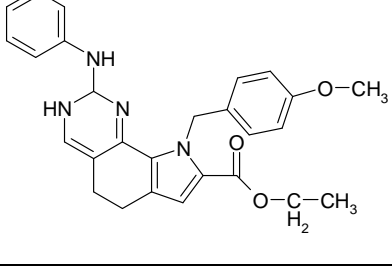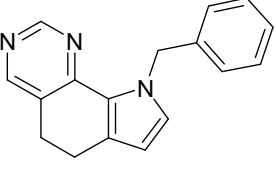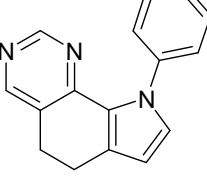
BQ50		

This series has been widely explored. After the evaluation of spectroscopic properties, cytotoxicity was determined on various tumoral cell lines; the most active molecules were then analysed with regard to cell death mechanism, cell cycle studies and mechanism of action.

The LCQ compounds are 17 pyrrolo[2,3-h]quinazoline derivatives:

LCQ1	LCQ2	LCQ3
LCQ4	LCQ5	LCQ6
LCQ7	LCQ8	LCQ9

LCQ10	LCQ11	LCQ12
LCQ13	LCQ14	LCQ15
LCQ16	LCQ17	
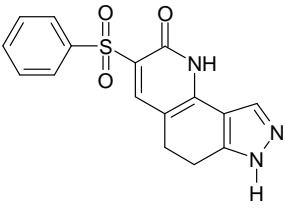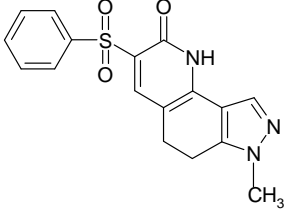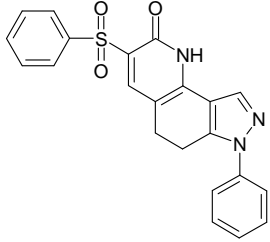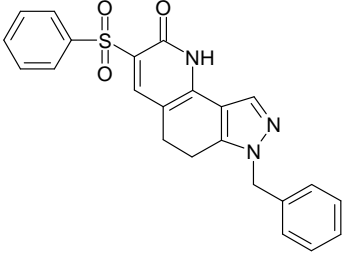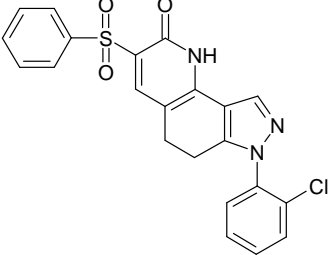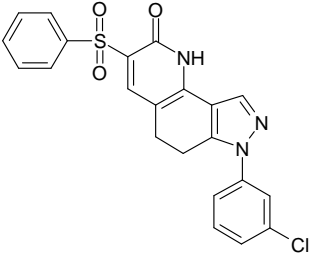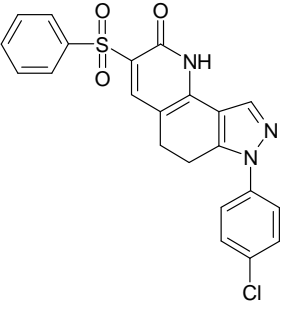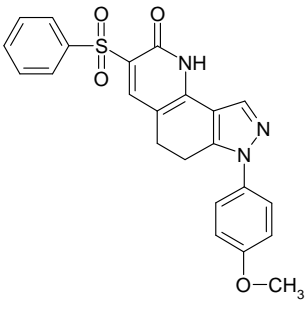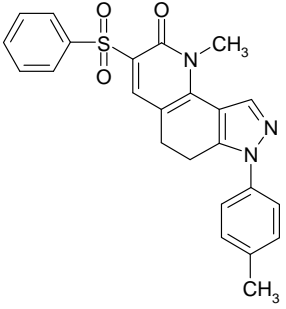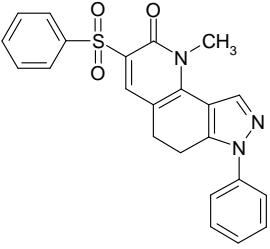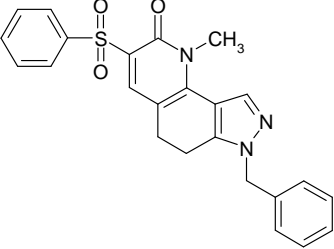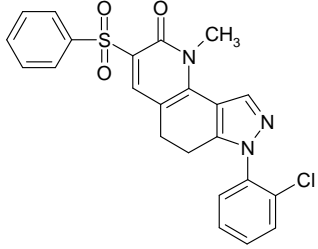
These compounds have shown to be less active than BQ derivatives, so photocytotoxicity was tested with remarkable results: these molecules, in fact, are heteroanalogues of angelicin, so they were investigated as photoactivable agents. The most active compounds were afterwards analysed with flow cytometry assays and tested to identify their potential target.
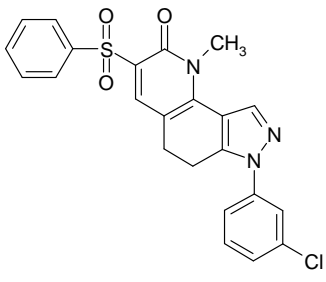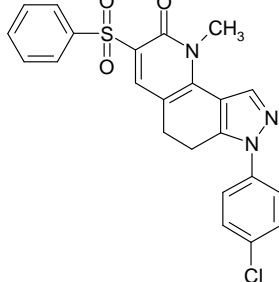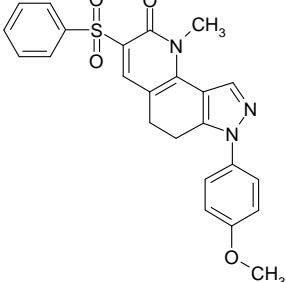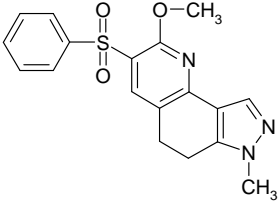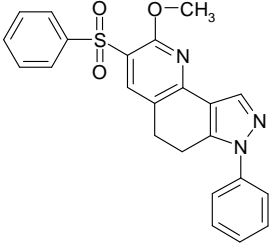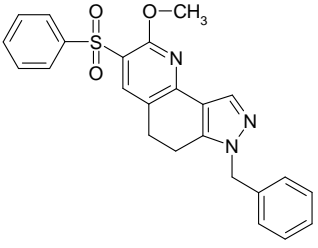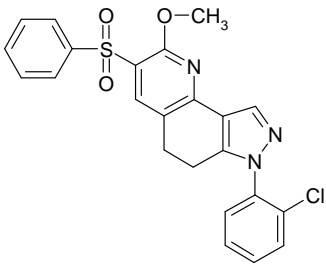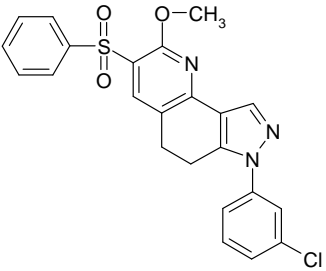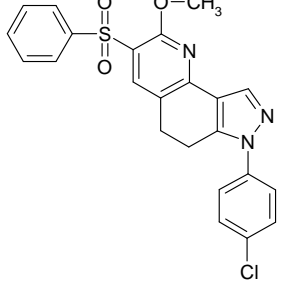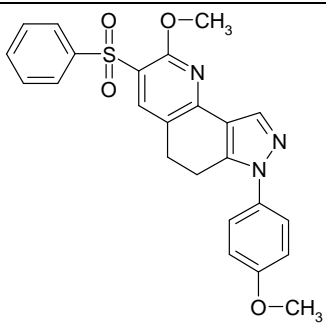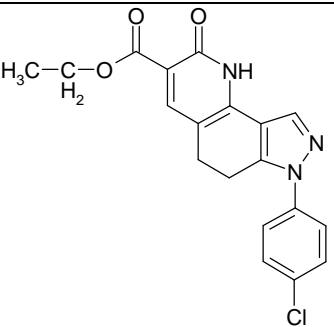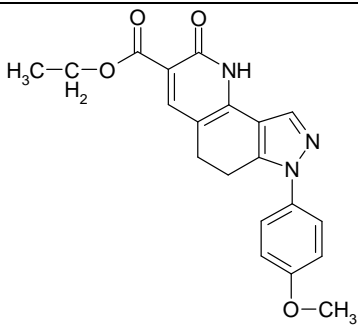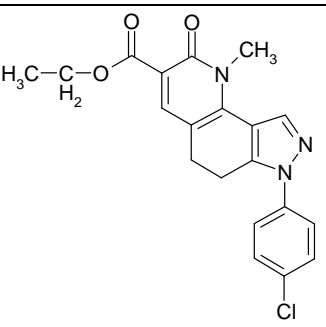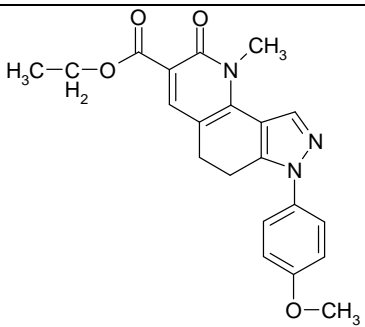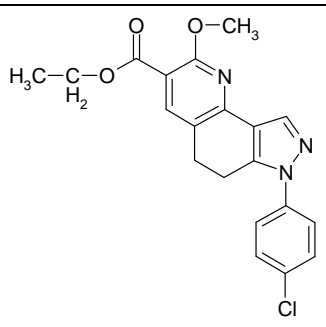
2.2 <u>PZQ series</u>

PZQ series is composed by 38 pyrazolo[3,4-h]quinolines, synthesized as angelicin analogues with photochemotherapeutic activity.
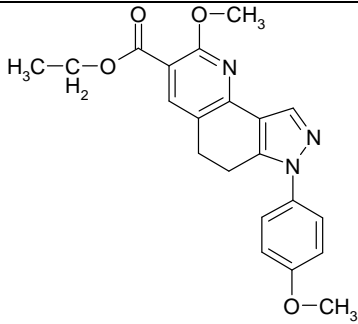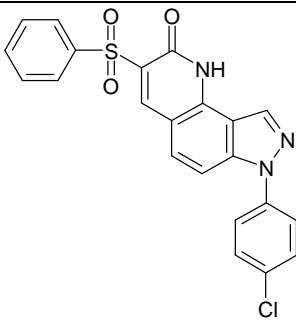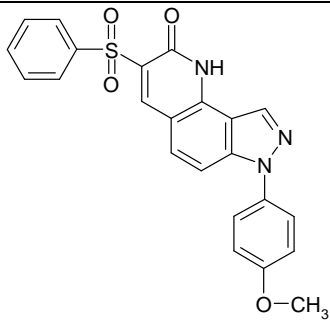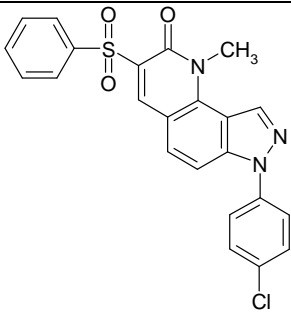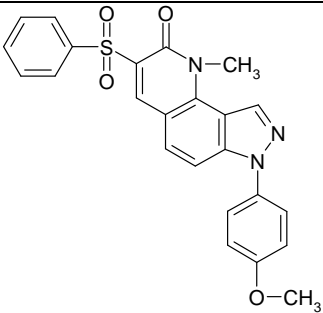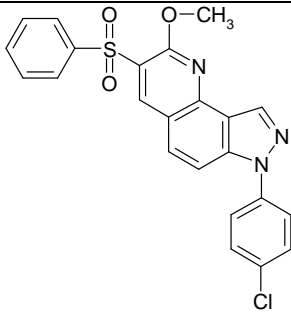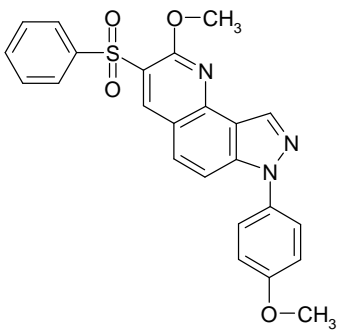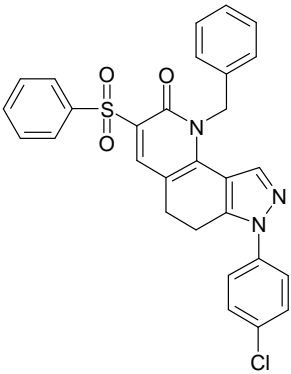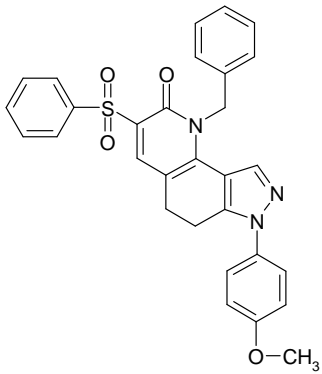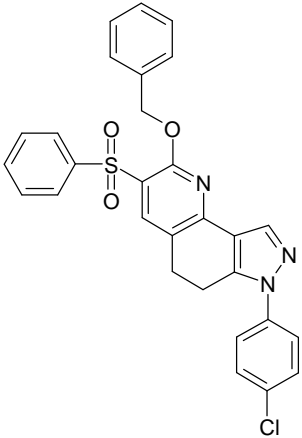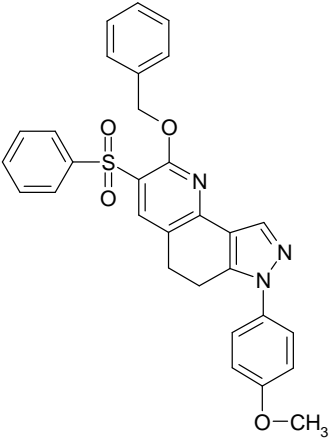
PUVA has been used for more than 2 decades as a very effective therapeutic modality for various diseases such as psoriasis, chronic eczema, cutaneous T-cell lymphoma and other primary and secondary lymphoproliferative disorders, and cutaneous graft-versus-host disease after allogeneic

stem cell transplantation [37]. The combination of psoralens and UV-light controls excess cell division in the skin by its ability to damage DNA. The lesions in DNA lead to inhibition of DNA synthesis, skin pigmentation and erythema production. On the other hand, psoralens show mutagenic and carcinogenic effects [38]. Much effort has gone into finding more active compounds with diminished side effects. In PZQ derivatives the oxygen atom at position 1 of angelicin has been substituted with a nitrogen atom and the furan ring with a pyrazole ring; furthermore, C3 has been replaced by a phenylsulphonyl or an ethoxycarbonyl group and the nitrogen atom at position 7 has been substituted in most cases by a group with remarkable steric hindrance.

PZQ1	PZQ2	PZQ3
PZQ4	PZQ5	PZQ6
PZQ7	PZQ8	PZQ9
PZQ10	PZQ11	PZQ12

PZQ13	PZQ14	PZQ15
PZQ16	PZQ17	PZQ18
PZQ19	PZQ20	PZQ21
PZQ22	PZQ23	PZQ24
PZQ25	PZQ26	PZQ27

PZQ28	PZQ29	PZQ30
PZQ31	PZQ32	PZQ33
PZQ34	PZQ35	PZQ36
PZQ37	PZQ38	

First of all, spectroscopic and photochemical features have been determined for these compounds; successively, cytotoxicity and photocytotoxicity were evaluated on tumour and non-tumour cell lines, with and without scavengers. The most active molecules were then further analysed to establish cell death mechanism and to characterize their potential targets.

3. Pyrrolo[3,4-h]quinazolines

3.1   Physicochemical properties

BQ compounds are 49 new molecules, therefore physicochemical properties are to be examined. Absorbance and emission spectra are determined in DMSO or in phosphate buffer and molar extinction coefficient (ε) is calculated, as described in Materials and methods section; the results are listed in table 3.1.

Compounds	λ_{max} abs in DMSO (nm)	ε ($M^{-1}*cm^{-1}$) in DMSO	λ_{max} abs in phosphate buffer (nm)	λ_{max} emiss in DMSO (nm)
BQ1	262	5545	320	376
BQ2	313	49072	316	417
BQ3	313	20224	315	374
BQ4	314	49701	316	398
BQ5	314	26925	316	405
BQ6	313	20378	313, 264	365
BQ7	311	22904	314, 266	371
BQ8	266, 307	24530	312, 266	374
BQ9	268	21382	269, 286, 312	370
BQ10	308	21693	313	376
BQ11	288	35144	281	424
BQ12	283	23808	274, 314	420
BQ13	277	46359	268	422
BQ14	276	32527	269	422
BQ15	277	28023	270	421
BQ16	334	14669	334	373

BQ17	335	14667	335	375
BQ18	335	15219	335	375
BQ19	335	14741	335	372
BQ20	332, 261	13706	329	374
BQ21	332, 261	15518	331	372
BQ22	332, 261	17792	330	376
BQ23	332, 261	9915	328	377
BQ25	263, 336	23176	262, 336	377
BQ26	263, 337	28524	262, 338	377
BQ27	264, 336	15681	266, 341	377
BQ28	267, 337	14997	266, 338	376
BQ29	319	24554	334	448
BQ30	319	27373	332	445
BQ31	319	28275	332	446
BQ32	320	19216	334	358
BQ33	329	32901	342	458
BQ34	324, 260	33376	327	400
BQ35	323, 260	25575	335	400
BQ36	324, 260	29526	332	400
BQ37	324, 261	27842	331	400
BQ38	324	26303	332	464
BQ39	324	29714	327	451
BQ40	320	32267	332	461
BQ41	321	33022	332	456
BQ42	321	31560	327	459
BQ43	321	33367	327	459
BQ44	285, 346	78297	278, 344	423
BQ45	285, 346	108007	304, 361	421
BQ46	287, 353	69527	298, 366	442
BQ47	281, 344	79645	290, 361	429
BQ48	278, 344	94012	267, 356	427

| BQ49 | 281, 345 | 76558 | 296 | 433 |
| BQ50 | 285, 345 | 89431 | 303 | 428 |

Tab. 3.1 Spectrophotometric features of pyrrolo[3,4-h]quinazolines.

3.2   <u>Cytotoxic activity</u>

As pyrrolo[3,4-h]quinazolines are synthesized as antiproliferative compounds, their cytotoxic effect is observed in a panel of 5 human tumour cell lines: K-562 (chronic myeloid leukaemia), Jurkat (T-cell leukaemia), LoVo (colon adenocarcinoma), MCF-7 (breast adenocarcinoma) and A-431 (vulvar squamous cell carcinoma).

Cytotoxicity is evaluated with MTT test after 72 hours from the incubation with BQ molecules in the presence of different concentrations of compounds, as described in Materials and methods section; results are summarized in the following table as IC_{50} (molecules concentration which leads to death 50% of cell population).

IC_{50} (μM)					
Compounds	*K-562*	*Jurkat*	*LoVo*	*MCF-7*	*A-431*
BQ1	> 20	> 20	> 20	> 20	> 20
BQ2	> 20	> 20	> 20	> 20	> 20
BQ3	> 20	> 20	> 20	> 20	> 20
BQ4	> 20	> 20	> 20	> 20	> 20
BQ5	> 20	> 20	> 20	> 20	> 20
BQ6	> 20	> 20	> 20	> 20	> 20
BQ7	> 20	> 20	> 20	> 20	> 20
BQ8	> 20	> 20	$11,3 \pm 1,8$	> 20	> 20
BQ9	$3,9 \pm 0,6$	$3,7 \pm 0,5$	$5,0 \pm 0,4$	$7,5 \pm 0,3$	$11,3 \pm 1,8$
BQ10	$3,8 \pm 0,4$	$3,1 \pm 0,1$	$5,4 \pm 0,3$	$14,1 \pm 0,9$	$17,3 \pm 2,3$
BQ11	> 20	$8,4 \pm 0,5$	$6,9 \pm 1,9$	> 20	> 20
BQ12	> 20	$10,7 \pm 1,3$	$9,1 \pm 1,4$	> 20	> 20
BQ13	> 20	> 20	> 20	> 20	> 20

BQ14	13,1 ± 2,5	3,2 ± 0,5	9,9 ± 1,8	11,7 ± 0,4	> 20
BQ15	10,9 ± 2,3	1,3 ± 0,2	7,1 ± 0,7	7,0 ± 0,4	> 20
BQ16	> 20	> 20	> 20	> 20	> 20
BQ17	> 20	> 20	> 20	> 20	> 20
BQ18	19,1 ± 2,1	> 20	6,8 ± 0,4	> 20	> 20
BQ19	> 20	8,1 ± 1,9	> 20	> 20	> 20
BQ20	> 20	> 20	10,7 ± 1,1	> 20	> 20
BQ21	> 20	> 20	> 20	> 20	> 20
BQ22	> 20	11,7 ± 1,1	12,8 ± 0,2	> 20	11,8± 1,5
BQ23	> 20	6,3 ±0,4	9,4 ± 0,2	> 20	> 20
BQ25	> 20	5,0 ± 1,0	> 20	> 20	> 20
BQ26	> 20	5,9 ± 0,5	10,5 ± 1,2	> 20	> 20
BQ27	15,3 ± 3,0	3,9 ± 0,8	9,0 ± 1,7	15,3 ± 0,8	> 20
BQ28	> 20	8,1 ± 1,2	8,0 ± 0,9	> 20	> 20
BQ29	> 20	> 20	> 20	> 20	> 20
BQ30	> 20	> 20	> 20	> 20	> 20
BQ31	> 20	> 20	> 20	> 20	> 20
BQ32	> 20	> 20	> 20	> 20	> 20
BQ33	> 20	9,4 ± 0,8	> 20	> 20	> 20
BQ34	> 20	12,5 ± 1,7	> 20	> 20	> 20
BQ35	> 20	> 20	> 20	> 20	> 20
BQ36	> 20	8,5 ± 2,1	> 20	> 20	> 20
BQ37	> 20	> 20	> 20	> 20	> 20
BQ38	> 20	> 20	> 20	> 20	> 20
BQ39	> 20	> 20	> 20	> 20	> 20
BQ40	> 20	6,2 ± 0,6	14,6 ± 1,6	> 20	> 20
BQ41	> 20	7,4 ± 0,4	> 20	> 20	> 20
BQ42	> 20	9,3 ± 1,3	> 20	17,9 ± 1,6	8,5 ± 1,2
BQ43	> 20	> 20	> 20	> 20	> 20
BQ44	> 20	8,6 ± 1,9	7,4 ± 1,2	> 20	7,7 ± 0,5
BQ45	> 20	> 20	> 20	> 20	7,6 ± 1,3
BQ46	11,0 ± 1,0	> 20	8,8 ± 1,0	> 20	> 20
BQ47	8,8 ± 1,41	7,3 ± 1,5	9,9 ± 1,0	> 20	9,7 ± 0,4

BQ48	> 20	> 20	> 20	> 20	$3,0 \pm 0,5$
BQ49	> 20	$13,0 \pm 1,6$	$9,2 \pm 0,6$	> 20	> 20
BQ50	$18,6 \pm 1,6$	> 20	$6,9 \pm 0,4$	> 20	> 20

Tab. 3.2 Antiproliferative activity of BQ molecules (μM).

Some molecules are inactive at the employed concentrations, some others inhibit the proliferation of some cell lines (e.g. BQ8, BQ11 and BQ12). The most active compounds are BQ9 and BQ10 (IC_{50} values are lower than 15μM in all cell lines) and, next, BQ14 and BQ15, with interesting cytotoxic effect.

Given that many molecules have been analysed, some hypotheses can be developed regarding the structure-activity relationships (SAR).

Pyrrolo[3,4-h]quinazolines are variably substituted at positions 2, 7, 8 and 9. Among quinazoline derivatives unsubstituted at position 2, the most cytotoxic ones are substituted at positions 7 and 8 with lipophilic groups with a remarkable steric hindrance (e.g. ethyl ester – BQ9 and BQ10 – or phenyl group – BQ14 and BQ15 – at position 7; p-methyl benzyl group – BQ9 and BQ14 – or p-methoxybenzyl group – BQ10 and BQ15 – at position 8); if the substitution is observed at only one of the two positions, we can see a complete loss of antiproliferative activity (e.g. BQ4, BQ5, BQ6) or cytotoxicity is remarkably reduced (e.g. BQ11, BQ12).

Moreover, cytotoxicity does not increase with the introduction of a substituent at position 2; particularly, a carbonyl group reduces cytotoxicity of some molecules or inactivates other derivatives. Instead, an amine group can remarkably increase cytotoxicity in Jurkat cells, but it does not lead to active compounds for other cell lines.

In analogy to the quinazoline derivatives which inhibit tyrosine kinase receptor [33, 34, 36, 39-41], some molecules with an aniline group at position 2 have been synthesized (BQ44 – BQ50); this group does not seem to increase the antiproliferative activity of these compounds, but tested compounds are not substituted at positions 7 and 8 as the most active ones in the 2-unsubstituted series.

3.2.1 <u>Cytotoxicity on resistant tumour cell lines</u>

Although many anticancer drugs in clinical use are effective in the treatment of different kinds of tumours, their potential is limited by the development of drug resistance. Resistance can be intrinsic

_____

or acquired, but in either case tumours become refractory to a variety of structurally different drugs. Thus, the antiproliferative activity is also tested on LoVo^{doxo} cells, a human cancer cell line expressing high level of 170-kDa P-glycoprotein (P-gp) drug efflux and resistant to doxorubicine; resistance index (RI) is determined comparing IC$_{50}$ values of the resistant line to the ones obtained with LoVo cells.

	IC$_{50}$ (μM)		
Compounds	*LoVo*	*LoVo^{doxo}*	*RI*
BQ8	11,26 ± 1,76	19,43 ± 0,50	1,72
BQ9	5,01 ± 0,44	15,17 ± 1,03	3,03
BQ10	5,44 ± 0,27	8,65 ± 0,13	1,59
BQ11	6,88 ± 1,89	8,70 ±1,31	1,26
BQ12	9,11 ± 1,43	12,45 ± 1,33	1,37
BQ14	9,90 ± 4,83	9,47 ± 2,49	0,96
BQ15	7,11 ± 0,78	12,50 ± 3,91	1,76
BQ18	6,80 ± 0,36	9,46 ± 0,28	1,39
BQ20	10,67 ± 1,08	9,15 ± 0,40	0,86
BQ22	12,76 ± 0,17	> 20	n.a.
BQ23	9,36 ± 0,23	> 20	n.a.
BQ26	10,47 ± 1,16	10,31 ± 1,53	0,98
BQ27	9,07 ± 1,67	12,92 ± 1,26	1,42
BQ28	7,96 ± 0,92	12,15 ± 2,11	1,53
BQ40	14,62 ± 1,64	> 20	n.a.
BQ44	7,41 ± 1,23	3,50 ± 0,52	0,47
BQ46	8,77 ± 1,03	> 20	n.a.
BQ47	9,91 ± 1,03	> 20	n.a.
BQ49	9,19 ± 0,64	> 20	n.a.
BQ50	6,92 ± 0,42	> 20	n.a.

n.a. = not available

Tab. 3.3 IC$_{50}$ values on LoVo^{doxo} cell line (μM).

As we can see in this table, many molecules maintain their cytotoxic effect on the resistant subclone: IC$_{50}$ values, in fact, are often similar in both cell lines and RI is next to 1. Nevertheless, some compounds are not cytotoxic on the resistant cell line, particularly when they are substituted

with an aniline group at position 2, so RI cannot be calculated; instead, other molecules are more active on the resistant cell line.

We can notice two extreme cases: BQ9 has RI of 3,3, probably because it is P glycoprotein substrate, but BQ44 cytotoxic activity is higher on LoVo^{doxo} cells (RI = 0,47).

3.2.2 <u>Colony formation assay</u>

Colony formation assay is a cell survival test based on the ability of a single cell to grow into a colony, hence this test is performed to confirm our previous results about the effectiveness of the most active pyrrolo[3,4-h]quinazolines: cell colony formation, in fact, has been found to be a more sensitive parameter of toxicity than cell viability since colony formation is assessed while the cells are in a state of proliferation, and thus more susceptible to toxic effects.

In this test, A-431 cells are seeded in their proper medium (7000 cells/well); after 24 hours incubation with BQ9, BQ10, BQ14, BQ15 and BQ47 at five different concentrations, the growth medium is restored and colony formation is tested every 2-3 days. After 10-15 days, cells are stained with crystal violet dye and observed with a light microscope; colony formation percentage is then calculated. A colony is formed at least by 50 cells.

	BQ9	*BQ10*	*BQ14*	*BQ15*	*BQ47*
50 µM	0%	23,53%	0%	10,39%	4,62%
20 µM	0%	40,00%	20,22%	20,78%	18,46%
10 µM	0%	34,12%	34,83%	48,05%	13,85%
5 µM	3,95%	50,59%	40,45%	46,75%	55,38%
2,5 µM	32,89%	58,82%	56,18%	64,94%	66,15%
0 µM (C)	100%	100%	100%	100%	100%

Tab. 3.4 Percentage of colonies formed after incubation with BQ9, BQ10, BQ14, BQ15 and BQ47 at various concentrations; C = control.

As we can see, every compound remarkably inhibits colony formation, in almost all cases in a dose-dependent mode: these results, therefore, confirm our previous data.

3.3 Cell death mechanism

Cell death mechanism is investigated with a flow cytometry test performed with the most active compounds: BQ9, BQ10, BQ14, BQ15 and BQ47.

It is very important to distinguish the mechanism that leads to cell death both to understand the mechanism of action and to predict some side effects; necrosis, for example, leads to an inflammatory reaction, but apoptosis does not: this could be an interesting property to evaluate for a potential therapeutic purpose.

To determine the mechanism that leads to cell death, we perform the Annexin-V/PI test, which uses FITC-conjugated Annexin-V to check the translocation of phosphatidylserine (PS) from the inner side of the plasma membrane to the outer layer, and propidium iodide (PI) to test the plasmatic membrane integrity: the exposure of PS, in fact, is one of the earlier events in apoptosis, but it occurs also during cell necrosis; the difference between these two forms of cell death is that during the initial stages of apoptosis the cell membrane remains intact, while at the very moment that necrosis occurs the cell membrane looses its integrity and becomes leaky [42].

This experiment is performed on Jurkat cells. After 24 hours from the incubation with two concentrations of each compound, most of the cells is in late apoptosis or in necrotic phase: cells, in fact, are positive to both FITC and PI fluorescence. A good percentage of cells treated with BQ47, nevertheless, is still in the early apoptotic phase: this can be explained with the lower cytotoxicity of this derivative, so cell death could be, in this case, less quick.
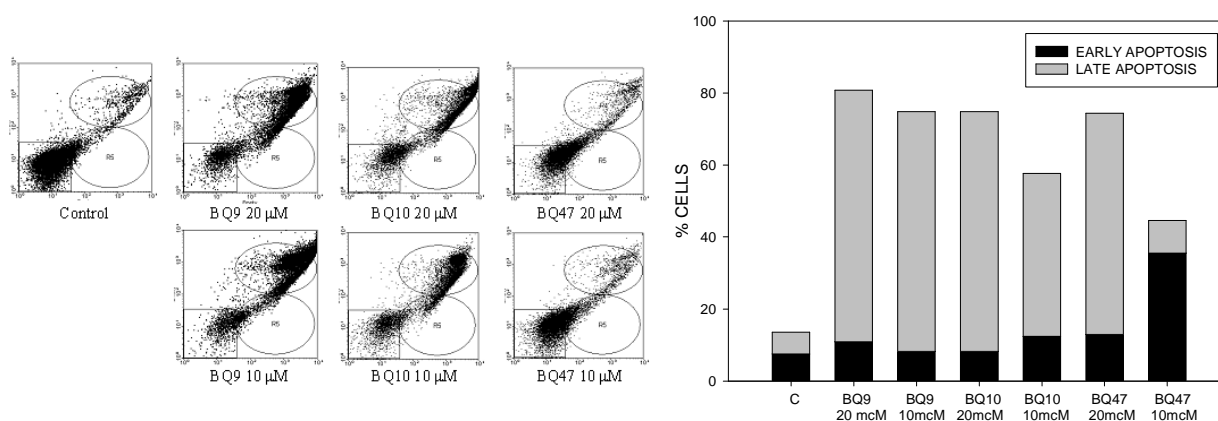
Fig. 3.1 Early and late apoptotic cells after 24 hours from incubation with BQ9, BQ10 and BQ47 20 μM and 10 μM; C = control.
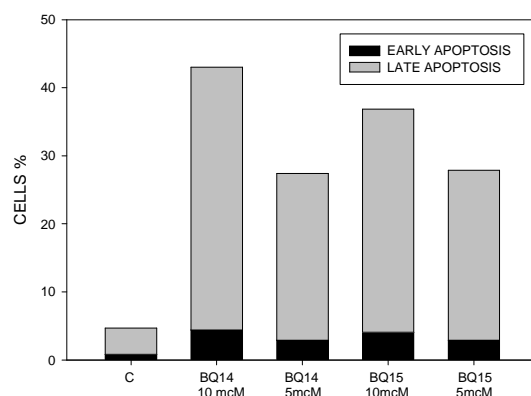
Fig. 3.2 Early and late apoptotic cells after 24 hours from incubation with BQ14 and BQ15 10 μM and 5 μM; C = control.

This test is reproduced after 6 hours to verify if apoptosis is the main cell death mechanism for these molecules. Reducing incubation period we can see more cells positive to FITC and negative to PI in comparison with the control (especially for BQ9, BQ10 and 20 μM BQ47): we can then hypothesize that cell death occurs by apoptosis, but this supposition will be further analysed.
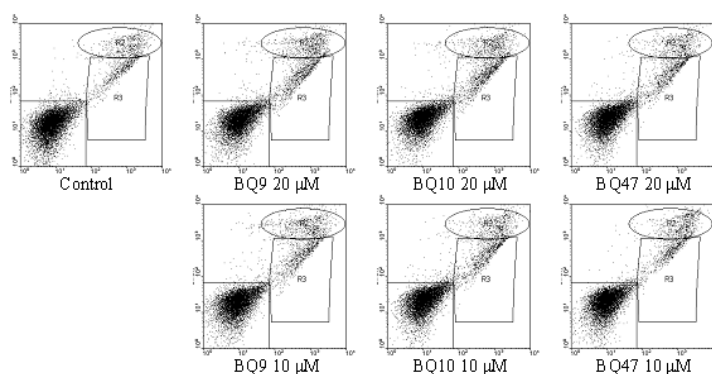
Fig. 3.3 Early and late apoptotic cells after 6 hours from incubation with BQ9, BQ10 and BQ47 20 μM and 10 μM; C = control.

3.4   <u>Involvement of mitochondria in cell death mechanism</u>

This feature is analysed to confirm the purposed cell death mechanism: mitochondria, in fact, have a key role in apoptosis and their involvement can be detected through some flow cytometric

_____

experiments which consider mitochondrial membrane potential and reactive oxygen species (ROS) production.

3.4.1 <u>Determination of mitochondrial membrane potential</u>

The collapse in mitochondrial membrane potential ($\Delta\Psi$) is one of the early events, if not the cause, of apoptosis [43]. Intracellular energy produced by the mitochondrial respiratory chain is stored as an electrochemical gradient consisting of a transmembrane electrical potential ($\Delta\Psi$) of 180 to 200 mV (negative inside). This energy drives the synthesis of ATP. It is possible to detect variations in $\Delta\Psi$ at the single-cell or single-organelle level using the lipophilic cation JC-1 [44].

As described in Materials and methods section, the JC-1 dye undergoes a reversible change in fluorescence emission from green to greenish orange as $\Delta\Psi$ increases: therefore, cells with high $\Delta\Psi$ form JC-1 aggregates and fluoresce orange, those with low $\Delta\Psi$ contain monomeric JC-1 and fluoresce green [45].

This assay is performed with Jurkat cells after 6 and 24 hours of incubation with the most active molecules and results are summarized in the following graphic.
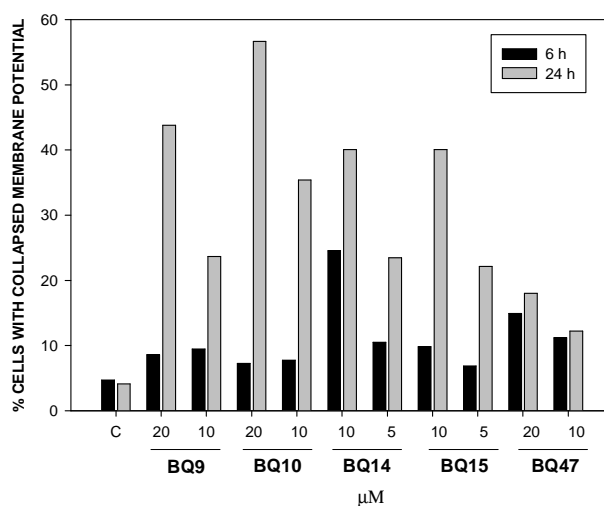
Fig. 3.4 Evaluation of mitochondrial membrane potential $\Delta\Psi$ after 6 and 24 hours of incubation with BQ9, BQ10, BQ14, BQ15 and BQ47; C = control.

In fig. 3.4 we can observe a significant dose-dependent depolarisation of mitochondrial membrane, feature that increases with treatment period, so we can hypothesize mitochondria involvement in cell death process.

3.4.2 <u>Determination of reactive oxygen species (ROS) production</u>

During apoptosis, mitochondria are subject to particular damages that compromise their activity, and ROS production is both the cause and the consequence of these injuries. The one-electron reduction of molecular oxygen produces a relatively stable intermediate, the superoxide anion ($O_2^{\cdot-}$), which serves as the precursor of most ROS; the dismutation of superoxide anions by superoxide dismutases results in H_2O_2 production. Subsequent reaction of H_2O_2 and $O_2^{\cdot-}$ can generate the highly reactive hydroxyl radical ($OH^{\cdot}$) [46]. Reactive oxygen species are usually present in cells in low concentration, but their production is improved in case of mitochondrial damage and oxidative stress, or when defence mechanisms lack.

To detect ROS production we utilise two probes, hydroethidine (HE) to reveal superoxide anion and 2',7'-dichlorodihydrofluorescein-diacetate (DCFDA) to reveal hydrogen peroxide.

The cytofluorimetric assay is carried out after incubating for 24 hours Jurkat cells with the most active compounds at two concentrations.
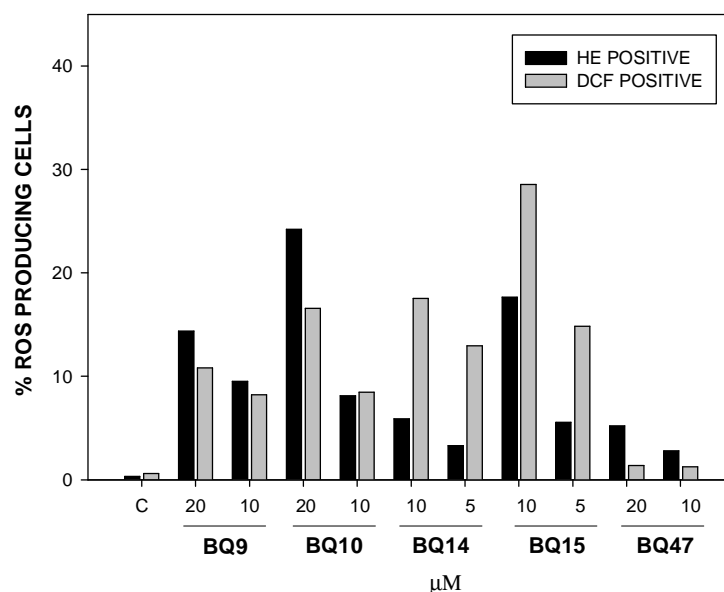
Fig. 3.5 Percentage of ROS producing cells after 24 hours incubation; C = control.

As we can see, ROS production is increased compared to control and it is a dose-dependent property: consequently, these results confirm the involvement of mitochondria in apoptosis process.

3.5 Involvement of lysosomes in cell death mechanism

Even lysosomes can take part in apoptosis process; their implication is detected with Acridine Orange (AO), which selectively enters lysosomes and forms aggregates which fluoresce red; if lysosomal membrane undergoes rupture, however, this probe migrates to cytosol and, in monomeric form, fluoresces green.

This analysis is led after incubating Jurkat cells for 6 and 24 hours; in the following graph, we can appreciate lysosomes involvement in apoptosis, especially after the longer exposure: this could suggest their secondary role in apoptosis evolution.
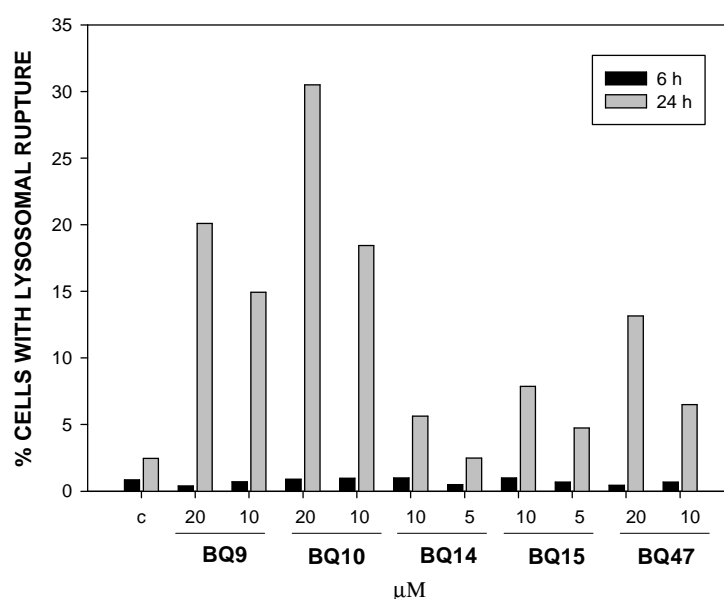
Fig. 3.6 Evaluation of lysosomal damage after 6 and 24 hours incubation; C = control.

3.6 Evaluation of EGFR inhibition

As seen before, pyrrolo[3,4-h]quinazolines were synthesized to identify new potential inhibitors of tyrosine kinase activity. Particularly, we evaluate their potential activity on EGFR.

To investigate whether these compounds could block EGF receptor signalling, we employ the human skin cancer cell line A-431, which overexpresses the EGFR.

After treating these cells with compounds for three hours, the blockage in EGFR signalling is detected by Western blotting using phospho-specific antibodies against the EGF receptor and the

downstream signalling molecules ERK1/2 and AKT. As a positive control, some cell samples are treated with a known EGFR inhibitor (AG1478).
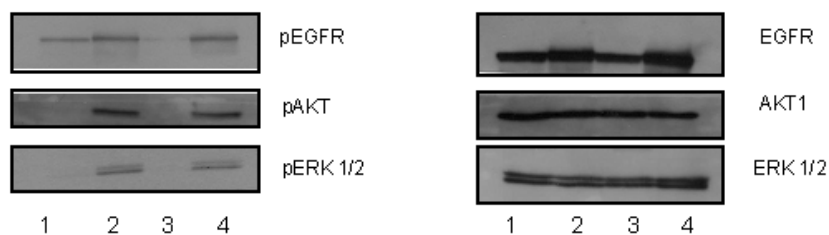
Fig. 3.7 Cells are serum-starved and either treated for 10 min with 100 ng/ml EGF after 3h of compound incubation. Cell lysates (100 μg) are separated by SDS-PAGE and the membrane probed with phospho-specific antibodies against the EGF receptor (P-Tyr1173) or AKT (Thr308) or ERK1/2 (P-Thr202/P-Tyr204). In addition, the membranes are probed with antibodies against total EGFR, AKT-1 and ERK 1/2. 1: control without EGF; 2: control + EGF; 3: AG1478 5 μM + EGF; 4: BQ9 20 μM + EGF.
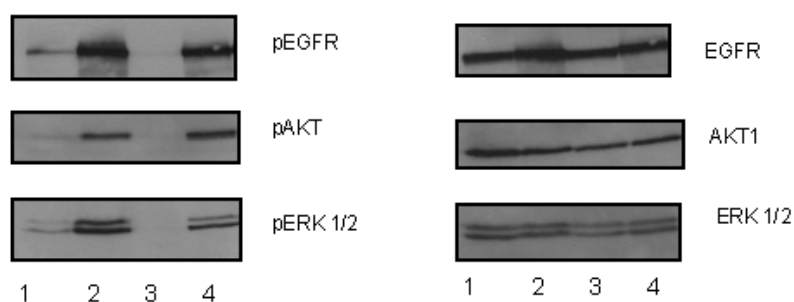
Fig. 3.8 Cells are serum-starved and either treated for 10 min with 100 ng/ml EGF after 3h of compound incubation. Cell lysates (100 μg) are separated by SDS-PAGE and the membrane probed with phospho-specific antibodies against the EGF receptor (P-Tyr1173) or AKT (Thr308) or ERK1/2 (P-Thr202/P-Tyr204). In addition, the membranes are probed with antibodies against total EGFR, AKT-1 and ERK 1/2. 1: control without EGF; 2: control + EGF; 3: AG1478 5 μM + EGF; 4: BQ10 20 μM + EGF.
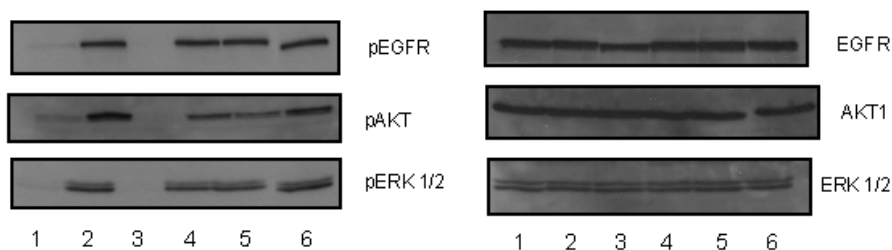
Fig. 3.9 Cells are serum-starved and either treated for 10 min with 100 ng/ml EGF after 3h of compound incubation. Cell lysates (100 μg) are separated by SDS-PAGE and the membrane probed with phospho-specific antibodies against the EGF receptor (P-Tyr1173) or AKT (Thr308) or ERK1/2 (P-Thr202/P-Tyr204). In addition, the membranes are probed with antibodies against total EGFR, AKT-1 and ERK 1/2. 1:

_____

control without EGF; 2: control + EGF; 3: AG1478 5 μM + EGF; 4: BQ42 20 μM + EGF; 5: BQ45 20 μM
+ EGF; 6: BQ48 20 μM + EGF.

As we can clearly observe in the upper and left western blot pictures, the analysed compounds are not able to inhibit the phosphorylation and the activity of EGFR upon EGF stimulation; moreover, the phosphorylation of the downstreaming protein ERK 1/2 and AKT is not also inhibited in the BQ treated cells. Consequently, we can hypothesize that EGFR is not the target for BQ compounds.

3.7   Evaluation of cell cycle

This assay is performed on Jurkat cells after 24 hours incubation to better understand the mechanism of action of BQ9, BQ10, BQ14, BQ15 and BQ47; with this flow cytometric test we can also draw some conclusions about cell death mechanism.

DNA contents are different in each phase of the cell cycle so, after fixation in ethanol, cells are stained with propidium iodide (PI) dye, which allows to perform rapid determinations of DNA per cell; then, we distribute cells according to their DNA contents and we obtain the following graphs.
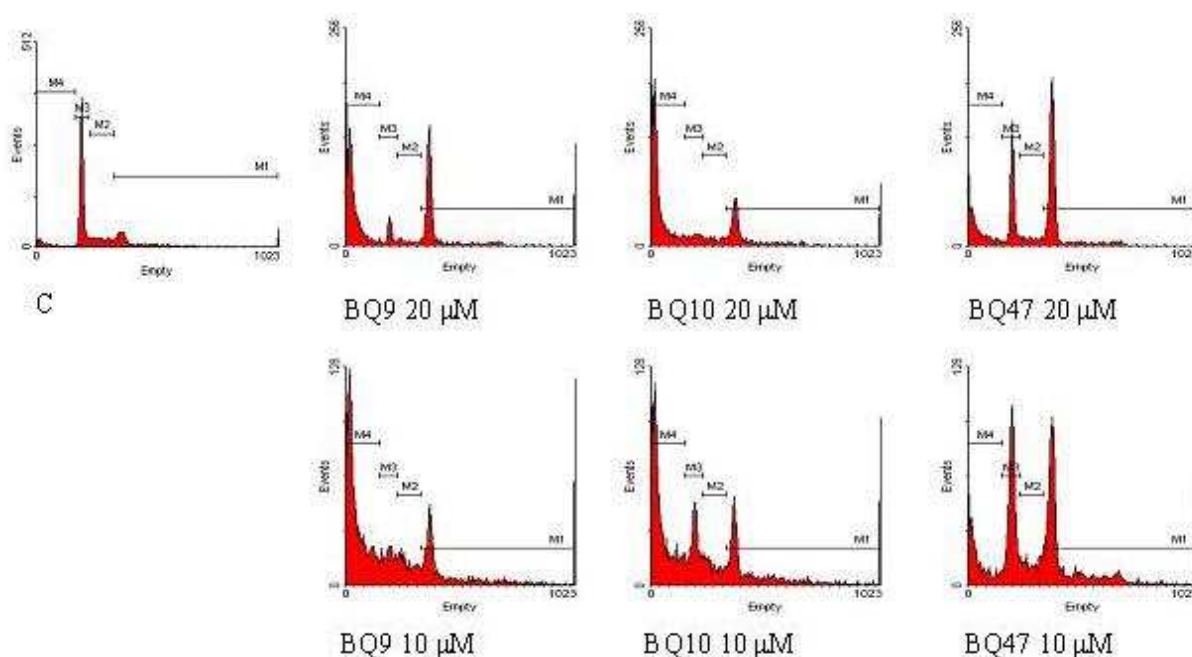
Fig. 3.10 DNA histograms of BQ9, BQ10 and BQ47 20 and 10 μM; C = control.

To better analyse cell cycle results, we can calculate cell percentages in each cell cycle phase:

	% G_1	% S	% G_2-M	% sub-G_1
Control	59,6	18,0	22,4	8,5
BQ9 20μM	12,8	8,4	78,8	55,4
BQ9 10μM	25,5	24,9	49,6	58,3
BQ10 20μM	18,9	17,1	64,0	62,8
BQ10 10μM	32,6	20,0	47,4	53,3
BQ14 10 μM	50,7	17,7	31,6	41,1
BQ14 5 μM	57,4	16,5	26,1	16,7
BQ15 10 μM	42,3	13,6	44,1	38,3
BQ15 5 μM	55,9	15,2	28,9	23,9
BQ47 20μM	27,4	7,9	64,7	23,3
BQ47 10μM	36,7	12,2	51,1	17,9

Tab. 3.5 Cell percentages in each cell cycle phase.

In comparison with control, we can notice deep changes in cell cycle profile: for every compound, in fact, cells in G_2/M phase increase considerably; we can also see a remarkable decrease in G_1 phase cells and the onset of a sub-G_1 peak, which is a consequence of the ordered degradation of DNA during cell death and represents apoptotic cells.

3.8   **Mitotic index**

Since cell cycle studies highlighted a block in G_2-M phase, we decided to reveal if the block occurs during G_2 phase or during mitosis.

In this assay, nuclei are stained with 4% Giemsa and observed with optical microscope: the amount of dispersed chromosomes in the cytoplasm and the disappearance of the nuclear membrane are a typical sign of mitotic metaphase.
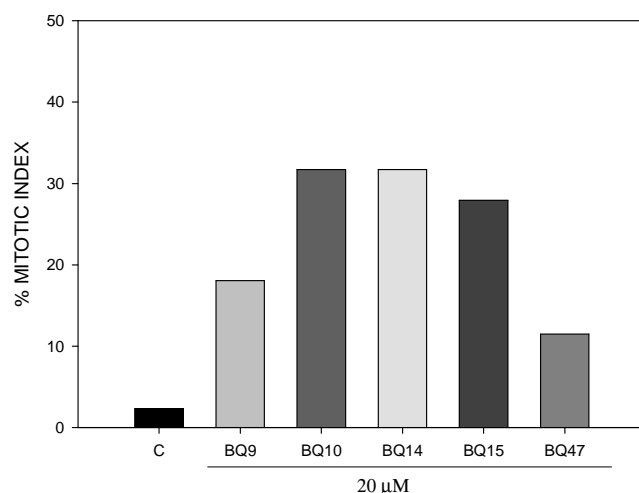
Fig. 3.11 Mitotic index in absence (C) or in presence of 20 µM BQ9, BQ10, BQ14, BQ15 and BQ47.

The most active BQ derivatives induce, at the concentration of 20 µM, a block in mitotic phase in treated Jurkat cells. BQ compounds could act as antimitotic drugs so further investigations will be performed to confirm their mechanism of action.

3.9   Evaluation of microtubule network as a possible target

Microtubules with actin and intermediate filaments constitute the cytoskeleton of all eukaryotic cells. They are directly involved in many cell functions, such as mitosis, intracellular movement, secretion, cell movement, and maintenance of cell shape. Microtubules are dynamic polymers made by the assembly of tubulin, a heterodimer consisting of α- and β-tubulin. Microtubule dynamics are involved in many microtubule dependent processes in cells, the most important being mitosis. During mitosis, the interphase microtubule network completely disassembles and a new assembly of microtubules occurs, leading to the mitotic spindle on which the chromosomes attach and segregate to the two spindle poles [47].

3.9.1 Microtubule network perturbation

Since the block of cell cycle in mitotic phase is a typical feature of microtubule-targeting drugs, we evaluated the perturbation of microtubule network induced by some BQ derivatives.

For this test, we observe treated cells by immunofluorescence microscopy. A panel of A-431 cells treated for 24 hours with the test compounds is treated with a β-tubulin antibody conjugated with the fluorophore FITC.

| CONTROL | BQ9 20 μM | BQ10 20 μM | BQ14 20 μM |

| BQ15 20 μM | BQ47 20 μM | Vinblastine 2 μM |
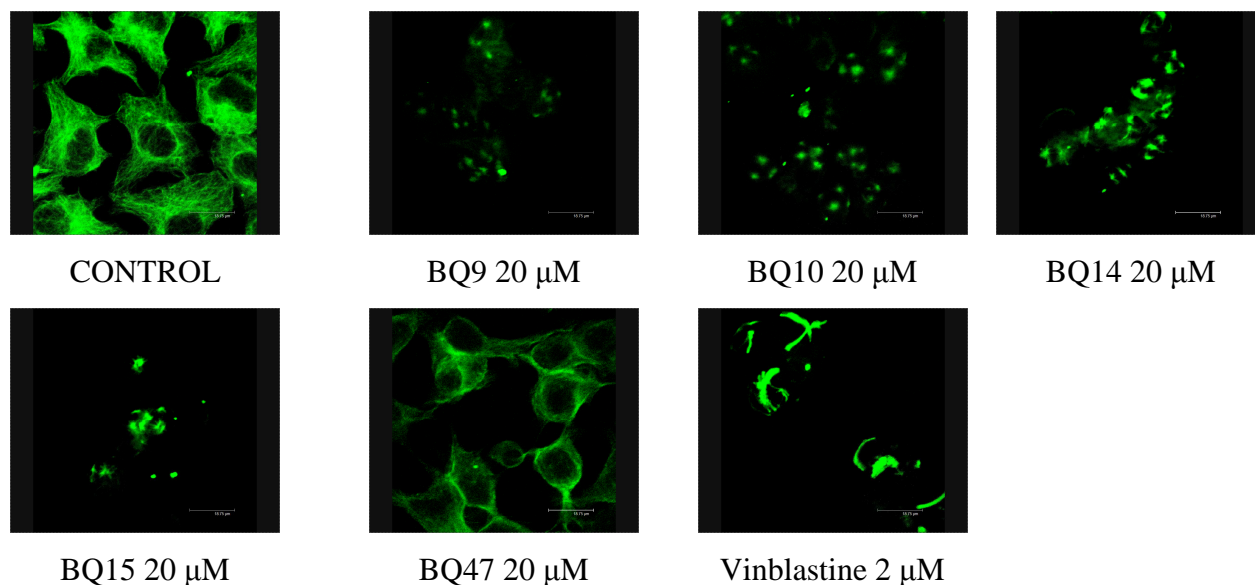
Fig. 3.12 Immunofluorescence images of A-431 cells treated with BQ9, BQ10, BQ14, BQ15 and BQ47 20 μM; control is represented by non-treated cells; as reference compound 2 μM vinblastine is used.

As shown in Fig 3.12, in control cells we can see normal organization and arrangement of tubulin network; on the contrary, BQ molecules disrupt microtubule cytoskeleton. Moreover, with the exception of BQ47, all compounds induce a clear modification in cell morphology with a "rounded-up" form, typical feature of cells with occurring microtubule disaggregation. These effects can be also observed in vinblastine treated cells (positive control).

3.9.2 <u>Effects on microtubule perturbation in vitro</u>

Since the immunofluorescence studies suggest that BQ compounds impair the formation or the stability of microtubule network, their effects on tubulin polymerisation in vitro are evaluated. Polymerisation is followed by fluorescent enhancement with the incorporation of a fluorescent reporter (DAPI) into the microtubules as polymerisation occurs: in fact, the fluorescence of this probe raises with microtubules formation.
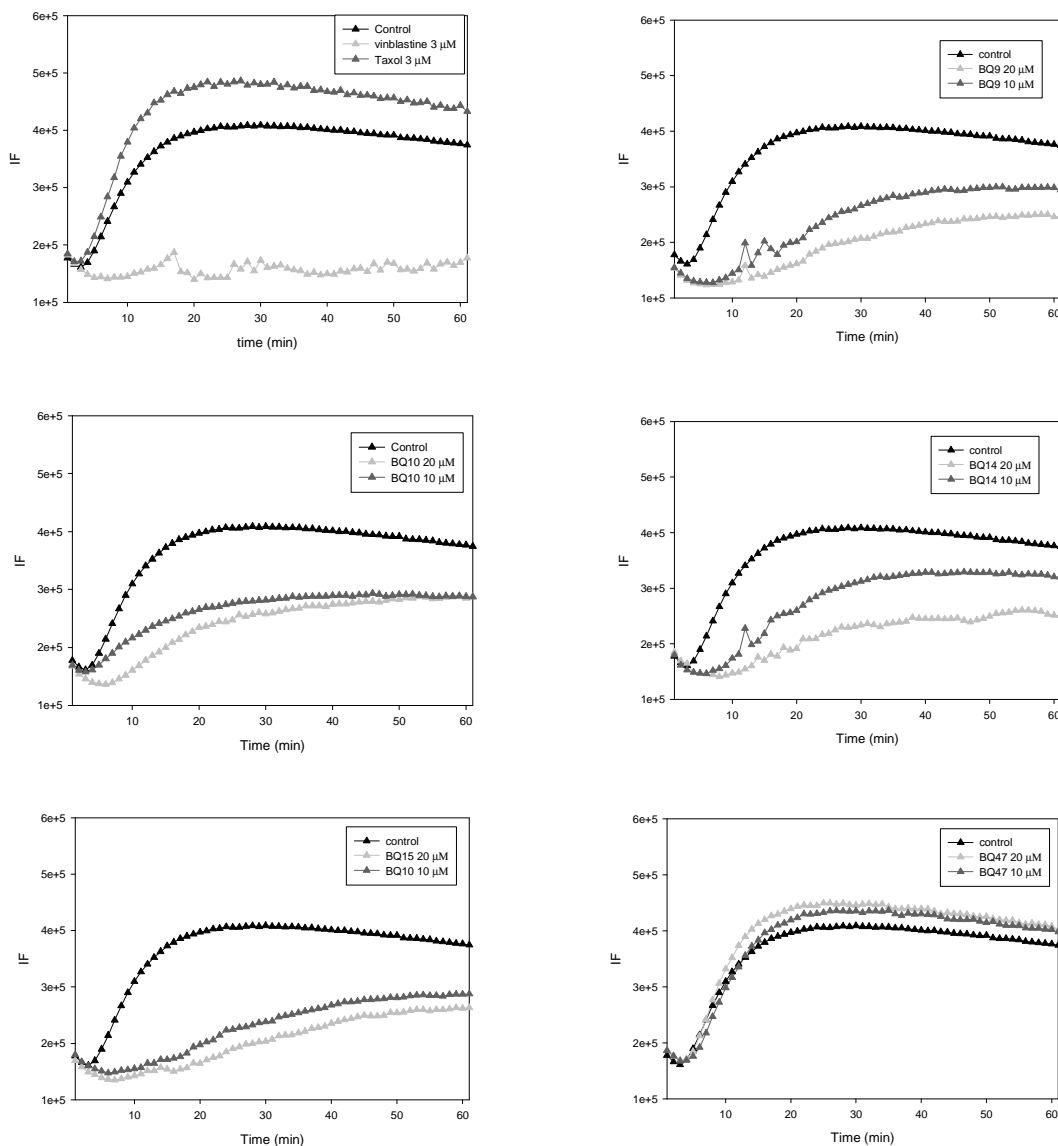
Fig. 3.13 Effect of vinblastine, taxol, BQ9, BQ10, BQ14, BQ15 and BQ47 on microtubule assembly.

In these graphs, at the beginning we can see a slow increase if fluorescence (nucleation phase), then an exponential growth and finally a steady state due to the dynamic structure of microtubules.

While in the control sample the fluorescence increases over time, when reaction is carried out in presence of vinblastine or taxol, we observe an inhibition or enhancement of tubulin polymerisation respectively. BQ compounds, with the exception of BQ47, reduce tubulin polymerisation in concentration-dependent manner: hence, these compounds show an antimitotic action.

3.10 <u>Evaluation of antivascular activity in vitro</u>

Since many antimitotic drugs (such as colchicine and combretastatin) can also have an effect on tumour immature and neo-formed vessel network, an antivascular effect is assessed performing some preliminary tests in vitro: thanks to their action on microtubules, in fact, many antimitotic compounds can disrupt cytoskeleton of the rapid-dividing tumour vessel endothelial cells, can affect their morphology leading to interferences of cell-to-cell junctional proteins, an increase in vascular permeability and a final blood collapse.

These preliminary assays are carried out on human umbilical vein endothelial cells (HUVECs). First of all, we study the effect of these molecules on cellular motility with a scratch test: HUVEC monolayers are scratched with a tip and, after different times of incubation with or without BQ, the width of the wound is measured.
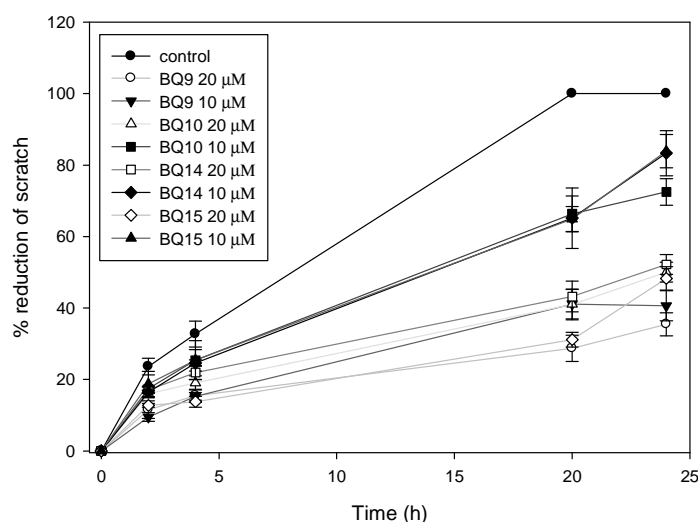
Fig. 3.14 Effect of BQ9, BQ10, BQ14, BQ15 and BQ47 on HUVECs motility; C = control.

All the compounds, at a concentration of 20 μM, inhibit the closure of the scratch in comparison to control (after 24 hours, the less active derivative BQ14 induces a closure only of the 40 %, while control is completely closed after 20 hours), so they can be considered active. Moreover BQ9 results very active at 10 μM too, while the other molecules reduce cell motility in a weaker way (after 24 hours, they induce a closure of 70-80 % of the scratch).
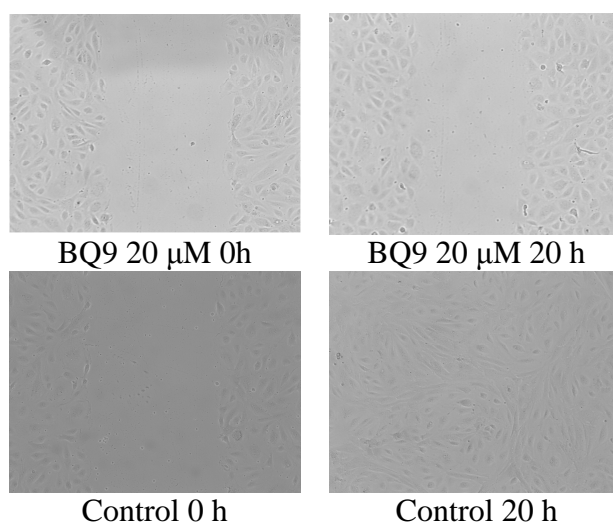
Fig. 3.15 Control and BQ9 20 μM treated HUVECs.

Then, the effect of BQ derivatives on vessel disruption is evaluated in vitro after growing HUVECs on Matrigel, which stimulates attachment, migration and differentiation of endothelial cells into tubule like structures [48]. After the formation of these capillary-like tubules, HUVECs are incubated with compounds at 20 μM concentration for 3 hours. Pictures of capillary network are taken after 3 hours of incubation and analysed by AngioJ plug-in of ImageJ software. Particularly, we consider 5 parameters that are associated with morphology of capillary network; results are presented in Figure 3.16; the pictures of control and of BQ9 treated cells are shown in Figure 3.17 as representative.
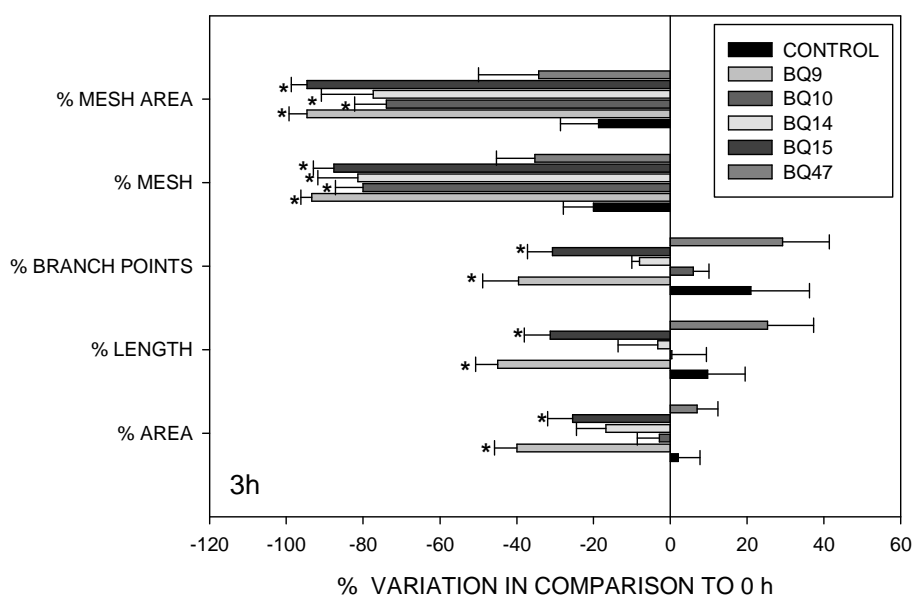
Fig. 3.16 Effects of BQ9, BQ10, BQ14, BQ15 and BQ47 on vessel disruption.

BQ9 20 μM 0h   BQ9 20 μM 3 h

Control 0 h   Control 3 h
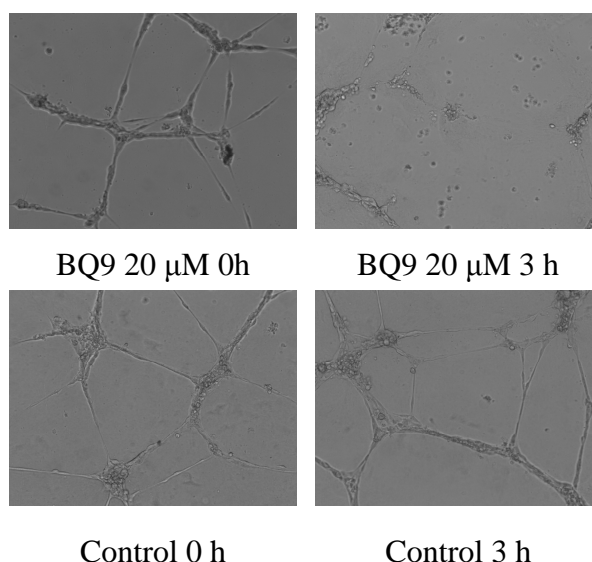
Fig. 3.17 HUVECs treated with BQ9 20 μM and control.

Quantitative image analysis shows that while BQ9 and BQ15 significantly decrease both dimensional (percent of area covered by HUVECs, total length per field and percent of area covered by meshes) and topological parameters (number of meshes per field, number of branching points) of the capillary-like network, BQ10 and BQ14 are mainly responsible for the decrease of the number of meshes and the percentage of their area. BQ47 is not able to induce significant changes in HUVECs morphology.

3.11 **Conclusions**

In this section 49 new pyrrolo[3,4-h]quinazoline derivatives were analysed.

These molecules were synthesised at Palermo University by the condensation of a pyrrolo ring to a quinazoline structure; this nucleus was then variously substituted at positions 2, 7, 8 and 9.

After observing BQ compounds chemical and physical properties, we evaluated their cytotoxic activity on a wide range of tumour cell lines; some molecules showed an interesting cytotoxicity, others were inactive at the employed concentrations.

Since the number of compounds was reasonable, we can make some structure-activity relationship considerations: among quinazoline derivatives unsubstituted at position 2, the most cytotoxic ones are substituted at positions 7 and 8 with lipophilic groups with a remarkable steric hindrance. Introducing a substitution at position 2, cytotoxicity does not increase; particularly, a carbonyl

group reduces cytotoxicity of some molecules or inactivates other derivatives. Instead, an amine group can remarkably increase cytotoxicity in Jurkat cells, but it does not lead to active compounds for others cell lines. Even an aniline group does not seem to increase the antiproliferative activity of these molecules.

BQ cytotoxic activity was then tested on a resistant tumour cell line, LoVo^{doxo}, and RI was calculated; many molecules maintain their cytotoxic effect on the resistant subclone and RI is next to 1: this could be really favourable because MDR is one of the most critical problems in chemotherapy.

This study analysed then the most active compounds among this series, BQ9, BQ10, BQ14, BQ15 and BQ47. These compounds induce cellular death through apoptosis, with a central role of mitochondria and lysosomes (involved later compared to mitochondria); this cell death mechanism is desirable because, unlike necrosis, it doesn't lead to an inflammatory response.

Then the possible mechanism of action was evaluated.

Because of their structural analogy with some EGFR inhibitors, we tested the most active compounds for this mechanism of action; nevertheless, they do not seem to be EGFR inhibitors, but further analysis will be carried out.

Moreover, in cell cycle study we can notice a block in G$_2$-M phase; further analysis demonstrated that the block occurs during mitosis. As antimitotic drugs induce a cell cycle block in G$_2$-M phase, we decided to verify a possible interference with microtubule network and we observed that BQ molecules disrupt microtubule cytoskeleton; moreover, with the exception of BQ47, all compounds induce a clear modification in cell morphology with a "rounded-up" form, typical feature of cells with occurring microtubule disaggregation. Furthermore, BQ compounds, with the exception of BQ47, reduce tubulin polymerisation in concentration-dependent manner: hence, these compounds show an antimitotic action.

Finally, we observed BQ antivascular activity in vitro with positive results: in fact these molecules can inhibit cell motility and disrupt a neo-formed HUVEC vessel network.

4. Pyrrolo[2,3-h]quinazolines

4.1 Physicochemical properties

Absorbance and emission spectra are determined in DMSO or in phosphate buffer and molar extinction coefficient (ε) is calculated; the results are listed in the following table.

Compounds	λ_{max} abs in DMSO (nm)	ε ($M^{-1}*cm^{-1}$) in DMSO	λ_{max} abs in phosphate buffer (nm)	λ_{max} emiss in DMSO (nm)
LCQ1	347	27300	351	471
LCQ2	349	34600	351	469
LCQ3	360	33600	358	439
LCQ4	362	28700	358	446
LCQ5	353	22700	350	385
LCQ6	349	23000	350	392
LCQ7	352	23800	350	387
LCQ8	361	27100	356	419
LCQ9	362	25700	362	417
LCQ10	363	26400	362	416
LCQ11	293	45700	284	420
LCQ12	293	46000	292	426
LCQ13	290	36500	384	426
LCQ14	292	32400	272	417
LCQ15	287	35700	295	418
LCQ16	336	13200	335	375
LCQ17	332	26400	333	410

Tab. 4.1 Spectrophotometric features of LCQ molecules.

All of these derivatives absorb in the UV range, essential feature for the further studies.

4.2 <u>Cytotoxic activity</u>

LCQ series is synthesised with the aim of obtaining new photochemotherapeutic agents; their cytotoxic effect is observed through MTT test in a panel of 5 human tumour cell lines: K-562 (chronic myeloid leukaemia), Jurkat (T-cell leukaemia), MCF-7 (breast adenocarcinoma), LoVo (colon adenocarcinoma) and A-431 (vulvar squamous cell carcinoma).

IC_{50} (μM)					
Compounds	*K-562*	*Jurkat*	*MCF-7*	*LoVo*	*A-431*
LCQ1	>20	>20	>20	>20	>20
LCQ2	>20	>20	>20	>20	>20
LCQ3	>20	6,0 ± 1,4	>20	>20	>20
LCQ4	>20	8,4 ± 1,2	>20	>20	>20
LCQ5	>20	>20	>20	>20	>20
LCQ6	>20	>20	>20	>20	>20
LCQ7	>20	>20	>20	>20	>20
LCQ8	>20	>20	>20	4,2 ± 0,8	>20
LCQ9	>20	14,0 ± 1,3	>20.	14,2 ± 0,2	>20
LCQ10	>20	>20	>20.	>20	>20
LCQ11	>20	12,0 ± 1,5	>20	14,7 ± 0,5	9,3 ± 1,2
LCQ12	>20	4,8 ± 0,8	>20	>20	5,0 ± 0,4
LCQ13	>20	>20	>20	>20	9,6 ± 0,4
LCQ14	13,1 ± 1,1	2,9 ± 0,5	>20	>20	1,4 ± 0,1
LCQ15	>20	>20	>20	>20	>20
LCQ16	>20	>20	>20	>20	>20
LCQ17	>20	>20	>20	>20	>20

Tab. 4.2 Antiproliferative activity of LCQ series (μM).

Many compounds have no effect on cell proliferation at the employed concentrations, others are active only in Jurkat cell line; LCQ14 is the only compound which demonstrates a quite good antiproliferative activity, with IC$_{50}$ values lower than 5 µM against both Jurkat and A-431 cell lines. As LCQ series seems to be almost inactive as antiproliferative line, we decided to test its photocytotoxicity: in fact, pyrrolo[2,3-h]quinazolines are also heteroanalogues of angelicin and they could be photoactivable compounds.

4.3 <u>Photostability</u>

As pyrrolo[2,3-h]quinazolines absorb in the UV range, we observe their photostability after UVA irradiation.

When irradiated in solution, furocoumarins undergo photolysis [49]. Thus, absorption spectra of 20 µM derivatives in DMSO are recorded after increasing doses of UVA: these spectra give information about the photostability of these molecules and about the formation of other species as a consequence of irradiation.
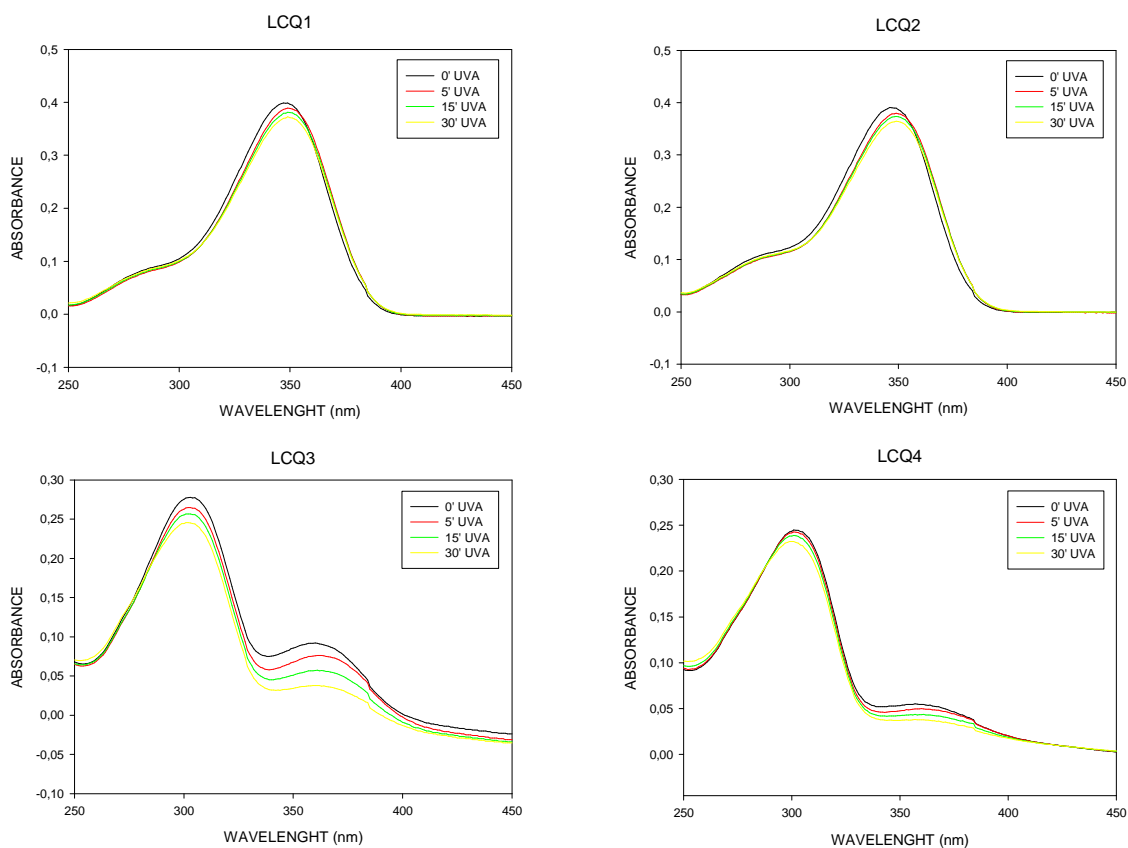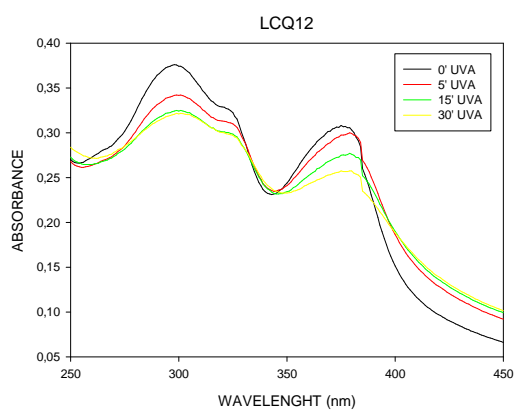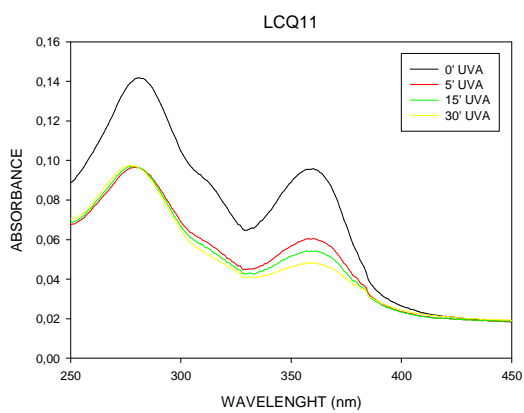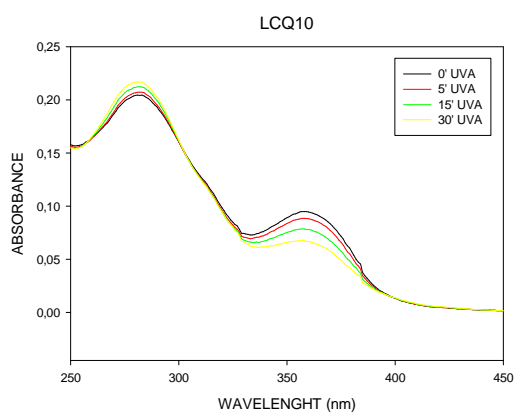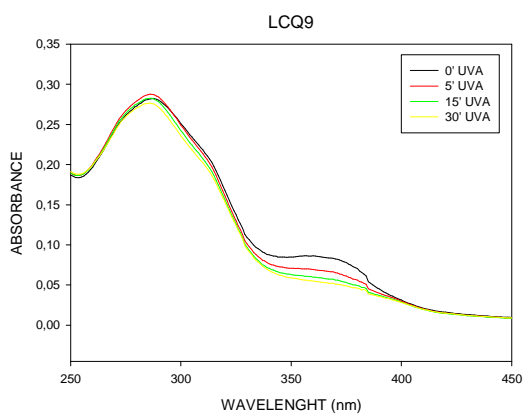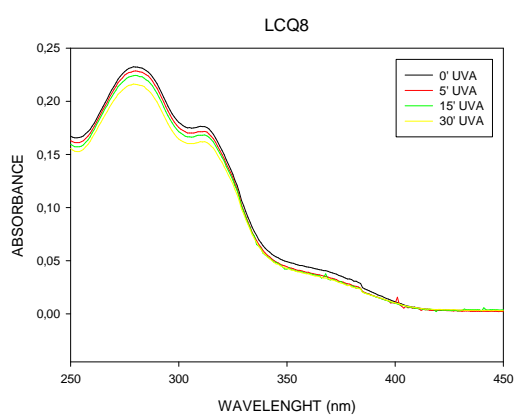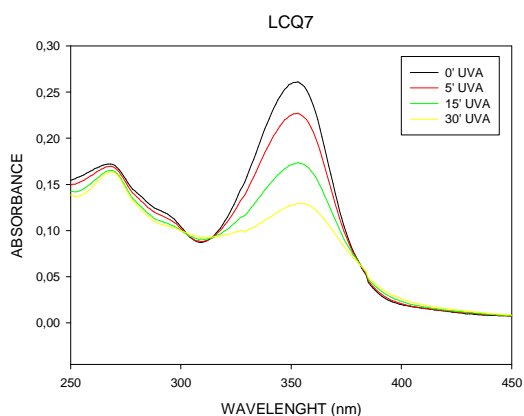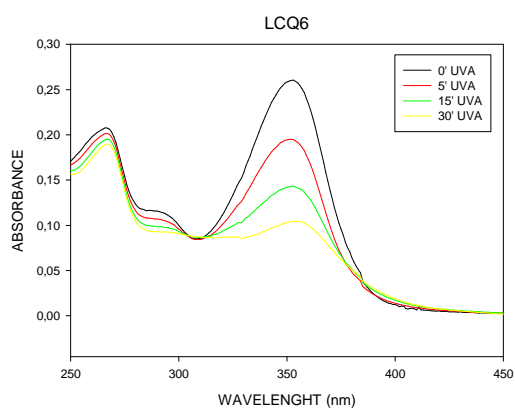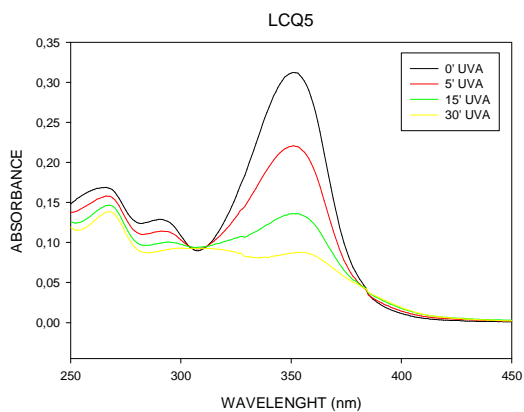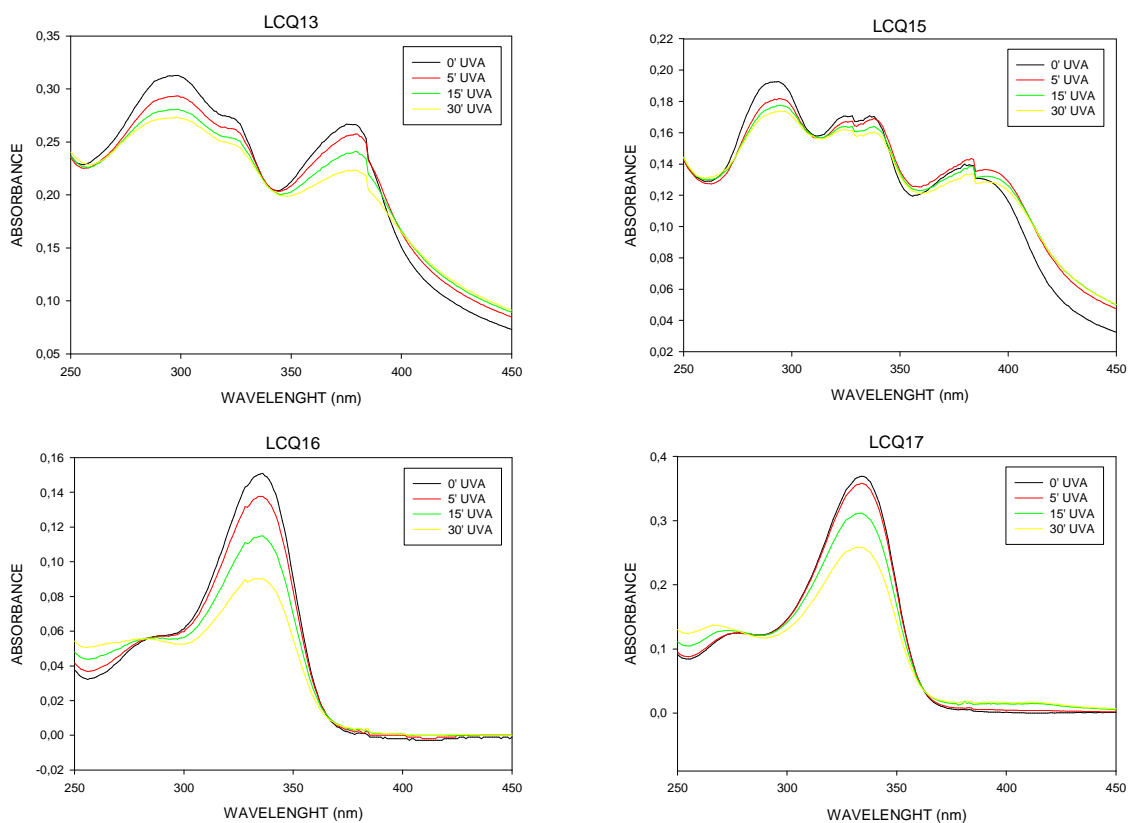
Fig. 4.1 Photodegradation of pyrrolo[2,3-h]quinazolines.

As we can see in fig. 4.1, pyrroloquinazolines undergo photolysis after UVA irradiation. In most cases, we can find simple reduction of maximum absorbance; moreover, in some spectra we observe the presence of isosbestic points that indicate the equilibrium in solution between the two species, the non-degraded compound and a photoproduct.

4.4 <u>Photocytotoxicity</u>

As pyrroloquinazolines absorb in the UV range and demonstrated to undergo photolysis after UVA irradiation, we analyse their antiproliferative effect after the irradiation of a panel of 4 human tumour cell lines (Jurkat, K-562, LoVo and A-431) in the presence of different concentrations of test compounds. Two UVA doses are used: 2,5 and 3,75 J/cm^2, corresponding to 10 and 15 irradiation minutes, respectively. For photocytotoxicity experiments, cells are incubated with compounds for 30 minutes prior to irradiation with Wood's lamps (emitting principally at 365 nm); cellular survival is checked by MTT test after 72 hours from irradiation.

IC$_{50}$ (μM)				
Compounds	**K-562**		**Jurkat**	
	2,5 J/cm^2	**3,75 J/cm^2**	**2,5 J/cm^2**	**3,75 J/cm^2**
LCQ1	>20	>20	>20	>20
LCQ2	>20	13,69 ± 1,09	>20	>20
LCQ3	5,70 ± 0,76	4,38 ± 0,44	4,85 ± 0,53	3,47 ± 0,11
LCQ4	7,96 ± 1,46	2,92 ± 0,42	2,05 ± 0,62	1,08 ± 0,25
LCQ5	>20	>20	>20	8,42 ± 1,49
LCQ6	1,44 ± 0,12	0,72 ± 0,28	0,65 ± 0,13	0,39 ± 0,05
LCQ7	1,71 ± 0,17	0,53 ± 0,09	0,43 ± 0,08	0,28 ± 0,08
LCQ8	2,38 ± 0,70	1,16 ± 0,20	0,83 ± 0,16	0,46 ± 0,09
LCQ9	0,74 ± 0,13	0,48 ± 0,08	0,43 ± 0,08	0,21 ± 0,06
LCQ10	0,75 ± 0,18	0,41 ± 0,05	0,29 ± 0,02	0,23 ± 0,01
LCQ11	3,51 ± 0,80	1,82 ± 0,39	0,83 ± 0,08	0,55 ± 0,09
LCQ12	3,90 ± 0,70	2,85 ± 0,20	0,81 ± 0,07	0,52 ± 0,11
LCQ13	4,06 ± 0,60	2,16 ± 0,28	2,05 ± 0,12	0,68 ± 0,09
LCQ14	>20	>20	>20	8,53 ± 1,53
LCQ15	2,63 ± 0,36	1,88 ± 0,35	0,70 ± 0,11	0,50 ± 0,05
LCQ16	>20	>20	>20	>20
LCQ17	>20	>20	>20	>20

Tab. 4.3 Photocytotoxicity in some human leukaemia cell lines after UVA irradiation.

IC$_{50}$ (μM)				
Compounds	**LoVo**		**A-431**	
	2,5 J/cm^2	**3,75 J/cm^2**	**2,5 J/cm^2**	**3,75 J/cm^2**
LCQ1	>20	>20	>20	>20
LCQ2	>20	>20	>20	>20
LCQ3	9,72 ± 1,32	6,76 ± 0,57	9,72 ± 1,32	6,76 ± 0,57
LCQ4	3,07 ± 0,35	2,30 ± 0,24	3,07 ± 0,35	2,30 ± 0,24
LCQ5	>20	>20	>20	>20
LCQ6	0,85 ± 0,19	0,54 ± 0,09	0,85 ± 0,19	0,54 ± 0,09
LCQ7	1,12 ± 0,23	0,59 ± 0,18	1,12 ± 0,23	0,59 ± 0,18

LCQ8	$1,57 \pm 0,12$	$1,02 \pm 0,09$	$1,57 \pm 0,12$	$1,02 \pm 0,09$
LCQ9	$0,56 \pm 0,07$	$0,44 \pm 0,04$	$0,56 \pm 0,07$	$0,44 \pm 0,04$
LCQ10	$0,47 \pm 0,07$	$0,34 \pm 0,03$	$0,47 \pm 0,07$	$0,34 \pm 0,03$
LCQ11	$0,82 \pm 0,14$	$0,55 \pm 0,08$	$0,82 \pm 0,14$	$0,55 \pm 0,08$
LCQ12	$2,31 \pm 0,17$	$0,95 \pm 0,09$	$2,31 \pm 0,17$	$0,95 \pm 0,09$
LCQ13	$2,80 \pm 0,29$	$1,43 \pm 0,15$	$2,80 \pm 0,29$	$1,43 \pm 0,15$
LCQ14	$15,21 \pm 1,97$	$9,61 \pm 1,32$	$15,21 \pm 1,97$	$9,61 \pm 1,32$
LCQ15	$0,88 \pm 0,11$	$0,48 \pm 0,11$	$0,88 \pm 0,11$	$0,48 \pm 0,11$
LCQ16	>20	>20	>20	>20
LCQ17	>20	>20	>20	>20

Tab. 4.4 Photocytotoxicity in some human solid tumour cell lines after UVA irradiation.

Almost all compounds reveal dose-dependent IC_{50} values after UVA irradiation; the most active compounds are LCQ9 and LCQ10, with sub-micromolar IC_{50} results.

Given the considerable number of compounds tested, we can formulate some hypotheses regarding the structure-activity relationships.

Pyrrolo[3,2-h]quinazolines are variably substituted at positions 2, 8 and 9. The substitution at position 2 seems to play a key role in the induction of phototoxicity: in fact, the antiproliferative effect is maximum with an amino group and decreases progressively with an aniline group, a carbonyl group and without substituent. At position 9, the increase in steric hindrance (p-methoxybenzyl ≈ benzyl > methyl) improves the phototoxicity, as the introduction of an ethoxycarbonyl moiety at position 8, which even leads to active compounds.

4.4.1 <u>Photocytotoxicity in the presence of scavengers</u>

In this assay, we test the antiproliferative activity of LCQ9 and LCQ10, the most photocytotoxic compounds of this series, in the presence of some scavengers, which should exert their defensive action over treated LoVo cells.

In this test, we use three different scavengers: DMTU (1,3-dimethyl-2-thiourea), which protects cells by the formation of hydroxyl radical, DABCO (1,4-diazabicyclo[2.2.2]octane), which prevents the formation of singlet oxygen, and BHA (butylhydroxyanisole), which prevents the formation of alkyl radicals.

We carry out this test with one UVA dose (2,5 J/cm^2, corresponding to 10 minutes) and one compound concentration (0,5 μM); photocytotoxicity is evaluated after 72 hours with MTT test. Results are expressed as IC$_{50}$.

	LCQ9	*LCQ10*
No scavengers	64,53 ± 6,19	49,83 ± 5,20
+ DMTU	85,90 ± 3,72	57,58 ± 3,26
+ DABCO	64,32 ± 3,09	43,52 ± 1,19
+ BHA	66,75 ± 6,46	48,71 ± 2,05

Tab. 4.5 IC$_{50}$ values in presence of scavengers.

These results highlight the protective effect of DMTU on the treated cells; instead, the other scavengers do not seem to prevent radical formation: therefore, we can hypothesise that LCQ9 and LCQ10 act through the formation of hydroxyl radical.

4.5 <u>Evaluation of cell cycle</u>

Cell cycle studies are performed in the dark with the most cytotoxic compound LCQ14. In this study there is no evidence of cell death because no changes are detected for cells treated; particularly, there is not the onset of the characteristic apoptotic peak (sub-G$_1$). These results suggest the hypothesis that pyrrolo[2,3-h]quinazolines are cytostatic compounds.

4.6 <u>Cell death mechanism</u>

Cell death mechanism is investigated with the most active compounds by a flow cytometry test.
At first, we performed this test with LCQ14, the most cytotoxic derivative on Jurkat cell line, and results were adequate to the previous ones: in fact, there is no evidence of cell death because there is no increase in the percentage of cells showing exposure of phosphatidylserine nor in the number

of cells with augmented permeability to propidium iodide. The hypothesis that pyrrolo[2,3-h]quinazolines are cytostatic but not cytotoxic molecules in the dark is confirmed.

Then, we carried out this test with the two most phototoxic compounds, LCQ9 and LCQ10, at the concentration of 1 or 2 µM, 24 and 3 hours after irradiation (2,5 J/cm^2).
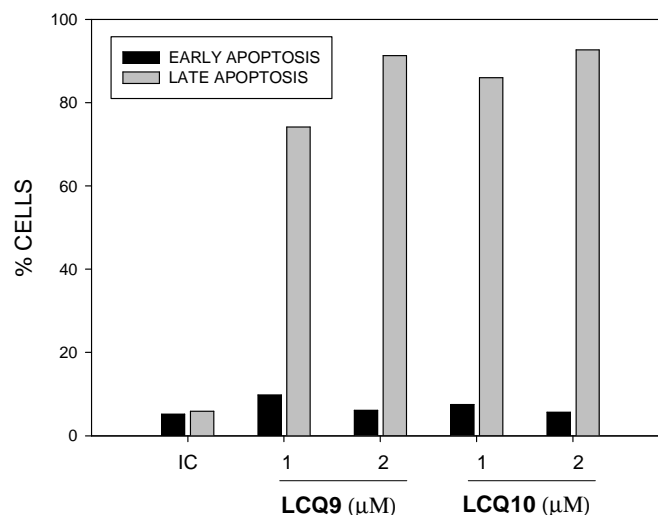
Fig. 4.2 Early and late apoptotic cells 24 hours after irradiation (2,5 J/cm^2); cells are incubated with LCQ9 and LCQ10 2 and 1 µM; IC = irradiated control.

After 24 hours, most cells are in late apoptotic phase, so we monitor cell death after a shorter incubation time.
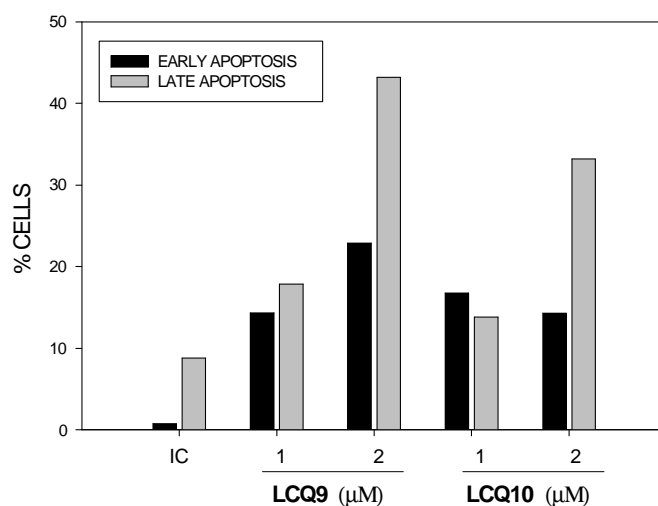
Fig. 4.3 Early and late apoptotic cells 3 hours after irradiation (2,5 J/cm^2); cells are incubated with LCQ9 and LCQ10 2 and 1 µM; IC = irradiated control.

After 3 hours from irradiation, an increase in early apoptotic cells is detected in a dose-dependent manner relative to control; a small percentage of necrotic cells is also detected, but the primary mechanism of cell death seems to be apoptosis.

4.7   Involvement of mitochondria in cell death mechanism

Psoralens and UVA are known to induce cell death by apoptosis with the involvement of mitochondria. Thus, we decided to perform some assays to evaluate a possible role of mitochondria in LCQ photoinduced apoptosis.

4.7.1 Determination of mitochondrial membrane potential

This test is performed with JC-1 dye after 3 hours irradiation; the mitochondrial membrane potential is monitored by the fluorescence of this probe. Results are summarised in the following graphic.
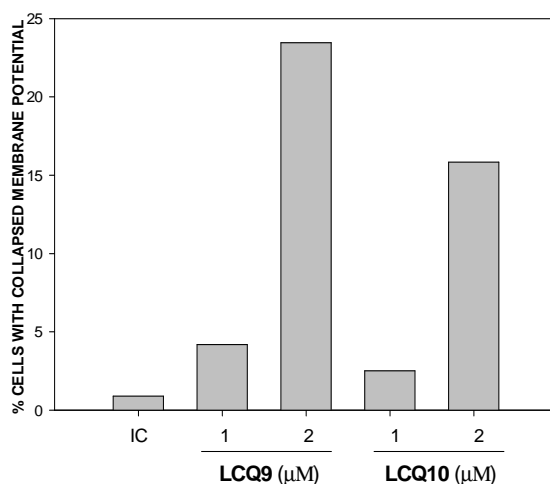
Fig. 4.4 Cells percentage with loss of mitochondrial membrane potential 3 hours after irradiation (2,5 J/cm^2) of cells treated with LCQ9 and LCQ10 2 and 1 µM; IC = irradiated control.

Irradiated Jurkat cells (2,5 J/cm^2), in the presence of LCQ9 and LCQ10 2 and 1 µM, undergo a depolarisation of mitochondrial membrane, with a dose-dependent shift in fluorescence respect to control, so we can hypothesise mitochondrial involvement in cell death process.

4.7.2 <u>Determination of ROS production</u>

ROS production is examined by flow cytometry 6 hours after irradiation of Jurkat cells in the presence of LCQ9 and LCQ10 2 and 1 μM.
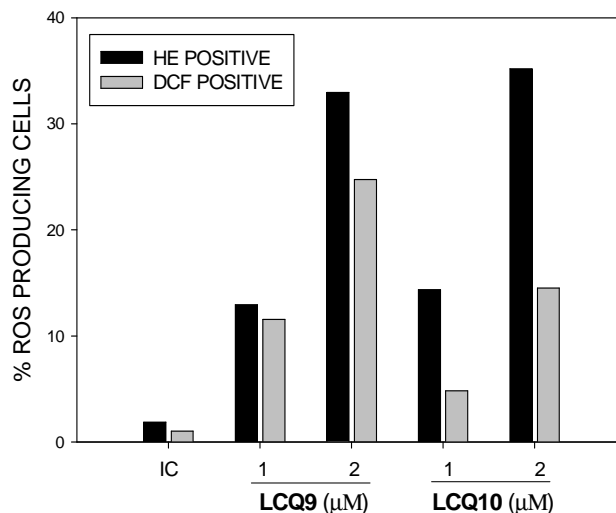
Fig. 4.5 Percentage of ROS production 6 hours after irradiation (2,5 J/cm^2) and treatment with LCQ9 and LCQ10 2 and 1 μM; IC = irradiated control.

As we can see, ROS production is increased compared to control and it is a dose-dependent property: consequently, these results confirm the involvement of mitochondria in apoptosis process.

4.8 <u>Involvement of lysosomes in cell death mechanism</u>

To investigate the integrity of lysosomes after UVA irradiation (2,5 J/cm^2) in the presence of LCQ9 and LCQ10, this flow cytometric analysis is performed with acridine orange dye; the percentage of Jurkat cells with intact lysosomes is evaluated by assaying red fluorescence after AO staining.

As we can see in the following graph, a significant extent of lysosomal damage is photo-induced by LCQ9 and LCQ10 3 hours after irradiation, so we can hypothesise lysosomal involvement in cell death mechanism.
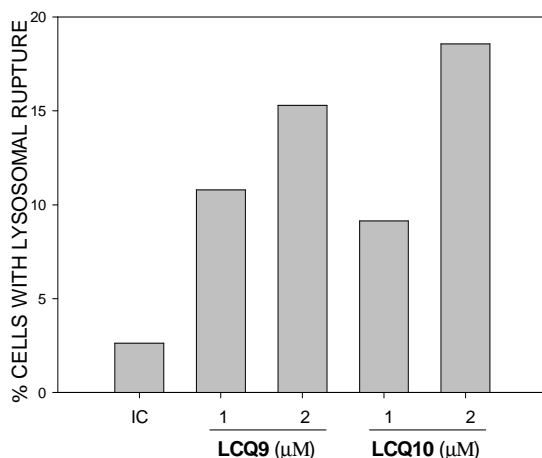
Fig.4.6 Cells percentage with lysosomal damage 3 hours after irradiation (2,5 J/cm^2) in the presence of LCQ9 and LCQ10 2 and 1 μM; IC = irradiated control.

4.9 <u>Photoreaction with the main biomolecules: lipid peroxidation</u>

This test is performed to reveal any possible photodamage against lipids 24 hours after the irradiation of Jurkat cells in the presence of LCQ9 and LCQ10. This assay involves the reaction of one molecule of malondialdehyde (MDA), which is a secondary product of lipid peroxidation, with two molecules of thiobarbituric acid (TBA): the formation of the reaction product, a pink complex, is monitored by fluorescence. This test is performed on the supernatant medium.
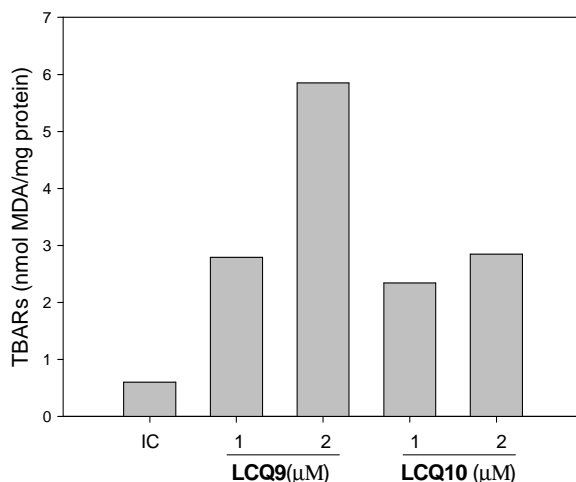
Fig. 4.7 Lipid peroxidation induced by LCQ9 and LCQ10 2 and 1 μM 24 hours after irradiation (2,5 J/cm^2); IC = irradiated control.

In this graphic, a significant dose-dependent production of thiobarbituric acid reactive substances (TBARs) is observed.

4.10 <u>Conclusions</u>

LCQ series is composed by 17 pyrrolo[2,3-h]quinazolines synthesised at Palermo University by the condensation of a pyrrolo ring to a quinazoline structure; this nucleus was then variously substituted at positions 2, 8 and 9.

Some of these derivatives inhibit cell proliferation in vitro, even in the absence of UVA irradiation, but their antiproliferative effect is very limited; furthermore, after flow cytometric analysis, cytotoxic activity can be excluded, because there is no increase in cell death in treated samples relative to control cells, but cytostatic activity could explain the decrease in cellular metabolic activity observed by MTT tests.

Pyrrolo[3,2-h]quinazolines absorb in the UV and UVA range; many of these derivatives undergo photolysis, as evidenced by monitoring changes in their structure after UVA irradiation. Most derivatives show remarkable photocytotoxicity in many human tumour cell lines, reaching IC_{50} values in the low micromolar and sub-micromolar range. The most phototoxic compounds, LCQ9 and LCQ10, bear an amino group, an ethoxycarbonyl moiety and a substituent of steric bulk at positions 2, 8 and 9, respectively.

Pyrrolo[3,2-h]quinazolines induce significant cell death by apoptosis at only 3 hours after UVA irradiation, as detected by Annexin V/PI test. We also carried out some experiments to determine that two organelles, mitochondria and lysosomes, are heavily involved in inducing cell death: in fact, we demonstrated the collapse in mitochondrial membrane potential, the production of ROS and the disruption of lysosomal integrity induced by the most active compounds.

Finally, the lipid peroxidation induced by pyrrolo[3,2-h]quinazolines could explain their phototoxic activity.

Although we have identified a very interesting class of new derivatives with high phototoxicity, further studies are required to identify the initial signals and downstream events involved in the activation of apoptosis and to reveal the mechanism of action.

5. Pyrazolo[3,4-h]quinolines

5.1 Physicochemical properties

As pyrazoloquinolines are new compounds, their physicochemical properties are determined. Absorbance and emission spectra are determined in DMSO or in phosphate buffer and molar extinction coefficient (ε) is calculated.

Compounds	λ_{max} abs in DMSO (nm)	ε ($M^{-1}*cm^{-1}$) in DMSO	λ_{max} abs in phosphate buffer (nm)	λ_{max} emiss in DMSO (nm)
PZQ1	402, 267	15856	383, 262	429
PZQ2	401, 268	33255	384	429
PZQ3	402, 272	29730	381	432
PZQ4	401, 268	30532	382	428
PZQ5	401, 265	21690	383	431
PZQ6	402, 265	24988	380	429
PZQ7	403, 263	32686	412	437
PZQ8	403, 263	34073	414	435
PZQ9	403, 263	32057	384	439
PZQ10	404, 262	29176	383	438
PZQ11	403, 263	31815	384	437
PZQ12	402, 262	30079	384	533
PZQ13	404, 264	31358	383	444
PZQ14	405, 264	32825	388	449
PZQ15	405, 262	29620	384	445
PZQ16	342, 268	35660	338, 262	382
PZQ17	342, 262	35657	364	385
PZQ18	342, 262	37471	343	386

PZQ19	338, 262	36739	349	380
PZQ20	338, 262	23660	355	379
PZQ21	338, 263	23655	357	384
PZQ22	342, 262	40331	364	397
PZQ23	393, 262	38908	373, 262	434
PZQ24	396, 262	20530	358	417
PZQ25	396, 262	36168	380	434
PZQ26	396, 262	41061	379	437
PZQ27	336, 262	46288	341	395
PZQ28	337, 262	49615	337, 273	390
PZQ29	369, 280	30094	397	443
PZQ30	373, 280	65204	414, 301	463
PZQ31	371, 281	47623	379, 279	426
PZQ32	379, 279	44061	379, 279	442
PZQ33	347, 264	40785	358, 268	422
PZQ34	344, 262	42862	354, 262	434
PZQ35	403	2865	378	427
PZQ36	406	39003	410	436
PZQ37	338	106096	359	425
PZQ38	344	32075	361	420
Ang	306	14602	305	413

Tab. 5.1 Spectrophotometric properties of PZQ series.

PZQ compounds absorb in UV range; these molecules exhibit a batochromic shift compared to angelicin (λ_{max} = 305 nm), selected as reference compound: this could be explained with the conjugation with substituents in position 3 and 7.

5.2 <u>Photostability</u>

As pyrrolo[2,3-h]quinazolines absorb in the UV range, we observe their photostability after UVA irradiation. The absorption spectra of 20 µM derivatives in DMSO are recorded after increasing doses of UVA: these spectra give information about the photostability of these molecules and about the formation of other species as a consequence of irradiation.
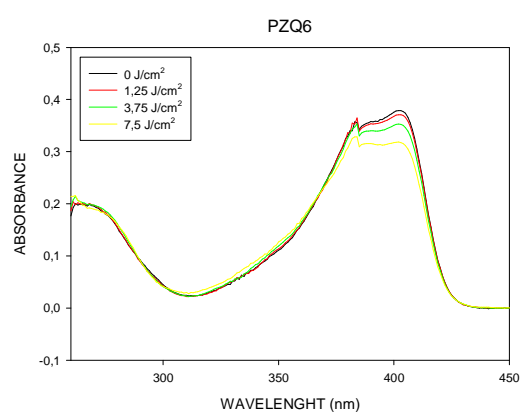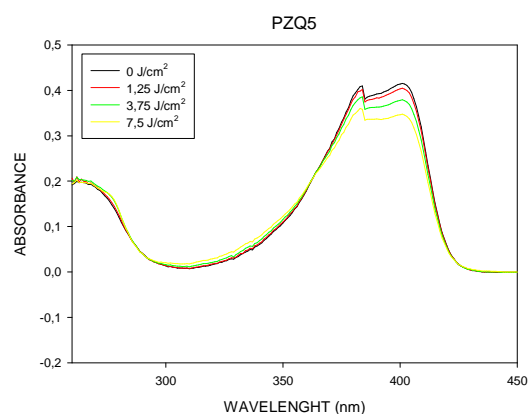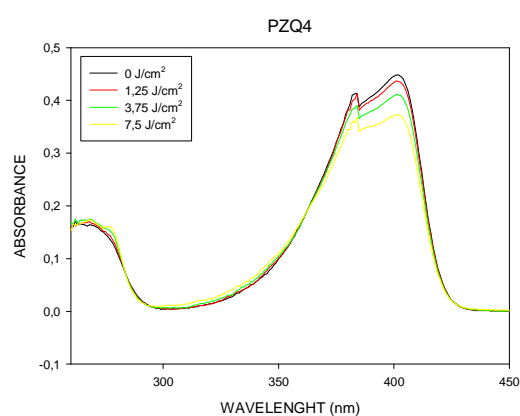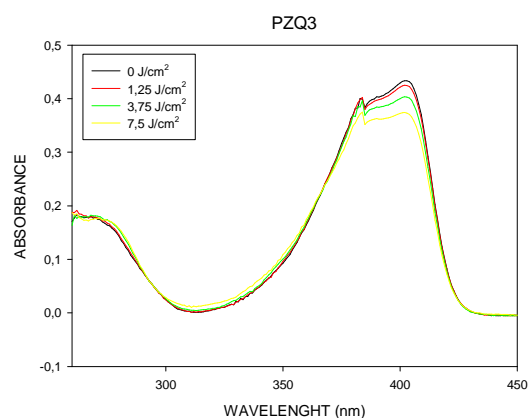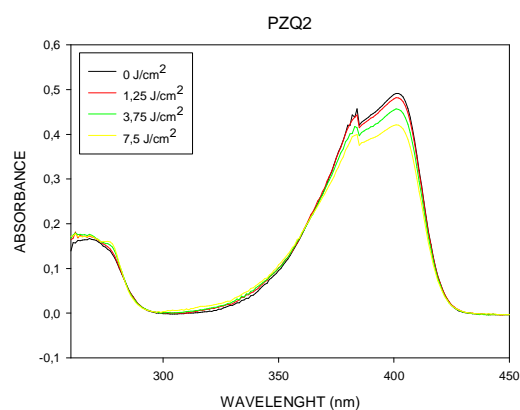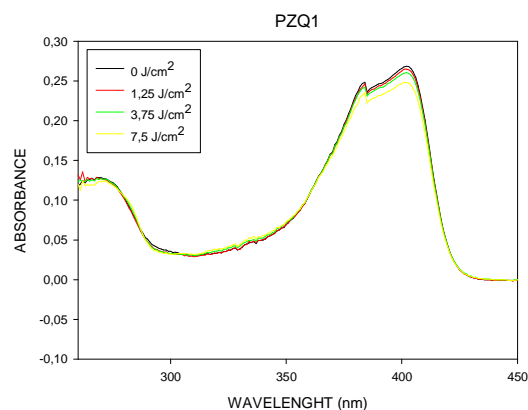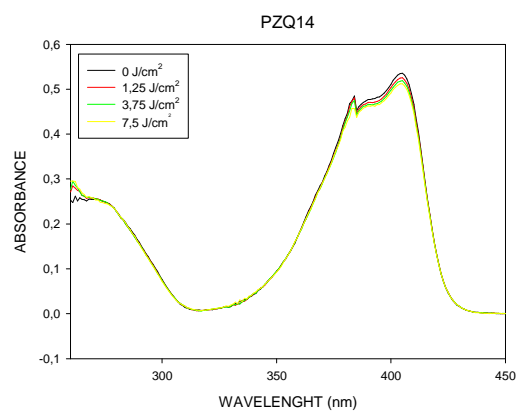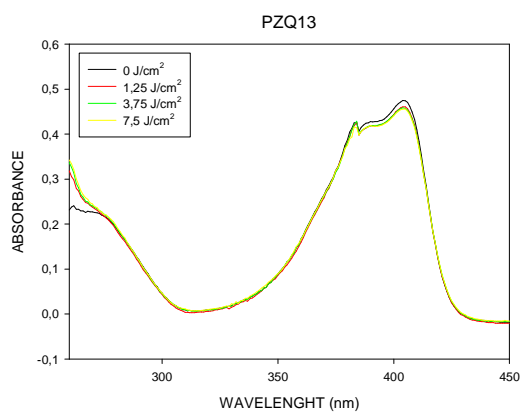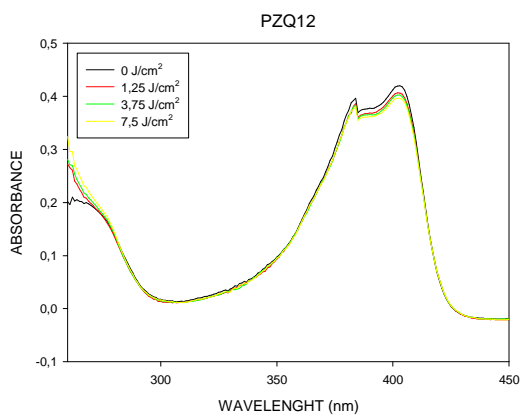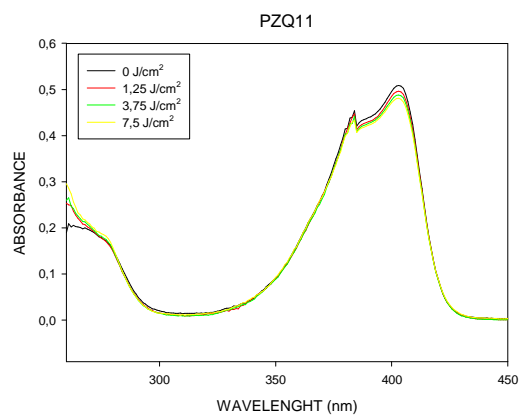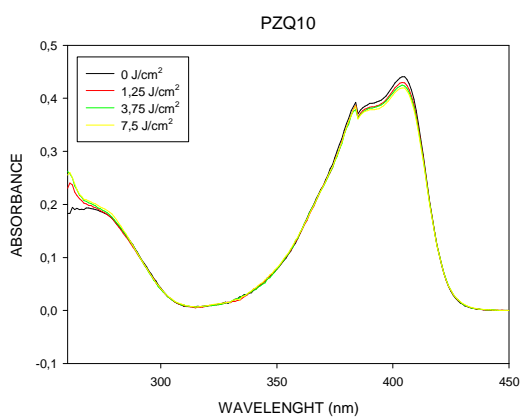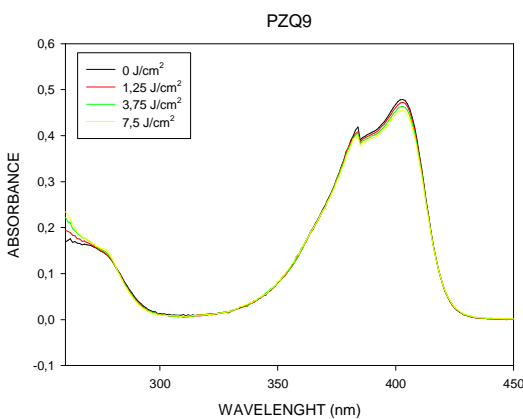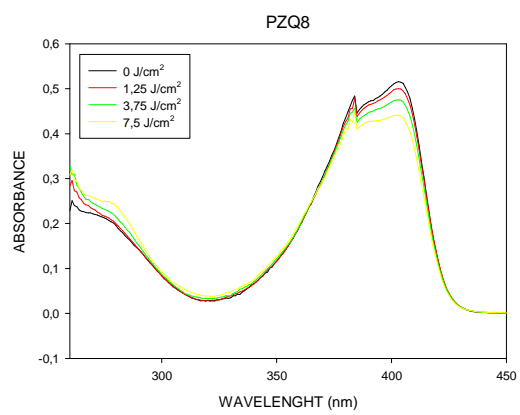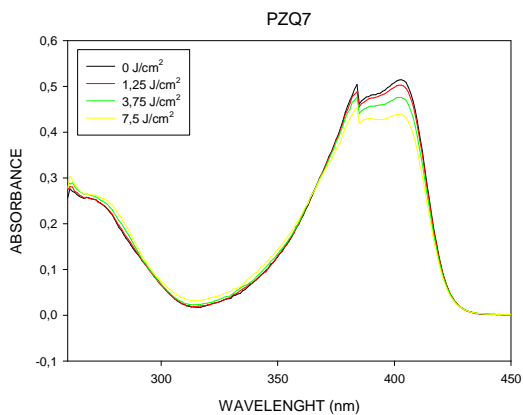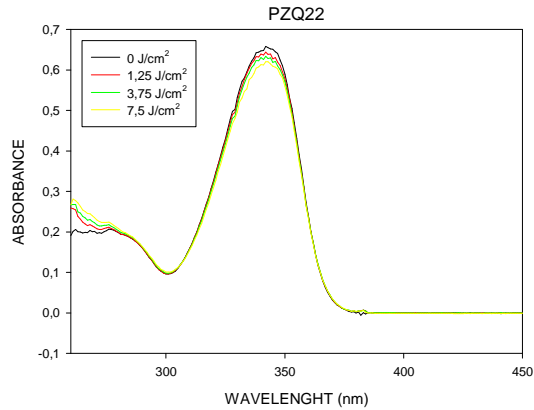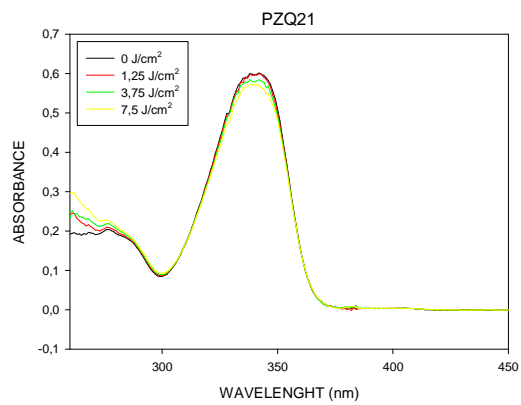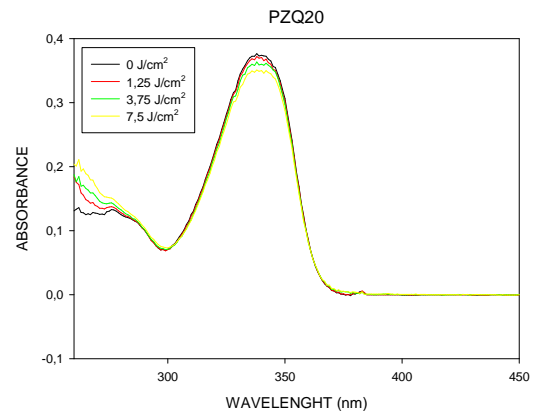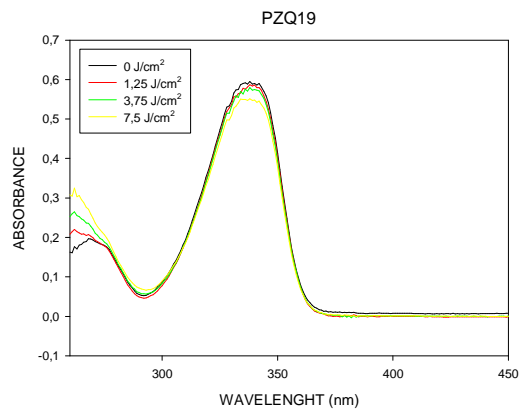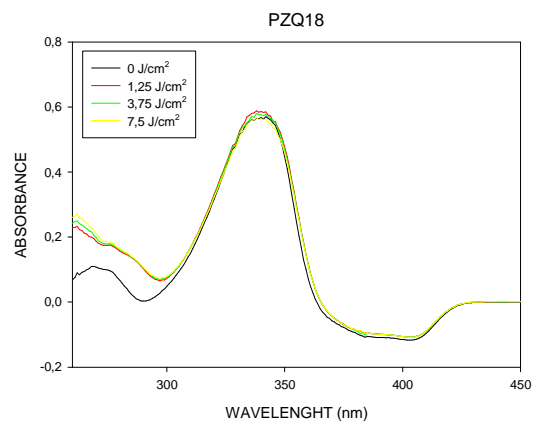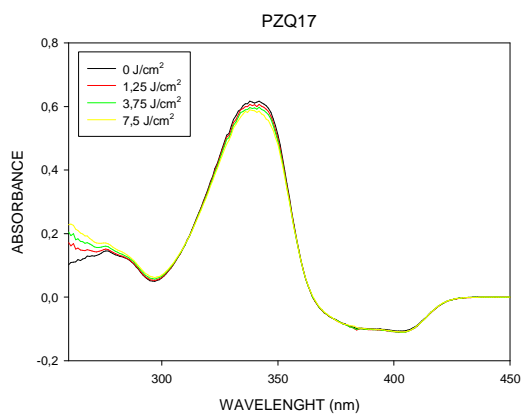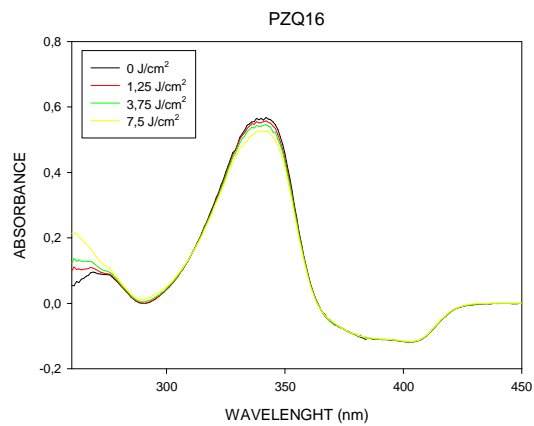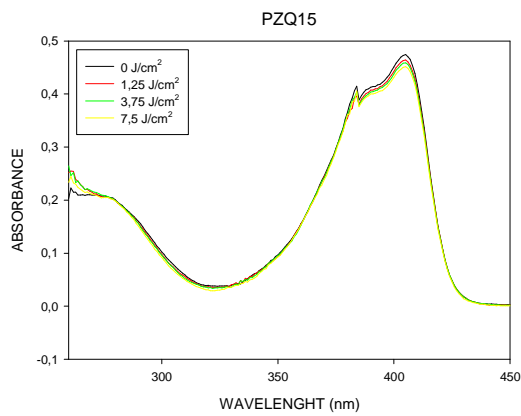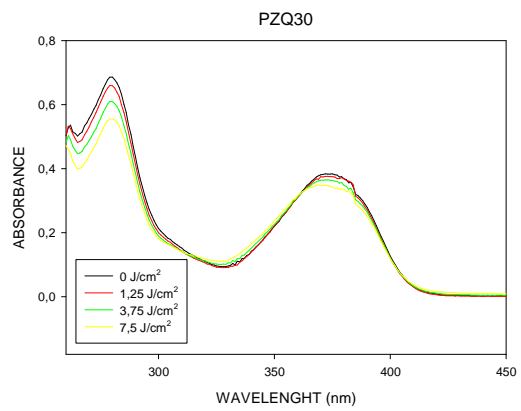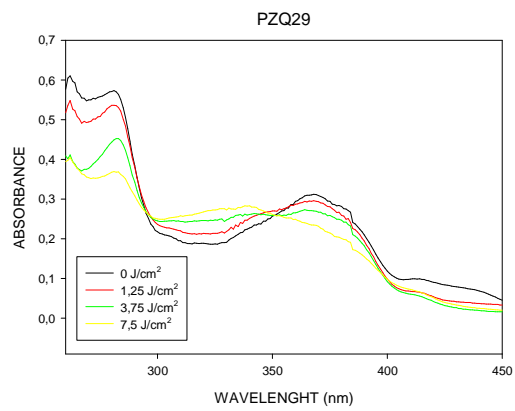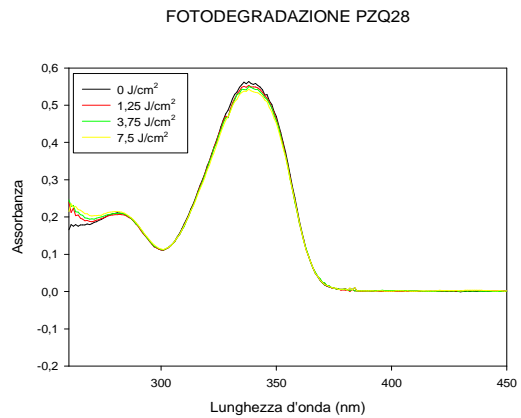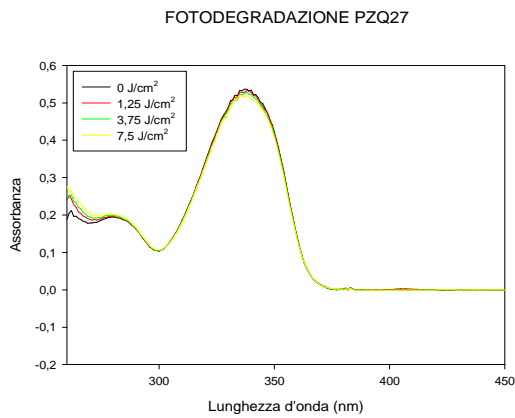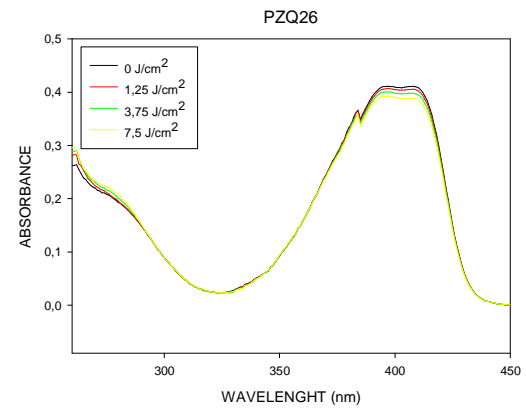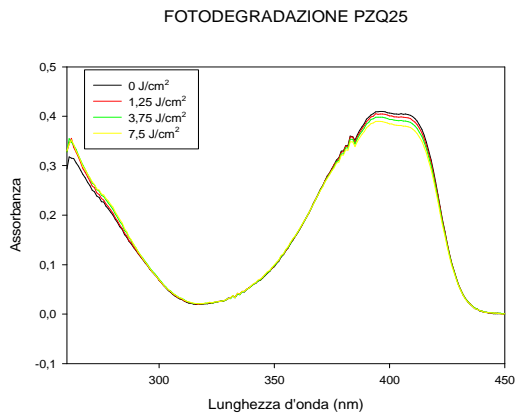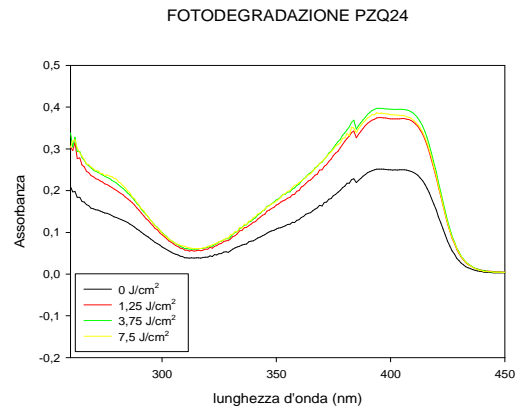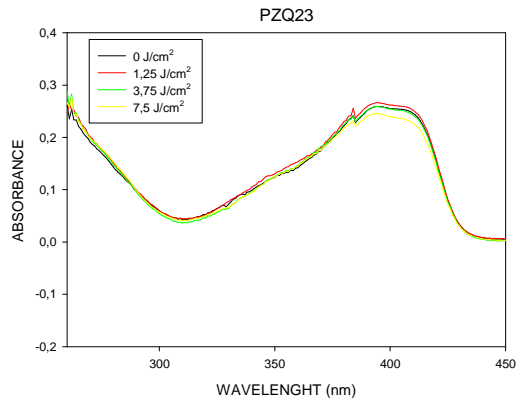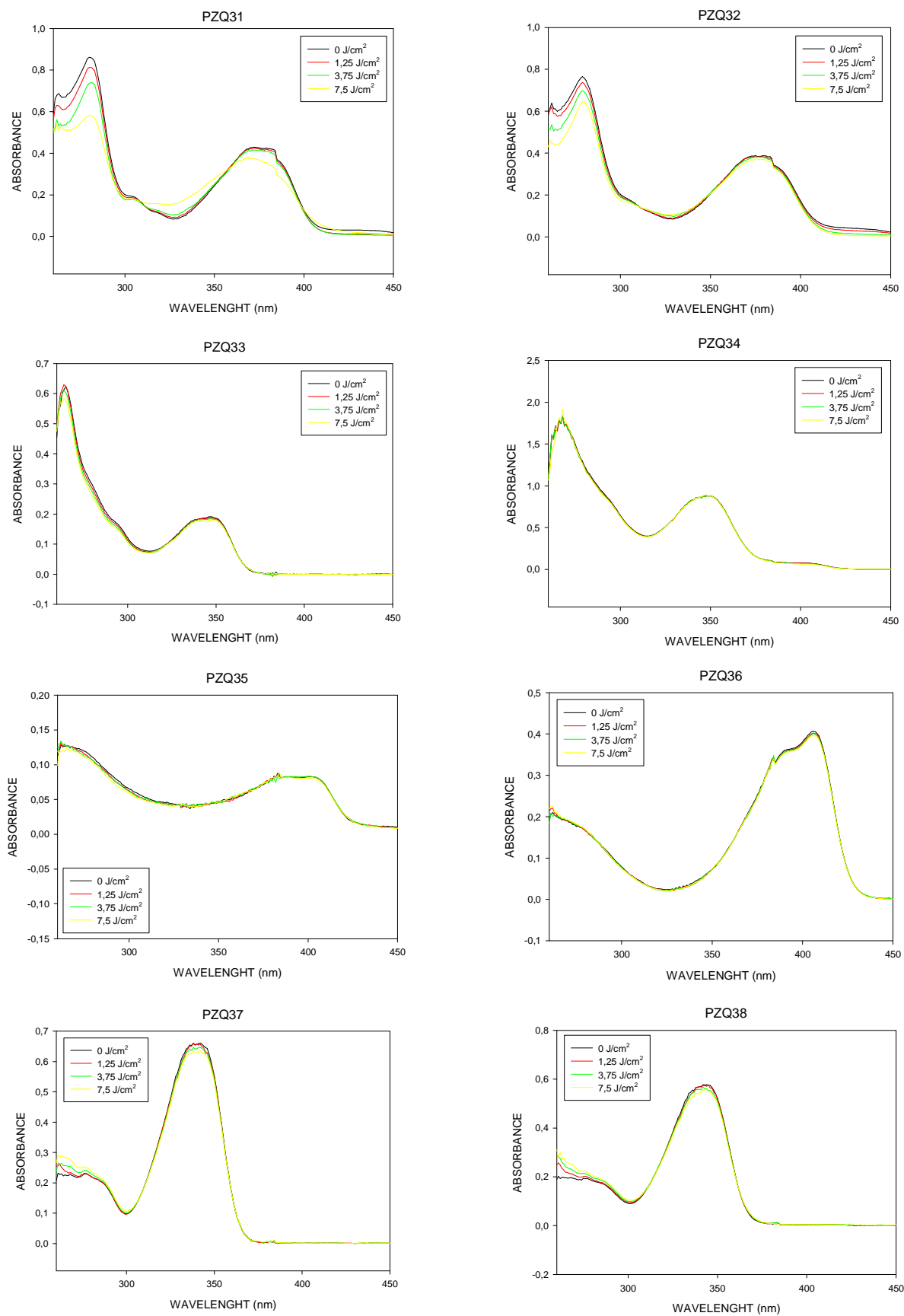
Fig. 5.1 Photodegradation of pyrazolo[3,4-h]quinolines.

Most of these molecules does not undergo photolysis; for those which degrade, furthermore, we detect a weak reduction of the maximum peak and the presence of one or more isosbestic points that reveal the presence of photoproduct(s) in equilibrium with the non-degraded molecule.

5.3 <u>Antiproliferative activity</u>

PZQ series is synthesised to obtain new photochemotherapeutic agents; their cytotoxic effect is observed through MTT test in a panel of 7 human tumour cell lines, K-562 (chronic myeloid leukaemia), Jurkat (T-cell leukaemia), HL-60 (promyelocytic leukaemia), A-431 (vulvar squamous cell carcinoma), A-549 (alveolar basal epithelial adenocarcinoma), LoVo (colon adenocarcinoma) and MCF-7 (breast adenocarcinoma), and in an immortalised line of human keratinocytes, NCTC-2544.

First of all, we observe the results obtained in the dark.

IC_{50} (µM)			
Compounds	K-562	Jurkat	HL-60
PZQ1	>20	>20	>20
PZQ2	>20	>20	>20
PZQ3	>20	>20	>20
PZQ4	>20	>20	>20
PZQ5	>20	>20	>20
PZQ6	>20	4,55 ± 0,66	>20
PZQ7	>20	>20	>20
PZQ8	>20	>20	>20
PZQ9	>20	>20	>20
PZQ10	>20	>20	>20
PZQ11	>20	>20	>20
PZQ12	13,85 ± 1,81	>20	>20
PZQ13	>20	11,26 ± 1,08	>20
PZQ14	>20	>20	>20
PZQ15	>20	>20	>20

PZQ16	>20	>20	>20
PZQ17	>20	12,07 ± 1,69	>20
PZQ18	>20	8,43 ± 1,43	6,10 ± 1,35
PZQ19	>20	9,80 ± 1,60	7,17 ± 0,77
PZQ20	>20	13,24 ± 1,67	>20
PZQ21	>20	11,35 ± 1,22	>20
PZQ22	>20	12,54 ± 1,53	>20
PZQ23	>20	> 20	>20
PZQ24	>20	>20	>20
PZQ25	>20	>20	>20
PZQ26	>20	>20	>20
PZQ27	>20	>20	>20
PZQ28	>20	>20	>20
PZQ29	>20	>20	>20
PZQ30	>20	>20	>20
PZQ31	>20	>20	>20
PZQ32	>20	>20	>20
PZQ33	>20	>20	>20
PZQ34	>20	>20	>20
PZQ35	>20	13,59 ± 1,70	11,56 ± 1,98
PZQ36	>20	>20	>20
PZQ37	>20	>20	>20
PZQ38	>20	>20	>20

Tab.5.2 Antiproliferative activity of PZQ series in some human leukaemia cell lines in the dark.

IC_{50} (μM)					
Compounds	*A-431*	*A-549*	*LoVo*	*MCF-7*	*NCTC-2544*
PZQ1	>20	>20	>20	>20	> 20
PZQ2	>20	>20	>20	>20	>20
PZQ3	4,41 ± 0,42	10,81 ± 0,66	>20	11,53 ± 2,02	>20
PZQ4	>20	>20	>20	>20	>20

PZQ5	>20	>20	>20	>20	>20
PZQ6	2,68 ± 0,32	6,41 ± 0,48	>20	>20	> 20
PZQ7	2,87 ± 0,58	6,25 ± 0,68	>20	11,17 ± 1,29	> 20
PZQ8	1,63 ± 0,33	4,04 ± 0,42	>20	8,54 ± 1,20	> 20
PZQ9	>20	>20	>20	>20	> 20
PZQ10	>20	>20	>20	>20	> 20
PZQ11	>20	>20	>20	>20	> 20
PZQ12	>20	>20	>20	>20	> 20
PZQ13	>20	>20	>20	>20	> 20
PZQ14	>20	>20	>20	>20	> 20
PZQ15	>20	>20	>20	>20	> 20
PZQ16	>20	>20	>20	>20	> 20
PZQ17	>20	>20	>20	>20	> 20
PZQ18	>20	>20	>20	>20	> 20
PZQ19	>20	>20	>20	>20	>20
PZQ20	>20	>20	>20	>20	> 20
PZQ21	>20	>20	>20	>20	> 20
PZQ22	>20	>20	>20	>20	> 20
PZQ23	0,83 ± 0,11	5 ± 0,93	>20	6,38 ± 0,90	8,39 ± 1,27
PZQ24	>20	>20	>20	> 20	> 20
PZQ25	>20	>20	>20	>20	> 20
PZQ26	>20	>20	>20	>20	>20
PZQ27	>20	>20	>20	>20	> 20
PZQ28	>20	>20	>20	>20	> 20
PZQ29	>20	12,49 ± 0,65	>20	9,26 ± 1,41	3,96 ± 0,92
PZQ30	2,64 ± 0,17	9,03 ± 0,65	>20	8,36 ± 0,75	5,61 ± 1,17
PZQ31	7,66 ± 0,69	>20	>20	> 20	9,78 ± 1,10
PZQ32	8,94 ± 0,92	>20	>20	9,60 ± 1,48	6,50 ± 0,73
PZQ33	2,95 ± 0,45	0,32 ± 0,75	>20	7,51 ± 1,30	4,72 ± 0,70
PZQ34	8,73 ± 0,25	>20	>20	16,19 ± 1,34	14,03 ± 1,27
PZQ35	>20	>20	>20	> 20	> 20
PZQ36	>20	>20	>20	>20	>20
PZQ37	>20	>20	>20	>20	>20

_____

PZQ38	>20	>20	>20	>20	>20

Tab. 5.3 Cytotoxicity in some human solid tumour cell lines in the dark.

Pyrazolo[3,4-h]quinazolines do not seem to be particularly cytotoxic molecules at the employed concentrations, especially in the leukaemic cell lines; the human solid tumour cell lines demonstrate to be more sensitive to these compounds, particularly when the derivative has a carbonyl group at position 2.

Then, we analyse the photocytotoxicity in the presence of different concentrations of test compounds; two UVA doses are used: 1,25 and 2,5 J/cm^2 in leukaemic cell lines, corresponding to 5 and 10 irradiation minutes, or 2,5 and 3,75 J/cm^2 in carcinoma cell lines, corresponding to 10 and 15 irradiation minutes, respectively. For photocytotoxicity experiments, cells are incubated with the molecules for 30 minutes prior to irradiation with Wood's lamps (emitting principally at 365 nm); cellular survival is checked by MTT test after 72 hours from irradiation.

	IC_{50} (μM)			
Compounds	***Jurkat***		***HL-60***	
	1,25 J/cm^2	***2,5 J/cm^2***	***1,25 J/cm^2***	***2,5 J/cm^2***
PZQ1	>20	>20	>20	>20
PZQ2	>20	>20	>20	>20
PZQ3	>20	>20	>20	>20
PZQ4	>20	6,88 ± 0,94	< 20	5,06 ± 0,63
PZQ5	11,27 ± 1,46	3,95 ± 0,34	11,48 ± 1,69	2,76 ± 0,40
PZQ6	>20	>20	>20	>20
PZQ7	>20	>20	>20	>20
PZQ8	>20	>20	>20	>20
PZQ9	>20	>20	>20	>20
PZQ10	>20	6,99 ± 1,15	>20	>20
PZQ11	>20	5,67 ± 0,93	>20	6,79 ± 0,54
PZQ12	>20	5,21 ± 0,84	>20	4,82 ± 0,24
PZQ13	>20	2,81 ± 0,41	>20	2,44 ± 0,24
PZQ14	>20	3,01 ± 0,60	>20	2,88 ± 0,42
PZQ15	>20	6,68 ± 0,42	>20	7,65 ± 0,55
PZQ16	>20	12,68 ± 1,58	>20	9,79 ± 1,46

PZQ17	3,65 ± 0,47	0,71 ± 0,13	2,83 ± 0,31	0,79 ± 0,06
PZQ18	2,48 ± 0,48	1,40 ± 0,15	3,83 ± 0,57	1,30 ± 0,16
PZQ19	1,93 ± 0,14	0,90 ± 0,13	3,78 ± 0,53	0,81 ± 0,15
PZQ20	1,95 ± 0,35	1,34 ± 0,27	3,42 ± 0,46	0,53 ± 0,14
PZQ21	0,72 ± 0,11	0,43 ± 0,13	4,03 ± 1,19	0,48 ± 0,10
PZQ22	1,15 ± 0,18	0,64 ± 0,15	5,29 ± 1,21	0,72 ± 0,12
PZQ23	>20	>20	> 20	>20
PZQ24	>20	>20	> 20	>20
PZQ25	>20	>20	> 20	7,67 ± 1,10
PZQ26	>20	>20	> 20	>20
PZQ27	4,47 ± 0,72	1,81 ± 0,35	5,38 ± 1,01	1,71 ±0,27
PZQ28	9,93 ± 1,31	6,43 ± 0,55	7,71 ± 1,41	4,69 ± 0,67
PZQ29	> 20	>20	> 20	> 20
PZQ30	> 20	> 20	> 20	> 20
PZQ31	0,20 ± 0,06	0,10 ± 0,02	0,39 ± 0,05	0,31 ± 0,02
PZQ32	0,58 ± 0,15	0,25 ± 0,04	0,61 ± 0,08	0,44 ± 0,03
PZQ33	4,23 ± 1,15	0,96 ± 0,20	1,80 ± 0,31	1,2 ± 0,14
PZQ34	1,50 ± 0,40	0,54 ± 0,11	0,82 ± 0,09	0,6 ± 0,09
PZQ35	> 20	4,97 ± 1,45	> 20	7,17 ± 1,44
PZQ36	> 20	>20	> 20	> 20
PZQ37	> 20	>20	> 20	> 20
PZQ38	> 20	> 20	> 20	9,09 ± 1,38

Tab. 5.4 Photocytotoxicity in some human leukaemia cell lines after UVA irradiation.

IC_{50} (μM)						
Compounds	*MCF-7*		*LoVo*		*A-549*	
	2,5 J/cm^2	*3,75 J/cm^2*	*2,5 J/cm^2*	*3,75 J/cm^2*	*2,5 J/cm^2*	*3,75 J/cm^2*
PZQ1	>20	>20	>20	>20	>20	>20
PZQ2	>20	>20	>20	>20	>20	>20
PZQ3	>20	>20	>20	>20	>20	14,06 ± 0,94
PZQ4	>20	>20	>20	14,52 ± 2,43	>20	>20

PZQ5	12,99 ± 1,48	10,43 ± 0,60	>20	10,14 ± 1,09	13,33 ± 2,20	8,97 ± 0,95
PZQ6	>20	>20	>20	>20	14,14 ± 1,51	9,53 ± 1,18
PZQ7	>20	>20	>20	>20	>20	> 20
PZQ8	>20	>20	>20	>20	>20	>20
PZQ9	>20	>20	>20	>20	>20	>20
PZQ10	>20	>20	>20	>20	>20	>20
PZQ11	>20	>20	>20	13,04 ± 2,2	>20	>20
PZQ12	>20	12,62 ± 1,04	>20	13,06 ± 1,85	>20	13,02 ± 1,27
PZQ13	12,67 ± 1,74	9,01 ± 1,19	13,12 ± 1,05	7,54 ± 1,17	>20	8,40 ± 1,43
PZQ14	>20	>20	>20	11,11 ± 2,40	>20	>20
PZQ15	>20	>20	>20	>20	>20	>20
PZQ16	>20	>20	>20	>20	>20	>20
PZQ17	2,47 ± 0,34	1,84 ± 0,19	3,14 ± 0,30	1,10 ± 0,20	7,56 ± 0,69	2,89 ± 0,32
PZQ18	4,00 ± 0,51	3,05 ± 0,48	5,32 ± 0,51	1,41 ± 0,25	10,37 ± 1,48	5,74 ± 1,04
PZQ19	3,13 ± 0,35	1,59 ± 0,12	5,73 ± 0,78	1,78 ± 0,36	14,32 ± 2,66	4,80 ± 0,50
PZQ20	5,15 ± 1,10	2,52 ± 0,40	9,84 ± 1,14	2,99 ± 0,87	13,33 ± 3,48	6,61 ± 0,85
PZQ21	7,09 ± 2,02	1,69± 0,18	5,53 ± 1,00	0,73 ± 0,15	5,28 ± 1,03	1,49 ± 0,35
PZQ22	2,53 ± 0,24	1,18 ± 0,12	3,56 ± 0,63	0,53 ± 0,11	4,02 ± 0,44	1,52 ± 0,15
PZQ23	7,32 ± 0,98	9,85 ± 0,93	>20	>20	>20	>20
PZQ24	>20	>20	>20	>20	>20	>20
PZQ25	>20	>20	>20	>20	>20	>20
PZQ26	>20	>20	>20	>20	>20	>20
PZQ27	>20	>20	2,79 ± 0,47	1,13 ± 0,41	3,68 ± 0,61	2,30 ± 0,31
PZQ28	>20	>20	5,81 ± 0,32	4,30 ± 0,52	6,99 ± 0,74	4,67 ± 0,56
PZQ29	>20	>20	>20	>20	>20	>20
PZQ30	>20	>20	>20	>20	5,39 ± 0,93	4,26 ± 0,67
PZQ31	0,33 ±0,06	0,17 ± 0,03	0,16 ± 0,03	0,04 ± 0,02	0,26 ± 0,25	0,08 ± 0,03
PZQ32	0,29 ± 0,03	0,14 ± 0,03	0,19 ± 0,03	0,09 ± 0,02	0,27 ± 0,01	0,08 ± 0,03
PZQ33	5,36 ± 0,73	3,23 ± 0,46	1,43 ± 0,30	0,71 ± 0,15	3,09 ± 1,15	0,75 ± 0,21
PZQ34	1,23 ± 0,14	0,59 ±0,07	0,42 ± 0,02	0,16 ± 0,03	0,35 ± 0,05	0,09 ± 0,03
PZQ35	> 20	9,89 ± 1,45	11,08 ± 1,24	3,72 ± 0,91	>20	6,64 ± 1,12
PZQ36	>20	>20	>20	4,12 ± 1,19	>20	>20
PZQ37	>20	>20	>20	>20	>20	>20

_____

PZQ38	>20	>20	>20	$2,67 \pm 0,84$	>20	$5,74 \pm 0,96$

Tab. 5.5 Photocytotoxicity in some human solid tumour cell lines after UVA irradiation

After UVA irradiation, many molecules show an interesting antiproliferative activity; the photocytotoxicity is, in most cases, dose-dependent.

The most active compounds in this series are PZQ31 and PZQ32, with sub-micromolar IC_{50} values in all the tested cell lines, but also PZQ21 and PZQ22 show a remarkable effect, with sub-micromolar IC_{50} results in some cell lines.

Given that many derivatives have been analysed, some hypotheses can be developed regarding the SAR.

These molecules are variously substituted at positions 1, 2, 3 and 7; some of them have a double bond at positions 5-6, so they become fully aromatic compounds.

Among the derivatives devoid of the double bond 5,6, the ones with a methoxyl group at position 2 (e.g. PZQ21 and PZQ22) are more effective than molecules with a carbonyl group. In addition, a hydrophobic substitution at position 7 (i.e. benzyl, phenyl, chlorophenyl, methoxyphenyl) increases photocytotoxicity, as the presence of a phenyl sulfonyl group at position 3 respect to an ethoxycarbonyl derivative.

The most active fully aromatic analogues maintain the methoxyl substitution at position 2 (a carbonyl group leads to a loss of activity) and the hydrophobic group at position 7; finally, the insertion of a methyl group at position 1 produces the most active compounds of this line, PZQ31 and PZQ32.

5.3.1 <u>**Photocytotoxicity in the presence of scavengers**</u>

In this assay, we test the antiproliferative activity of the most photocytotoxic compounds of this series in the presence of some scavengers.

In this test, we use six different scavengers: E vitamin (α-tocopherol) and reduced glutathione (GSH), which protect cells by the formation of alkyl radicals, sodium azide (NaN_3) and DABCO (1,4-diazabicyclo[2.2.2]octane), which prevent the formation of singlet oxygen, and DMTU (1,3-dimethyl-2-thiourea) and mannitol, which protect cells by the formation of hydroxyl radical.

We carry out this test with one UVA dose (2,5 J/cm^2, corresponding to 10 minutes) and with a compound concentration next to its IC_{50} (0,5 μM for PZQ21, 0,75 μM for PZQ22 and 0,20 μM for

PZQ31 and PZQ32); photocytotoxicity is evaluated after 72 hours with MTT test on treated Jurkat cells.
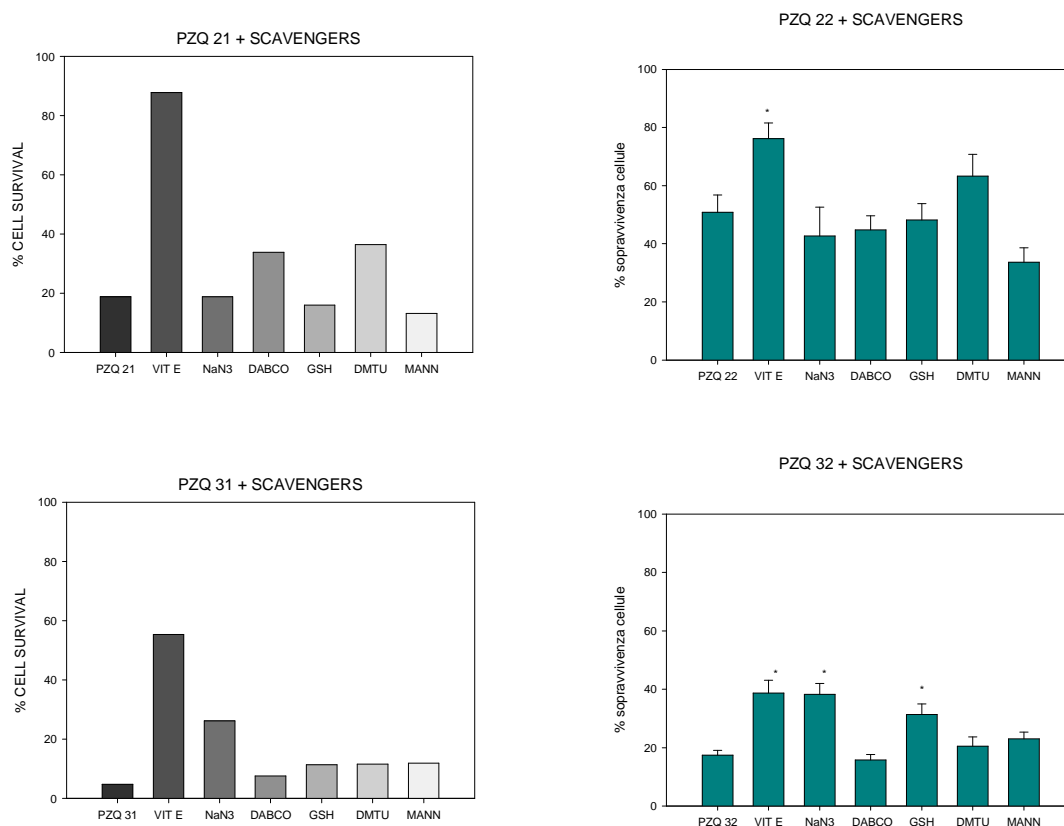
Fig. 5.2 Scavenger effect on treated cells after UVA irradiation (2,5 J/cm^2).

As we can see in figure 5.2, α-tocopherol is successful in protecting cells from PZQ injuries; since E vitamin is a lipophilic protein which can protect membranes, we can hypothesise the involvement of the plasma membrane structure in the mechanism of action of these compounds.

The other scavengers exert their action in a different manner for each molecule: for example, for PZQ21 and PZQ22, the lipophilic scavengers increase the cellular viability, while all scavengers lead to an augmentation of cellular survival in the presence of PZQ31. Anyway, the most effective scavengers have often lipophilic features, so they probably have the same localization of pyrazoloquinolines.

5.3.2 <u>Colony formation assay</u>

In this test, A-549 cells are seeded in their proper medium (7000 cells/well); after 30 minutes incubation with PZQ21, PZQ22, PZQ31 and PZQ32 at four different concentrations and UVA

irradiation (2,5 J/cm^2), cells are stored in their growth medium. After 5 days, cells are stained with crystal violet dye and observed with a light microscope; colony formation percentage is then calculated. A colony is formed at least by 50 cells.

C   IC

PZQ21 4 μM   PZQ21 2 μM   PZQ21 1 μM   PZQ21 0,5 μM

PZQ22 4 μM   PZQ22 2 μM   PZQ22 1 μM   PZQ22 0,5 μM

PZQ31 0,5 μM   PZQ31 0,25 μM   PZQ31 0,125 μM   PZQ31 0,0625 μM

PZQ32 0,5 μM   PZQ32 0,25 μM   PZQ32 0,125 μM   PZQ32 0,0625 μM
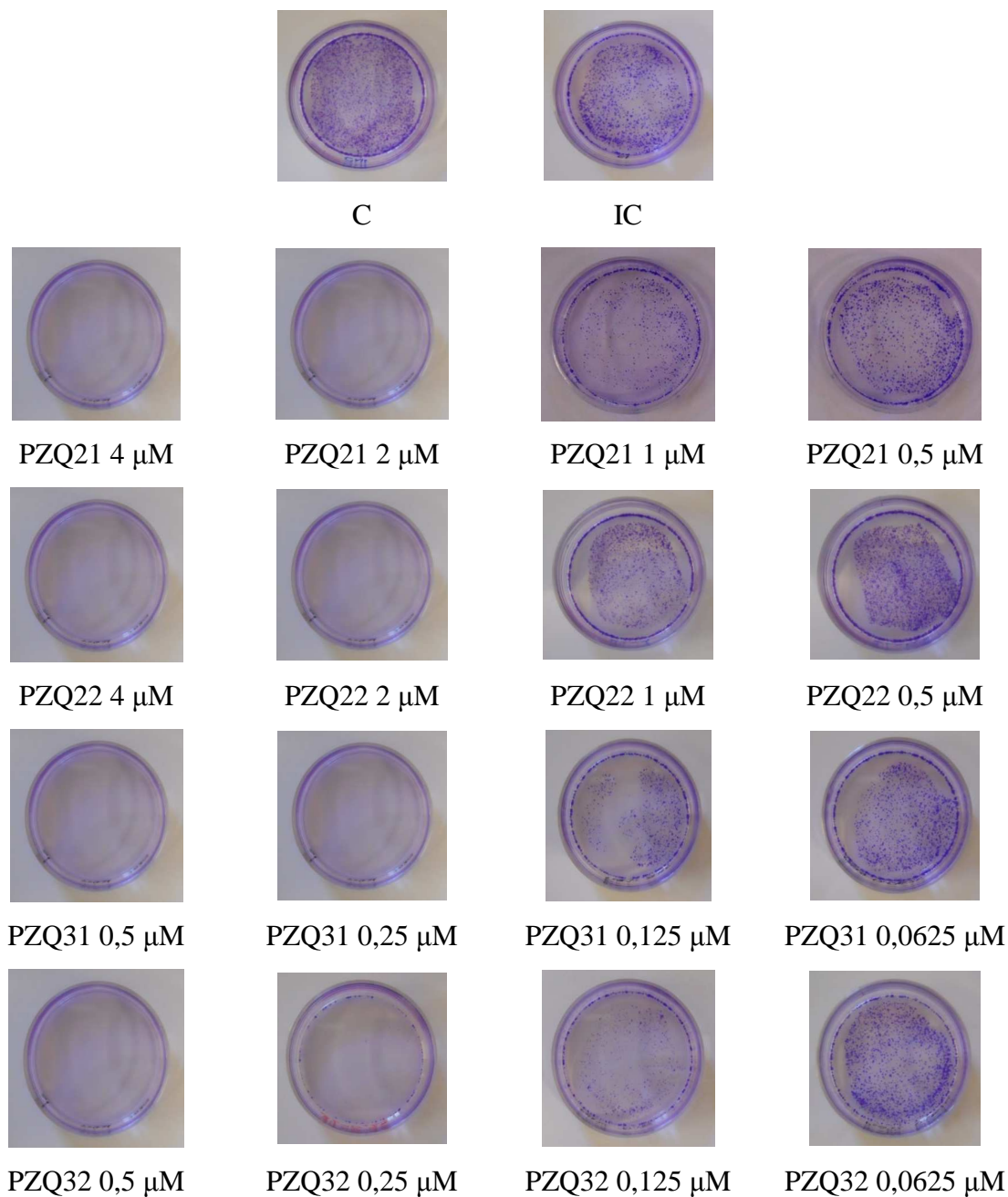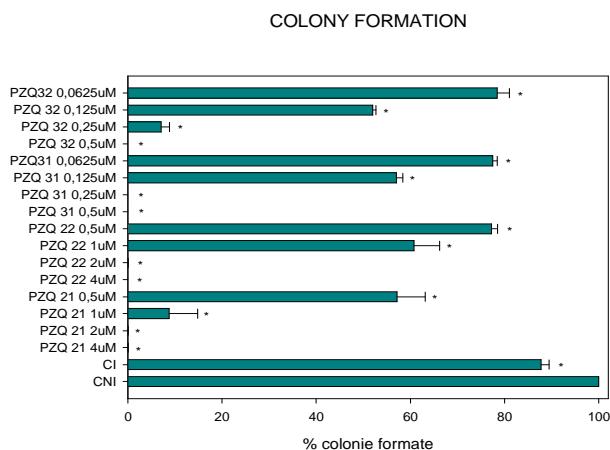
COLONY FORMATION

Fig.5.3 Colony formation assay; C = control, IC = irradiated control.

All these molecules can inhibit the colony formation at the employed concentrations in a dose-dependent manner; particularly, PZQ31 and PZQ32 can inhibit the colony formation at sub-micromolar concentrations, whereas PZQ21 and PZQ22 are effective at the concentration of about 1 μM.

5.4 <u>Cell death mechanism</u>

Cell death mechanism is studied with the most active compounds at the concentration of 1 or 2 μM, 24 and 3 hours after irradiation (2,5 J/cm^2), by the Annexin V/PI flow cytometry test.
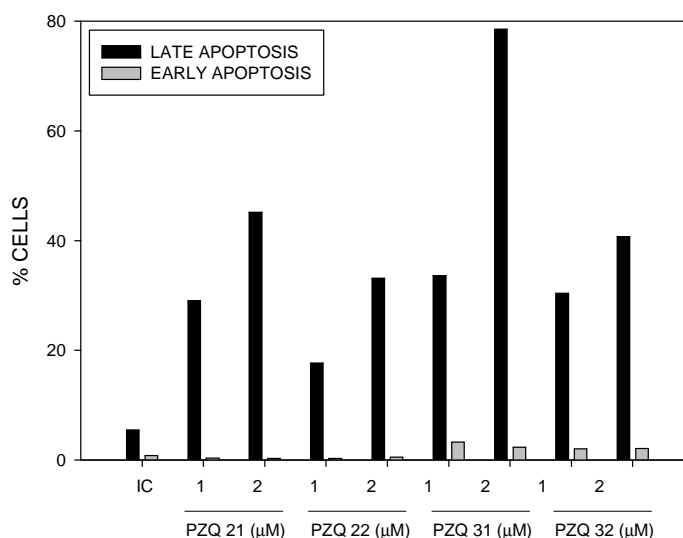
Fig. 5.4 Early and late apoptotic cells 24 hours after irradiation (2,5 J/cm^2); cells are incubated with PZQ21, PZQ22, PZQ31 and PZQ32 2 and 1 μM; IC = irradiated control.

_____

After 24 hours, most cells are in late apoptotic phase, so we monitor cell death after a shorter incubation time.

Fig. 5.4 Early and late apoptotic cells 3 hours after irradiation (2,5 J/cm^2); cells are incubated with PZQ21, PZQ22, PZQ31 and PZQ32 2 and 1 μM; IC = irradiated control.

After 3 hours from irradiation, an increase in early apoptotic cells is detected in a dose-dependent manner relative to control; a small percentage of necrotic cells is also detected, but the primary mechanism of cell death seems to be apoptosis.

5.5 Involvement of mitochondria in cell death mechanism

Psoralens and UVA are known to induce cell death by apoptosis with the involvement of mitochondria. Thus, we decided to perform some assays to evaluate a possible role of mitochondria in PZQ photoinduced apoptosis.

5.5.1 Determination of mitochondrial membrane potential

This test is performed with JC-1 dye after 24 and 3 hours from irradiation; the mitochondrial membrane potential is monitored by the fluorescence of this probe.

JC-1 24h
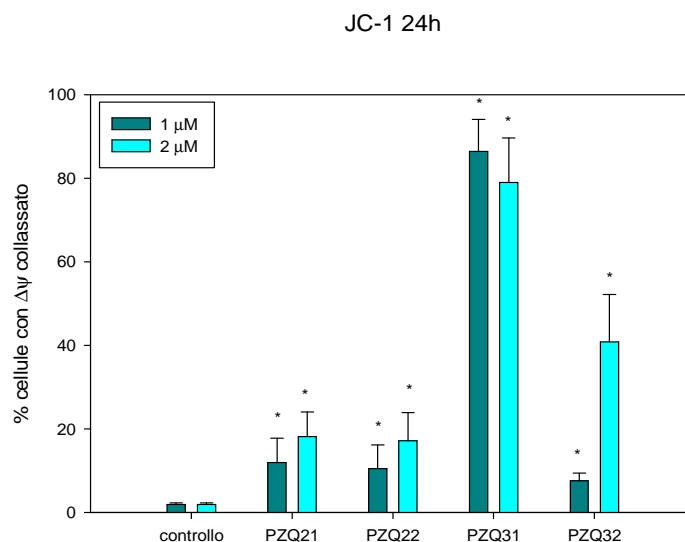
Fig. 5.5 Cells percentage with loss of mitochondrial membrane potential 24 hours after irradiation (2,5 J/cm²) of cells treated with PZQ21, PZQ22, PZQ31 and PZQ32 2 and 1 μM; IC = irradiated control.

JC-1 3h
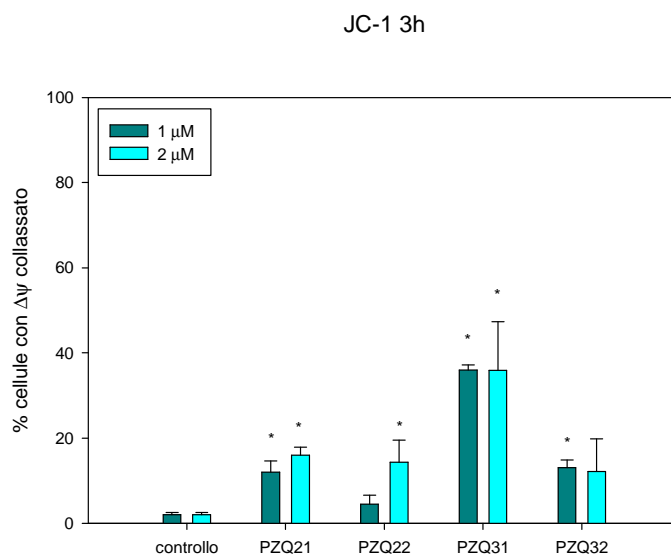
Fig. 5.6 Cells percentage with loss of mitochondrial membrane potential 3 hours after irradiation (2,5 J/cm²) of cells treated with PZQ21, PZQ22, PZQ31 and PZQ32 2 and 1 μM; IC = irradiated control.

In these graphics, we can detect a depolarisation of mitochondrial membrane, with a dose-dependent shift in fluorescence respect to control. Particularly, PZQ31 is the most effective compound; 3 hours after irradiation, we can see about 40% cells with collapsed membrane potential and, 24 hours after irradiation, about 80% cells. Moreover, for this compound we do not notice concentration-dependence but only UV dose-dependence because of the high efficacy of this molecule.

Consequently, we can hypothesise mitochondrial involvement in cell death process.

5.5.2 <u>Determination of ROS production</u>

ROS production is examined by flow cytometry 24 hours after irradiation of Jurkat cells in the presence of PZQ21, PZQ22, PZQ31 and PZQ32 at the concentration of 2 μM.
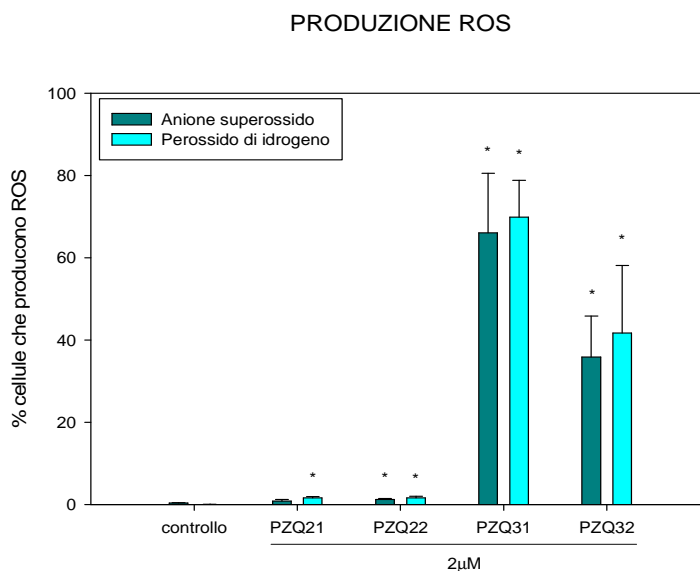
Fig. 5.7 Percentage of ROS production 24 hours after irradiation (2,5 J/cm^2) and treatment with PZQ21, PZQ22, PZQ31 and PZQ32 2 μM; IC = irradiated control.

PZQ21 and PZQ22 induce a weak increase in ROS production at the employed concentration; instead PZQ31 and PZQ32 provoke a remarkable increment in this parameter. These results confirm the previous ones, that is the mitochondria involvement in cell death process, in a weaker manner for PZQ21 and PZQ22 and preferentially for PZQ32 and, above all, for PZQ31.

5.6 <u>Involvement of lysosomes in cell death mechanism</u>

To investigate the involvement of lysosomes in the apoptotic mechanism 24 and 3 hours after UVA irradiation (2,5 J/cm^2), we perform a flow cytometric analysis with acridine orange dye; the percentage of Jurkat cells with intact lysosomes is evaluated by assaying red fluorescence after AO staining.
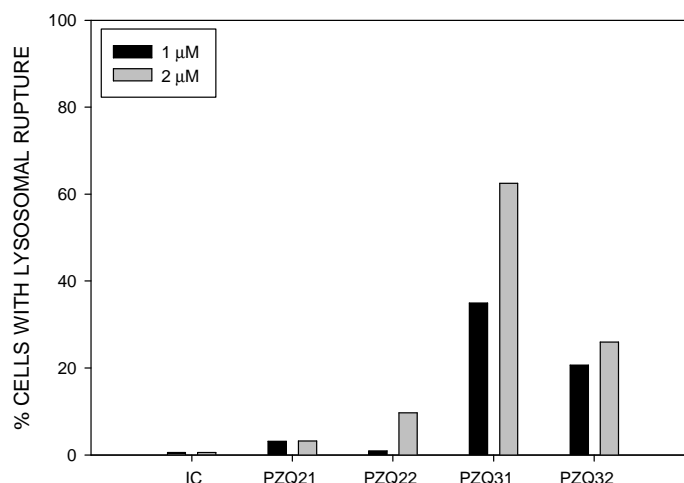
Fig.5.8 Cells percentage with lysosomal damage 24 hours after irradiation (2,5 J/cm^2) in the presence of PZQ21, PZQ22, PZQ31 and PZQ32 2 and 1 μM; IC = irradiated control.

AO 3h
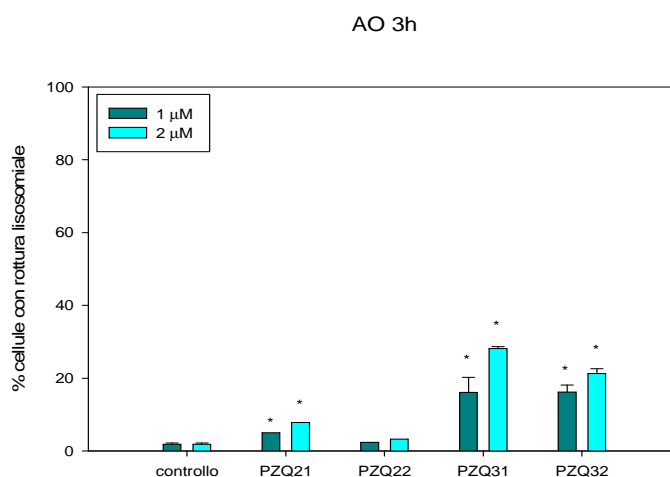
Fig.5.9 Cells percentage with lysosomal damage 3 hours after irradiation (2,5 J/cm^2) in the presence of PZQ21, PZQ22, PZQ31 and PZQ32 2 and 1 μM; IC = irradiated control.

The lysosomal damage is concentration- and time-dependent; as seen before, PZQ32 and particularly PZQ31 are the most active compounds. In conclusion, we can hypothesise lysosomal involvement in cell death mechanism.

5.7 **Photoreaction with the main biomolecules**

In this section we analyse PZQ photoreaction with lipids and proteins.

5.7.1 <u>Lipid peroxidation</u>

This assay is performed to reveal a potential photodamage against lipids 24 hours after the irradiation of Jurkat cells in the presence of test compounds at the concentration of 2 μM.
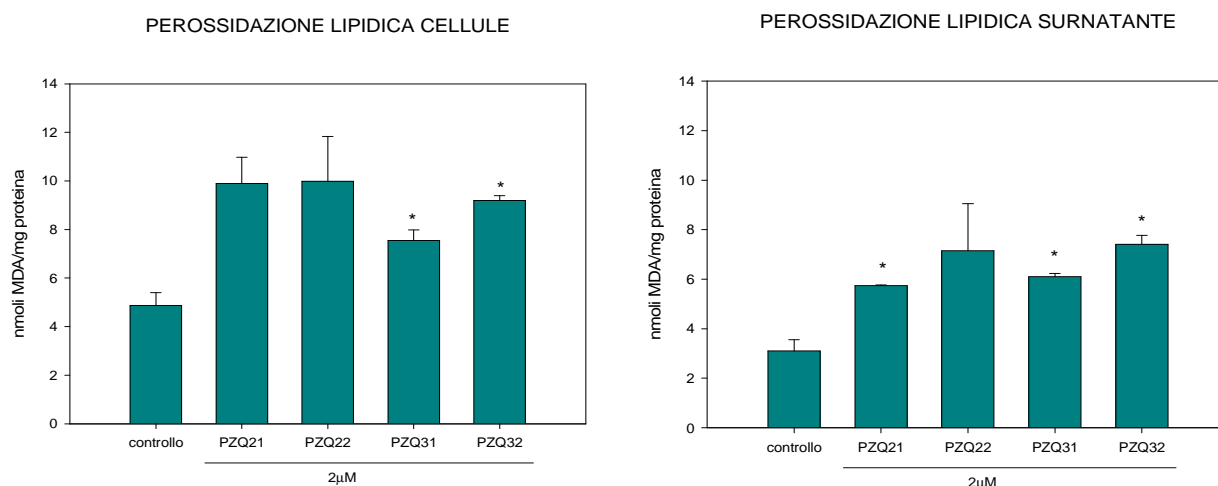
Fig. 5.10 Lipid peroxidation induced by PZQ21, PZQ22, PZQ31 and PZQ32 2 μM 24 hours after irradiation (2,5 J/cm^2); IC = irradiated control.

In these graphics, a considerable production of thiobarbituric acid reactive substances (TBARs) is observed, particularly in cells extract (intracellular MDA) respect to the surnatant (extracellular MDA): therefore, lipids could be a possible target of pyrazoloquinolines.

5.7.2 <u>Photoreaction with model proteins</u>

This experiment is carried out to discover another potential target of these molecules; particularly, tryptophan (Trp) and tyrosine (Tyr) amino acids are monitored through fluorimetric assays to detect a photodamage on two model proteins, BSA (bovine serum albumin, containing Trp) and RNAse (containing Tyr, but not Trp).

Protein solutions treated with 10 μM test compounds are irradiated with different UVA doses (1,25 J/cm^2, 2,5 J/cm^2, 5 J/cm^2, 7,5 J/cm^2, 11,25 J/cm^2, 15 J/cm^2) and fluorescence spectra are recorded: changes in protein fluorescence highlight a photodamage.

FOTOREAZIONE CON RNAsi A
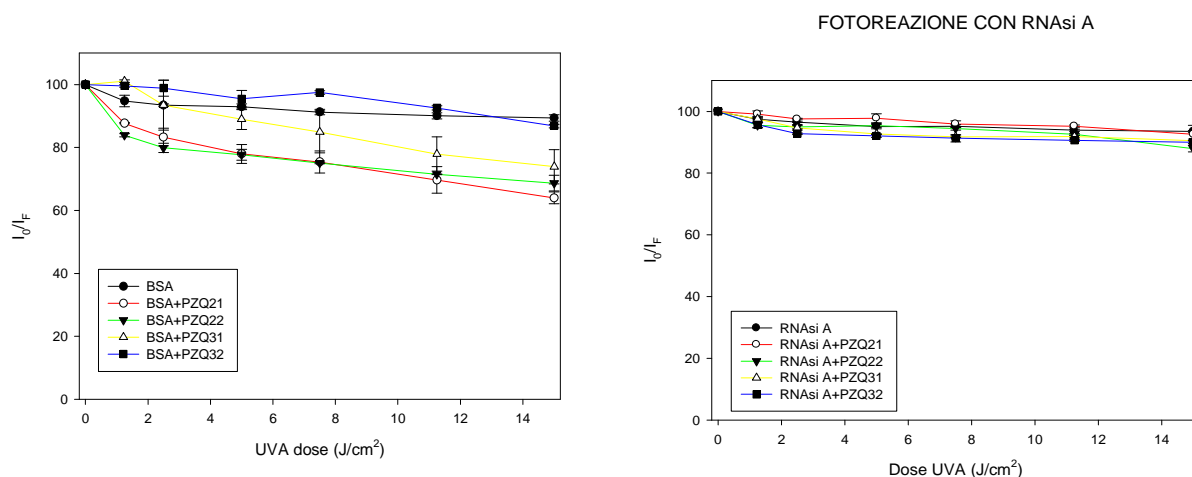
Fig. 5.11 Photoreaction with BSA and RNAse of test compounds in the presence of increasing UVA doses.

In these graphs we can notice that PZQ compounds cause a dose-dependent decrease in Trp fluorescence and this fact is indicative of photoreaction with BSA; instead, RNAse fluorescence is not affected by irradiation in the presence of these compounds.

5.8 <u>Conclusions</u>

In this section 38 new pyrazolo[3,4-h]quinolines were analysed.

These molecules were synthesised at Palermo University as angelicin heteroanalogues: the aim was to obtain new photochemotherapic agents with minor toxicity but improved activity in comparison to angelicin and its derivatives. Their nucleus was variously substituted at positions 1, 2, 3 and 7 and some of them have a double bond at positions 5-6, so they become fully aromatic compounds.

Some of these derivatives inhibit cell proliferation in vitro, even in the absence of UVA irradiation, but their antiproliferative effect is not very pronounced at the employed concentrations, especially in the leukaemic cell lines; the human solid tumour cell lines demonstrated to be more sensitive to these compounds, particularly when the derivative has a carbonyl group at position 2.

Pyrazolo[3,4-h]quinolines absorb in the UV and UVA range, but in most cases they do not undergo photolysis, as we can see by monitoring changes in their structure after UVA irradiation; for those which degrade, we detected a weak reduction of the maximum peak and the presence of one or more isosbestic points that reveal the presence of photoproduct(s) in equilibrium with the non-degraded molecule.

Most derivatives showed remarkable photocytotoxicity in many human tumour cell lines, reaching IC$_{50}$ values in the sub-micromolar range; the most phototoxic compounds are PZQ21, PZQ22, PZQ31 and PZQ32. Among the not fully aromatic derivatives, the ones with a methoxyl group at position 2 (e.g. PZQ21 and PZQ22) are more effective than molecules with a carbonyl group. In addition, a hydrophobic substitution at position 7 increases photocytotoxicity, as the presence of a phenyl sulfonyl group at position 3 respect to an ethoxycarbonyl derivative. The most active fully aromatic analogues maintain the methoxyl substitution at position 2 (a carbonyl group leads to a loss of activity) and the hydrophobic group at position 7; finally, the insertion of a methyl group at position 1 produces the most active compounds of this line, PZQ31 and PZQ32.

With flow cytometry studies we demonstrated that these compounds induce cellular death through apoptosis, with the involvement of mitochondria and lysosomes (involved later respect to mitochondria); PZQ31 is the most effective compound.

Finally, we analysed the photoreaction with the main biomolecules to identify a possible target of these derivatives: these compounds react with lipids and BSA, so lipids and proteins could be involved in their mechanism of action. This is confirmed by the protective action of α-tocopherol on cells treated with test compounds; since E vitamin is a lipophilic protein that can protect membranes, we can hypothesise the involvement of the membrane structures in the mechanism of action of these compounds.

6. Materials and methods

6.1 Materials

- Compounds: 104 new compounds, synthesised at Palermo University by Cirrincione's group, were analysed:
  - BQ1: 6,8-dihydro-5H-pyrrolo[3,4-h]quinazoline
  - BQ2: 8-methyl-6,8-dihydro-5H-pyrrolo[3,4-h]quinazoline
  - BQ3: 8-benzyl-6,8-dihydro-5H-pyrrolo[3,4-h]quinazoline
  - BQ4: 8-(4-methylbenzyl)-6,8-dihydro-5H-pyrrolo[3,4-h]quinazoline
  - BQ5: 8-(4-methoxybenzyl)-6,8-dihydro-5H-pyrrolo[3,4-h]quinazoline
  - BQ6: ethyl 9-methyl-6,8-dihydro-5H-pyrrolo[3,4-h]quinazoline-7-carboxylate
  - BQ7: ethyl 8,9-dimethyl-6,8-dihydro-5H-pyrrolo[3,4-h]quinazoline-7-carboxylate
  - BQ8: ethyl 8-benzyl-9-methyl-6,8-dihydro-5H-pyrrolo[3,4-h]quinazoline-7-carboxylate
  - BQ9: ethyl 9-methyl-8-(4-methylbenzyl)-6,8-dihydro-5H-pyrrolo[3,4-h]quinazoline-7-carboxylate
  - BQ10: ethyl 9-methyl-8-(4-methoxybenzyl)-6,8-dihydro-5H-pyrrolo[3,4-h]quinazoline-7-carboxylate
  - BQ11: 7-phenyl-6,8-dihydro-5H-pyrrolo[3,4-h]quinazoline
  - BQ12: 8-methyl-7-phenyl-6,8-dihydro-5H-pyrrolo[3,4-h]quinazoline
  - BQ13: 8-benzyl-7-phenyl-6,8-dihydro-5H-pyrrolo[3,4-h]quinazoline
  - BQ14: 8-(4-methylbenzyl)- 7-phenyl-6,8-dihydro-5H-pyrrolo[3,4-h]quinazoline
  - BQ15: 8-(4-methoxybenzyl)- 7-phenyl-6,8-dihydro-5H-pyrrolo[3,4-h]quinazoline
  - BQ16: 8-methyl-6,8-dihydro-5H-pyrrolo[3,4-h]quinazolin-2-amine
  - BQ17: 8-benzyl-6,8-dihydro-5H-pyrrolo[3,4-h]quinazolin-2-amine
  - BQ18: 8-(4-methylbenzyl)-6,8-dihydro-5H-pyrrolo[3,4-h]quinazolin-2-amine
  - BQ19: 8-(4-methoxybenzyl)-6,8-dihydro-5H-pyrrolo[3,4-h]quinazolin-2-amine
  - BQ20: ethyl 2-amino-6,8-dihydro-5H-pyrrolo[3,4-h]quinazoline-7-carboxylate

- BQ21: ethyl 2-amino-8,9-dimethyl-6,8-dihydro-5H-pyrrolo[3,4-h]quinazoline-7-carboxylate

- BQ22: ethyl 2-amino-8-benzyl-9-methyl-6,8-dihydro-5H-pyrrolo[3,4-h]quinazoline-7-carboxylate

- BQ23: ethyl 2-amino-9-methyl-8-(4-methylbenzyl)-6,8-dihydro-5H-pyrrolo[3,4-h]quinazoline-7-carboxylate

- BQ25: 8-methyl-7-phenyl-6,8-dihydro-5H-pyrrolo[3,4-h]quinazolin-2-amine

- BQ26: 8-benzyl-7-phenyl-6,8-dihydro-5H-pyrrolo[3,4-h]quinazolin-2-amine

- BQ27: 8-(4-methylbenzyl)-7-phenyl-6,8-dihydro-5H-pyrrolo[3,4-h]quinazolin-2-amine

- BQ28: 8-(4-methoxybenzyl)-7-phenyl-6,8-dihydro-5H-pyrrolo[3,4-h]quinazolin-2-amine

- BQ29: 8-methyl-3,5,6,8-tetrahydro-2H-pyrrolo[3,4-h]quinazolin-2-one

- BQ30: 8-benzyl-3,5,6,8-tetrahydro-2H-pyrrolo[3,4-h]quinazolin-2-one

- BQ31: 8-(4-methylbenzyl)-3,5,6,8-tetrahydro-2H-pyrrolo[3,4-h]quinazolin-2-one

- BQ32: 8-(4-methoxybenzyl)-3,5,6,8-tetrahydro-2H-pyrrolo[3,4-h]quinazolin-2-one

- BQ33: 8-phenyl-3,5,6,8-tetrahydro-2H-pyrrolo[3,4-h]quinazolin-2-one

- BQ34: ethyl 8,9-dimethyl-2-oxo-3,5,6,8-tetrahydro-2H-pyrrolo[3,4-h]quinazoline-7-carboxylate

- BQ35: ethyl 8-benzyl-9-methyl-2-oxo-3,5,6,8-tetrahydro-2H-pyrrolo[3,4-h]quinazoline-7-carboxylate

- BQ36: ethyl 8-(4-methylbenzyl)-9-methyl-2-oxo-3,5,6,8-tetrahydro-2H-pyrrolo[3,4-h]quinazoline-7-carboxylate

- BQ37: ethyl 8-(4-methoxybenzyl)-9-methyl-2-oxo-3,5,6,8-tetrahydro-2H-pyrrolo[3,4-h]quinazoline-7-carboxylate

- BQ38: 8,9-dimethyl-3,5,6,8-tetrahydro-2H-pyrrolo[3,4-h]quinazolin-2-one

- BQ39: 8-benzyl-9-methyl-3,5,6,8-tetrahydro-2H-pyrrolo[3,4-h]quinazolin-2-one

- BQ40: 8-methyl-7-phenyl-3,5,6,8-tetrahydro-2H-pyrrolo[3,4-h]quinazolin-2-one

- BQ41: 8-benzyl-7-phenyl-3,5,6,8-tetrahydro-2H-pyrrolo[3,4-h]quinazolin-2-one

- BQ42: 8-(4-methylbenzyl)-7-phenyl-3,5,6,8-tetrahydro-2H-pyrrolo[3,4-h]quinazolin-2-one

- BQ43: 8-(4-methoxybenzyl)-7-phenyl-3,5,6,8-tetrahydro-2H-pyrrolo[3,4-h]quinazolin-2-one

- BQ44: 8-methyl-N-phenyl-6,8-dihydro-5H-pyrrolo[3,4-h]quinazolin-2-amine

- BQ45: 8-benzyl-N-phenyl-6,8-dihydro-5H-pyrrolo[3,4-h]quinazolin-2-amine
- BQ46: N,8-diphenyl-6,8-dihydro-5H-pyrrolo[3,4-h]quinazolin-2-amine
- BQ47: ethyl 2-anilino-8,9-dimethyl-6,8-dihydro-5H-pyrrolo[3,4-h]quinazoline-7-carboxylate
- BQ48: ethyl 2-anilino-9-methyl-6,8-dihydro-5H-pyrrolo[3,4-h]quinazoline-7-carboxylate
- BQ49: ethyl 2-anilino-8-benzyl-9-methyl-6,8-dihydro-5H-pyrrolo[3,4-h]quinazoline-7-carboxylate
- BQ50: 2-anilino-8-benzyl-7-phenyl-6,8-dihydro-5H-pyrrolo[3,4-h]quinazoline
- LCQ1: 9-methyl-3,5,6,9-tetrahydro-2H-pyrrolo[3,2-h]quinazolin-2-one
- LCQ2: 9-benzyl-3,5,6,9-tetrahydro-2H-pyrrolo[3,2-h]quinazolin-2-one
- LCQ3: ethyl 9-methyl-3,5,6,9-tetrahydro-2H-pyrrolo[3,2-h]quinazolin-2-one-8-carboxylate
- LCQ4: ethyl 9-benzyl-3,5,6,9-tetrahydro-2H-pyrrolo[3,2-h]quinazolin-2-one-8-carboxylate
- LCQ5: 2-amine-9-methyl-6,9-dihydro-5H-pyrrolo[3,2-h]quinazoline
- LCQ6: 2-amine-9-benzyl-6,9-dihydro-5H-pyrrolo[3,2-h]quinazoline
- LCQ7: 2-amine-9-(4-methoxybenzyl)-6,9-dihydro-5H-pyrrolo[3,2-h] quinazoline
- LCQ8: ethyl 2-amino-9-methyl-6,9-dihydro-5H-pyrrolo[3,2-h] quinazoline-8-carboxylate
- LCQ9: ethyl 2-amino-9-benzyl-6,9-dihydro-5H-pyrrolo[3,2-h]quinazoline-8-carboxylate
- LCQ10: ethyl 2-amino-9-(4-methoxybenzyl)-6,9-dihydro-5H-pyrrolo[3,2-h] quinazoline-8-carboxylate
- LCQ11: 2-anilino-9-methyl-6,9-dihydro-5H-pyrrolo[3,2-h]quinazoline
- LCQ12: 2-anilino-9-benzyl-6,9-dihydro-5H-pyrrolo[3,2-h]quinazoline
- LCQ13: 2-anilino-9-(4-methoxybenzyl)-6,9-dihydro-5H-pyrrolo[3,2-h]quinazoline
- LCQ14: ethyl 2-anilino-9-methyl-6,9-dihydro-5H-pyrrolo[3,2-h]quinazoline-8-carboxylate
- LCQ15: ethyl 2-anilino-9-(4-methoxybenzyl)-6,9-dihydro-5H-pyrrolo[3,2-h]quinazoline-8-carboxylate
- LCQ16: 9-benzyl-6,9-dihydro-5H-pyrrolo[3,2-h]quinazoline
- LCQ17: 9-phenyl-6,9-dihydro-5H-pyrrolo[3,2-h]quinazoline
- PZQ1: 3-(phenylsulfonyl)-1,5,6,7-tetrahydro-2H-pyrazolo[3,4-h]quinolin-2-one

- PZQ2: 7-methyl-3-(phenylsulfonyl)-1,5,6,7-tetrahydro-2H-pyrazolo[3,4-h]quinolin-2-one

- PZQ3: 7-phenyl-3-(phenylsulfonyl)-1,5,6,7-tetrahydro-2H-pyrazolo[3,4-h]quinolin-2-one

- PZQ4: 7-benzyl-3-(phenylsulfonyl)-1,5,6,7-tetrahydro-2H-pyrazolo[3,4-h]quinolin-2-one

- PZQ5: 7-(2-chlorophenyl)-3-(phenylsulfonyl)-1,5,6,7-tetrahydro-2H-pyrazolo[3,4-h]quinolin-2-one

- PZQ6: 7-(3-chlorophenyl)-3-(phenylsulfonyl)-1,5,6,7-tetrahydro-2H-pyrazolo[3,4-h]quinolin-2-one

- PZQ7: 7-(4-chlorophenyl)-3-(phenylsulfonyl)-1,5,6,7-tetrahydro-2H-pyrazolo[3,4-h]quinolin-2-one

- PZQ8: 7-(4-mthoxyphenyl)-3-(phenylsulfonyl)-1,5,6,7-tetrahydro-2H-pyrazolo[3,4-h]quinolin-2-one

- PZQ9: 1,7-dimethyl-3-(phenylsulfonyl)-1,5,6,7-tetrahydro-2H-pyrazolo[3,4-h]quinolin-2-one

- PZQ10: 1-methyl-7-phenyl-3-(phenylsulfonyl)-1,5,6,7-tetrahydro-2H-pyrazolo[3,4-h]quinolin-2-one

- PZQ11: 7-benzyl-1-methyl-3-(phenylsulfonyl)-1,5,6,7-tetrahydro-2H-pyrazolo[3,4-h]quinolin-2-one

- PZQ12: 7-(2-chlorophenyl)-1-methyl-3-(phenylsulfonyl)-1,5,6,7-tetrahydro-2H-pyrazolo[3,4-h]quinolin-2-one

- PZQ13: 7-(3-chlorophenyl)-1-methyl-3-(phenylsulfonyl)-1,5,6,7-tetrahydro-2H-pyrazolo[3,4-h]quinolin-2-one

- PZQ14: 7-(4-chlorophenyl)-1-methyl-3-(phenylsulfonyl)-1,5,6,7-tetrahydro-2H-pyrazolo[3,4-h]quinolin-2-one

- PZQ15: 7-(4-methoxyphenyl)-1-methyl-3-(phenylsulfonyl)-1,5,6,7-tetrahydro-2H-pyrazolo[3,4-h]quinolin-2-one

- PZQ16: 2-methoxy-7-methyl-3-(phenylsulfonyl)-6,7-dihydro-5H-pyrazolo[3,4-h]quinoline

- PZQ17: 2-methoxy-7-phenyl-3-(phenylsulfonyl)-6,7-dihydro-5H-pyrazolo[3,4-h]quinoline

- PZQ18: 2-methoxy-7-benzyl-3-(phenylsulfonyl)-6,7-dihydro-5H-pyrazolo[3,4-h]quinoline

- PZQ19: 7-(2-chlorophenyl)-2-methoxy-3-(phenylsulfonyl)-6,7-dihydro-5H-pyrazolo[3,4-h]quinoline

- PZQ20: 7-(3-chlorophenyl)-2-methoxy-3-(phenylsulfonyl)-6,7-dihydro-5H-pyrazolo[3,4-h]quinoline

- PZQ21: 7-(4-chlorophenyl)-2-methoxy-3-(phenylsulfonyl)-6,7-dihydro-5H-pyrazolo[3,4-h]quinoline

- PZQ22: 2-methoxy-7-(4-methoxyphenyl)-3-(phenylsulfonyl)-6,7-dihydro-5H-pyrazolo[3,4-h]quinoline

- PZQ23: 7-(4-chlorophenyl)-3-(ethoxycarbonyl)-1,5,6,7-tetrahydro-2H-pyrazolo[3,4-h]quinolin-2-one

- PZQ24: 7-(4-methoxyphenyl)-3-(ethoxycarbonyl)-1,5,6,7-tetrahydro-2H-pyrazolo[3,4-h]quinolin-2-one

- PZQ25: 7-(4-chlorophenyl)-1-methyl-3-(ethoxycarbonyl)-1,5,6,7-tetrahydro-2H-pyrazolo[3,4-h]quinolin-2-one

- PZQ26: 7-(4-methoxyphenyl)-1-methyl-3-(ethoxycarbonyl)-1,5,6,7-tetrahydro-2H-pyrazolo[3,4-h]quinolin-2-one

- PZQ27: 7-(4-chlorophenyl)-2-methoxy-3-(ethoxycarbonyl)-6,7-dihydro-5H-pyrazolo[3,4-h]quinoline

- PZQ28: 2-methoxy-7-(4-methoxyphenyl)-3-(ethoxycarbonyl)-6,7-dihydro-5H-pyrazolo[3,4-h]quinoline

- PZQ29: 7-(4-chlorophenyl)-3-(phenylsulfonyl)-1,7-dihydro-2H-pyrazolo[3,4-h]quinolin-2-one

- PZQ30: 3-(phenylsulfonyl)-7-(4-methoxyphenyl)-1,7-dihydro-2H-pyrazolo[3,4-h]quinolin-2-one

- PZQ31: 7-(4-chlorophenyl)-3-(phenylsulfonyl)-1-methyl-1,7-dihydro-2H-pyrazolo[3,4-h]quinolin-2-one

- PZQ32: 3-(phenylsulfonyl)-1-methyl-7-(4-methoxyphenyl)-1,7-dihydro-2H-pyrazolo[3,4-h]quinolin-2-one

- PZQ33: 7-(4-chlorophenyl)-3-(phenylsulfonyl)-2-methoxy-7H-pyrazolo[3,4-h]quinoline

- PZQ34: 3-(phenylsulfonyl)-2-methoxy-7-(4-methoxyphenyl)-7H-pyrazolo[3,4-h]quinoline

- PZQ35: 1-benzyl-7-(4-chlorophenyl)-3-(phenylsulfonyl)-1,5,6,7-tetrahydro-2H-pyrazolo[3,4-h]quinolin-2-one

- PZQ36: 1-benzyl-3-(phenylsulfonyl)-7-(4-methoxyphenyl)-1,5,6,7-tetrahydro-2H-pyrazolo[3,4-h]quinolin-2-one

- PZQ37: 2-benzyloxy-7-(4-chlorophenyl)-3-(phenylsulfonyl)-6,7-dihydro-5H-pyrazolo[3,4-h]quinoline

- PZQ38: 2-benzyloxy-3-(phenylsulfonyl)-7-(4-methoxyphenyl)-6,7-dihydro-5H-pyrazolo[3,4-h]quinoline

- DMSO (dimethyl sulfoxide), Sigma Aldrich (IT)

- Phosphate buffer, Sigma Aldrich (IT)

- RPMI-1640 Medium, Sigma Aldrich (IT)

- HAM'S (Nutrient Mixture F-12 HAM), Sigma Aldrich (IT)

- DMEM (Dulbecco's Modified Eagle's Medium), Sigma Aldrich (IT)

- Foetal bovine serum (FBS), Invitrogen (IT)

- Penicillin-Streptomycin solution, Sigma Aldrich (IT)

- HBSS (Hank's Balanced Saline Solution), Sigma Aldrich (IT)

- Trypsin, Sigma Aldrich (IT)

- MTT (3-[4,5-dimethylthiazol-2-yl]-2,5-diphenyl tetrazolium bromide), Sigma Aldrich (IT)

- PBS (Phosphate Buffer Solution) 10 mM, p.H. = 7.2

- Isopropanol, Carlo Erba (IT)

- HCl, Carlo Erba (IT)

- Tripan Blue, Sigma Aldrich (IT)

- Crystal violet (4-[(4-dimethylaminophenyl)-phenyl-methyl]-N,N-dimethyl-aniline), Sigma Aldrich (IT)

- Annexin V/PI staining kit, Roche (DE)

- JC-1 (5,5',6,6'-tetrachloro-1,1',3,3'-tetraethylbenzimidazol-carbocyanine), Molecular Probes Eugene (OR, USA)

- AO (Acridine Orange), Sigma Aldrich (IT)

- HE (hydroethidine), Molecular Probes Eugene (OR, USA)

- DCHF-DA (2',7'-dichlorofluorescin diacetate), Molecular Probes Eugene (OR, USA)

- 70% ethanol, Carlo Erba (IT)

- Cell cycle staining kit, Sigma Aldrich (IT)

- EGF (100 ng/ml), Sigma Aldrich (IT)

- Lysis buffer (50 mM Tris-HCl pH 8.5, 150 mM NaCl, 1% Triton X-100, 10% glycerol, 1 mM DTT, 30 mM NaPPi, 10 mM NaF, 1 mM Na3VO4, 100 nM okadaic acid, complete protease inhibitors), Roche (DE)

- PVDF membrane, Bio Rad (IT)

- Casein, Sigma Aldrich (IT)

- Tween-20, Sigma Aldrich (IT)

- Polyclonal anti-Phospho-EGFR (Tyr1173), Santa Cruz (TX, USA)

- Anti-Phospho-ERK1/2 (P-p42/p44) (Thr202/Tyr204), Cell Signaling (USA)

- Anti-EGFR, Santa Cruz (TX, USA)

- Alkaline phosphatase, Jackson Immunoresearch Laboratories (PA, USA)

- Giemsa stain, Sigma Aldrich (IT)

- Microtubule polymerisation assay kit Cytoskeleton (Denver, USA)

- DAPI (4',6-diamidino-2-phenylindole), Sigma Aldrich (IT)

- M200 Medium, Invitrogen (IT)

- LSGS (Low Serum Growth Supplement), Invitrogen

- Matrigel, BD Biosciences (NJ, USA)

- BHT (butylhydroxytoluen), Sigma Aldrich (IT)

- SDS (sodium dodecyl sulfate), Sigma Aldrich (IT)

- TCA (trichloroacetic acid), Sigma Aldrich (IT)

- TBA (thiobarbituric acid), Sigma Aldrich (IT)

- BHA (butylhydroxyanisole), Sigma Aldrich (IT)

- DABCO (1,4 diazabicyclo [2,2,2] octane), Acros Organics (N.J., USA)

- DMTU (N-N' dimethyl thiourea), Sigma Aldrich (IT)

- α-tocopherol, Sigma Aldrich (IT)

- GSH (reduced glutathione), Sigma Aldrich (IT)

- NaN3 (sodium azide), Sigma Aldrich (IT)

- MAN (mannitol), Sigma Aldrich (IT)

- BSA (Bovine Serum Albumin), Sigma Aldrich (IT)

- RNAse A (A ribonuclease), Sigma Aldrich (IT)

- UV-Vis double beam instrument Lambda 12, Perkin-Elmer (MA, USA)

- LS50B fluorimeter, Perkin-Elmer (MA, USA)

- Microtiter plate reader, Bio Rad (IT)

_____

- HPW 125 lamps, Philips (NL) and Cole-Parmer Instrument Company radiometer (IL, USA), equipped with a 365-CX sensor

- Flow cytometer BD FACSCalibur, Beckton Dickinson (NY, USA)

- Fluorescence microplate reader Fluoroskan Ascent FL, Labsystems (IT)

- Optical microscope Optika ProVision XDS, Optika (IT)

- Fluorescence microscope Nikon Eclipse 80i

- Confocal microscope TCS SP5, Leica (DE)

- HERACell incubator, Kendro (CT, USA)

- Centrifuge, Beckman Coulter (IT)

- Water bath, Julabo (DE)

- Vortex, IKA Works (NC, USA)

- Sonorex TK52, Bandelin (DE)

- Polaris cabinet, Steril

- Technical balance, KERN (DE)

- Analytical balance, Sartorius (DE)

- Digital photocamera Kodak DC256

6.2 <u>Methods</u>

6.2.1 <u>Spectrophotometric determinations</u>

All spectrophotometric measures were performed using UV-Vis Perkin Elmer instrument (Lambda12, double beam). For all the compounds, absorption spectra, molar extinction coefficients (ε) and determination of maxima peaks were carried out both in DMSO and phosphate buffer (10 mM and pH=7,2), solvents compatible with cells, at the concentration of 10 and 20 µM, respectively.

Solubility of all molecules in aqueous medium was determined through the construction of a calibration curve by spectrophotometer method in the range of concentration used for experiments and at maximum absorption peak.

6.2.2 <u>Spectrofluorimetric determinations</u>

Fluorimetric spectra were recorded in phosphate buffer or in DMSO by a Perkin Elmer LS50B fluorimeter with 10 μM solutions.

6.2.3 <u>Irradiation procedures</u>

HPW 125 Philips lamps, mainly emitting at 365 nm, were used for irradiation experiments. The spectral irradiance of the source was 4,0 mW/cm^2 as measured, at the sample level, by a Cole-Parmer Instrument Company radiometer (IL, USA), equipped with a 365-CX sensor.

6.2.4 <u>Photostability</u>

In this test, 20 μM compounds solutions in DMSO were irradiated with known UVA doses: 0 minutes, 5 minutes, 15 minutes, 30 minutes with 0,25 J/(cm^2 x min). The absorption spectra were recorded with UV-Vis double beam instrument Lambda 12, Perkin-Elmer.

6.2.5 <u>Cell cultures</u>

For experiments of cellular viability, various human cell lines were used: Jurkat, K-562, HL-60, LoVo, LoVo^{doxo}, MCF-7, A-431, A-549, NCTC-2544.

Jurkat were human lymphoblastoid cells taken in 14 years old boy in 1976; they were grown in RPMI medium supplemented with 115 units/ml of penicillin G, 115 μg/ml streptomycin and 10% heat-inactivated foetal bovine serum (complete RPMI 1640 medium). Cells were kept at 37 °C in 5% CO_2 humidified atmosphere and re-seeded into fresh medium three times a week.

K-562 were obtained by a 53 year old woman with chronic myelogenous leukaemia in terminal blast crisis; cells were kept at 37 °C in 5% CO_2 humidified atmosphere and re-seeded into fresh medium (complete RPMI 1640) three times a week.

HL-60 were promyelocytic leukaemia cells taken in a woman of 35 years in 1976; they were grown in complete RPMI 1640 medium, kept at 37 °C in 5% CO_2 humidified atmosphere and re-seeded into fresh medium three times a week

LoVo were human intestinal adenocarcinoma cells taken in a 56 years old man in 1971. LoVo were grown in HAM'S F12 medium, supplemented with 115 units/ml of penicillin G, 115 μg/ml streptomycin and 10% heat-inactivated foetal bovine serum (complete HAM'S medium); cells were kept at 37 °C in 5% CO_2 humidified atmosphere, trypsinised and re-seeded into fresh medium twice a week.

LoVo^{doxo} were doxorubicin resistant subclone of LoVo cells [50]; they were grown in complete HAM'S F12 medium supplemented with doxorubicin (0,1 μg/ml).

MCF-7 were human breast adenocarcinoma cells. They were grown in DMEM medium supplemented with 115 units/ml of penicillin G, 115 μg/ml streptomycin and 10% heatinactivated foetal bovine serum (complete DMEM medium); cells were kept at 37 °C in 5% CO_2 humidified atmosphere, trypsinised and reseeded into fresh medium once a week.

A-431 were obtained by a vulvar squamous cell carcinoma; they were grown in complete DMEM medium, kept at 37 °C in 5% CO_2 humidified atmosphere, trypsinised and reseeded into fresh medium twice a week.

A-549 derived from a non-small cell lung cancer. They were grown in complete DMEM medium; cells were kept at 37 °C in 5% CO_2 humidified atmosphere, trypsinised and reseeded into fresh medium twice a week.

NCTC-2544 were human immortalized keratinocytes; they were grown in complete DMEM medium, kept at 37 °C in 5% CO_2 humidified atmosphere, trypsinised and re-seeded into fresh medium twice a week.

6.2.6 Cellular toxicity and phototoxicity

Individual wells of a 96-well tissue culture microtiter plate were inoculated with 100 ml of complete medium containing $5x10^3$ cells; plates were harvested at 37 °C in a humidified 5% CO_2 incubator for 24 hours prior to the cell viability experiments. Drugs were dissolved in DMSO and then were diluted with Hank's Balanced Salt Solution (HBSS pH=7,2) for phototoxicity experiments or in the appropriated complete medium for the cytotoxicity ones.

In cytotoxicity tests, after medium removal, 100 μl of the drug solution at serial concentrations were added to each well and incubated at 37 °C for 72 hours.

In phototoxicity experiments, after medium removal, 100 μl of the drug solution at serial concentrations were put into each well and incubated at 37 °C for 30 minutes and then irradiated (1,25, 2,5 or 3,75 J/cm^2); after irradiation, drug solution was replaced by cellular medium and plates were incubated for 72 hours at 37 °C.

After the period of incubation, in both cases cell viability was assayed by the MTT [(3-(4,5-dimethylthiazol-2-yl)-2,5 diphenyl tetrazolium bromide)] test [51]; MTT is a yellow dye that can be absorbed by cells and reduced by mitochondrial dehydrogenases, producing insoluble blue crystals. In each well, 10 μl of MTT (5 mg/ml in PBS) were added and plates were put in incubator for 3 or 4 hours; after incubation, crystals were solubilised adding 100 μl of 0,08 N HCl in isopropanol and plates were detected through microplate Bio Rad reader at 570 nm.

The absorbance of each sample was corrected by instrument which subtracted the mean value of blanks (i.e. wells in which there were all the reactives except cells); the absorbance is proportional to cellular viability, so the cellular survival was calculated by the following equation:

$$\% \text{ CELL SURVIVAL} = \{[(A_{SAMPLE} - A_{100\%}) / A_{100\%}] + 1\} * 100$$

where $A_{100\%}$ is the mean of controls (i.e. cells without drug nor irradiation exposure, which represents 100% of survival) and A_{sample} is the absorbance of various samples in which cells were in contact with drug or irradiated in presence of drug.

For every cellular line, IC_{50} was measured through Sigma Plot software; IC_{50} represents the compound concentration which leads to death 50% of cell population.

In phototoxicity experiments, the protective effect of some scavengers was also evaluated. Various scavengers were employed: for LCQ compounds N-N' dimethyl thiourea (DMTU, 1 mM in ethanol), 1,4 diazabicyclo[2,2,2]octane (DABCO, 1 mM in PBS) and 2,6-di-tert-butylhydroxyanisole (BHA, 10 μM in ethanol); for PZQ molecules α-tocopherol (30 μM), sodium azide (NaN$_3$, 1 mM in PBS), 1,4 diazabicyclo[2,2,2]octane (DABCO, 1 mM in PBS), reduced glutathione (GSH, 1mM in PBS), N-N' dimethyl thiourea (DMTU, 1 mM in ethanol), mannitol (10 mM in PBS). Each experiment was repeated at least three times.

6.2.7 Colony formation assay

This test was performed with the most active molecules of BQ and PZQ series to confirm their cytotoxicity and photocytotoxicity, respectively.

_____

In this assay, 7 x 10^3 cells (A-431 or A-549 cells) were seeded in 2 ml of their proper medium and treated with serial concentrations of compounds; for BQ and PZQ treated cells, the growth medium was restored after 24 hours treatment and 30 minutes incubation plus 10 minutes irradiation, respectively. After a few days and some medium substitutions, cells were stained with crystal violet dye and observed with a light microscope; colony formation percentage was then calculated. A colony is formed at least by 50 cells.

6.2.8 **Flow cytometry**

Flow cytometry is a very important technique to obtain cellular characteristics: from the presence of membrane antigens with immunofluorescence methods to cellular volume, from cellular granularity to cellular membrane permeability; with this method we can reveal quantitative and qualitative features.

Flow cytometer is an instrument that makes statistical analysis in samples of microscopic dispersed particles in liquid suspension, through light diffusion and fluorescence phenomena. Modern flow cytometers are able to analyse several thousand particles every second, in "real time," and can actively separate and isolate particles having specified properties.
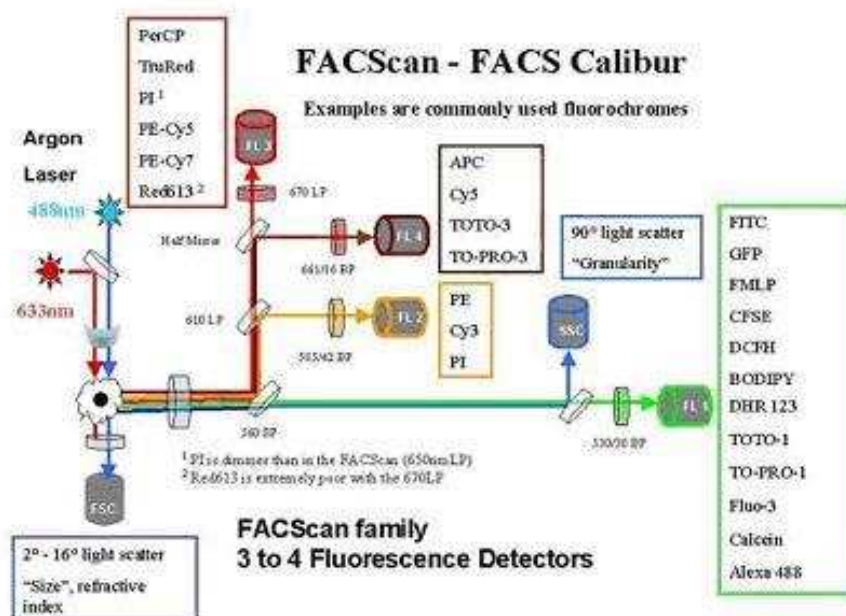
Fig. 6.1 Schematic representation of a flow cytofluorimeter.

A flow cytometer is similar to a microscope except that, instead of producing an image of the cell, flow cytometry offers "high-throughput" (for a large number of cells) automated quantification of set parameters.

Flow cytometer is formed by five components: fluidic system, optical system, electronic system, mechanic system and finally data SW-analysis system.

Fluidic system consists of a flow cell, a special capillary , usually in quartz, where an hydrodynamic apparatus permits to obtain the so called "hydrodynamic focalisation"; in this system, single particles are forced to flow at the centre of this capillary, where ideally they can perform laminar flow. Inside this flow cell, particles are in single line, so the instrument has the possibility to take single measures sequentially. The light source can be a laser or mercury vapour lamp.

The optical system lets the light beam arrive in the capillary core where it is focalised to each single cell flowing. Signals from cells are sent to respective photomultipliers; there is also an optical group parallel and orthogonal to light beam to check side scattering (SS) and forward scattering (FS), respectively. SS gives information about cellular morphology (shape, cytoplasmatic granularity and nucleus/cell rate), while FS about the size of objects [52]. In the SS, there are also fluorescent phenomena if fluorochromes are utilized for analysis (FITC, PE,etc). The emitted light is checked for spectral analysis (separation of wavelength through dichroic spectra) and is sent to photomultiplier to amplify signals. Signals are transformed to electric impulses and digitalised; a computer analyses the data and helps their visualization.

The process of collecting data from samples using the flow cytometer is termed "acquisition", and it is mediated by a computer physically connected to the flow cytometer; the software which handles the digital interface with the cytometer is capable of adjusting parameters (i.e. voltage, compensation, etc.) for the sample being tested, and also assists in displaying initial sample information while acquiring sample data to assure that parameters are set correctly.

Flow cytometry presents numerous advantages: the possibility of multiparametric analysis, the reproducibility, the high number of analysed cells (100000 events), the speed of analysis (seconds) and the simplicity of the preparation of samples. It is possible to isolate single populations of cell (for example living cells) and analyse only in this subpopulation parameters (gating).

6.2.8.1   <u>Determination of the cell death mechanism</u>

In the early stages of apoptosis, some changes occur at the cell surface: one of the first modifications is the loss of plasmatic membrane asymmetry, with the translocation of

phosphatidylserine (PS) from the inner side of the plasma membrane to the outer layer, by which PS becomes exposed at the external surface of the cell.

Annexin V is a calcium dependent phospholipid-binding protein with high affinity for PS; hence, this protein can be used as a sensitive probe for PS exposure upon the cell membrane when conjugated with the fluorophore fluorescein isothiocyanate (FITC).

Translocation of PS to the external cell surface is not unique to apoptosis, but occurs also during necrosis; the difference between these two forms of cell death is that during the initial stages of apoptosis the cell membrane remains intact, while at the very moment that necrosis occurs the cell membrane looses its integrity and becomes leaky. Therefore, the measurement of Annexin V binding to the cell surface as indicative for apoptosis has to be performed in conjunction with a dye exclusion test to establish integrity of the cell membrane [42].
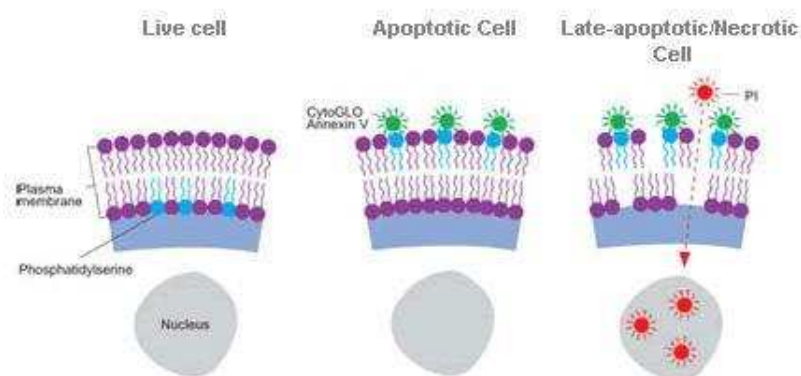
Fig. 6.2 Annexin V/PI assay.

In these assays, 4 x 10^5 Jurkat cells were treated with different concentrations of the most cytotoxic compounds or irradiated in the presence of the most photocytotoxic molecules; after different times of incubation (24 hours, 6 hours or 3 hours), samples were centrifuged and Annexin V-FITC/PI solution was added, according to the kit instructions. Samples were incubated for 15 minutes in the dark and then were analysed by cytofluorimeter by which the fluorescence of FITC (green, FL1) and of PI (red, FL3) were measured.

In conclusion, living cells do not show any fluorescence, late apoptosis cells demonstrate both fluorescence, early apoptotic cells present only the FITC one as their plasmatic membrane is still integer, necrotic cells demonstrate PI one.

6.2.8.2   Determination of mitochondrial membrane potential

One parameter of mitochondrial dysfunction is the loss of mitochondrial membrane potential.

The mitochondrial membrane potential was measured with the lipophilic cation 5,5',6,6' tetrachloro-1,1',3,3'-tetraethylbenzimidazol-carbocyanine (JC-1).
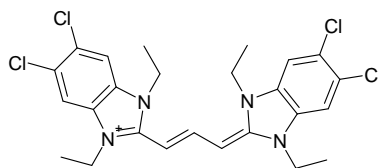
Fig. 6.3 JC-1 dye.

After 6 or 24 hours from the incubation with the most cytotoxic molecules or after 3 or 24 hours from the irradiation in the presence of the most photocytotoxic compounds, Jurkat cells were collected by centrifugation and resuspended in HBSS containing the JC-1 dye at the concentration of 1 μg/ml. Cells were then incubated at 37 °C for 10 minutes, centrifuged and resuspended again in HBSS; the cytofluorimetric analysis was performed collecting green (FL1) and orange (FL2) fluorescence in at least 10000 events for each sample.

This method is based on the ability of this fluorescent probe to enter selectively mitochondria and to change reversibly its colour from green to orange as membrane potential increases; this property is due to the reversible formation of JC-1 aggregates upon membrane polarization that causes shift in the emitted light from 530 nm (i.e. emission of JC-1 monomeric form) to 590 nm (emission of J-aggregate) when excited at 490 nm [53].

6.2.8.3   <u>Determination of reactive oxygen species (ROS) production</u>

ROS production was evaluated by flow cytometry with two different probes: hydroethidine (HE), which reveals superoxide anion, and dihydrochlorofluorescin-diacetate (DCFDA), which reveals the presence of hydrogen peroxide [54].

In the presence of superoxide anion, hydroethidine is oxidised to ethidium, which intercalates into DNA and can give the characteristic red fluorescence.
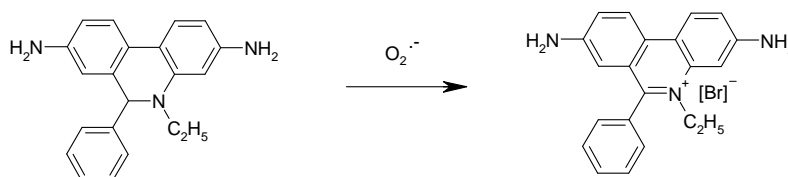
Fig.6.4 Oxidation of hydroethidine to ethidium by superoxide anion.

Otherwise, dihydrochlorofluorescin-diacetate penetrates very slowly the cell; then, inside of the cell, it is deacetilated by endogenous esterases, so it is trapped in the cytosol. It can be oxidised to dichlorofluorescein in the presence of peroxides and can give the characteristic fluorescence in the green region.
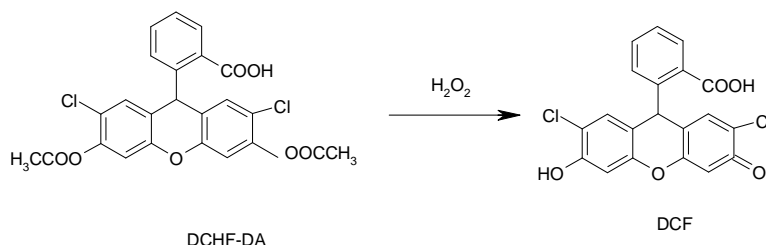
Fig. 6.5 Oxidation of DCHF-DA to DCF by hydrogen peroxide after deacetilation by endogenous esterases.

After 24 hours from the irradiation in the presence of LCQ and PZQ compounds or the treatment with BQ molecules, cells were collected by centrifugation and resuspended in HBSS containing the fluorescence probes HE or DCFDA at the concentration of 2,5 μM and 5,0 μM respectively. Cells were then incubated at 37 °C for 15 or 30 minutes, centrifuged and resuspended again in HBSS.

The fluorescence was finally recorded with the flow cytometer (Coulter Cytomics FC500) using the 488 nm wavelength as excitation, and the emission at 620 nm for HE and at 530 nm for DCFDA. At least 10000 events for each sample were acquired.

6.2.8.4   <u>Involvement of lysosomes in cell death mechanism</u>

To investigate the integrity of lysosomes, we performed flow cytometric analysis using the fluorescent dye acridine orange (AO).
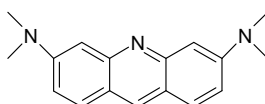
Fig. 6.6 Acridine orange dye (AO).

AO is a lysosomotropic base and a metachromatic fluorochrome exhibiting red fluorescence when highly concentrated, as in the case of intact lysosomes where AO is retained in its charged protonated form, and green fluorescence at low concentration as in damaged lysosomes. In this case, AO relocates to the cytosol where it is predominantly in the deprotonated form [23].

After 24 hours from the incubation with BQ derivatives or from the irradiation in the presence of LCQ and PZQ compounds, Jurkat cells were collected by centrifugation and resuspended in RPMI

containing AO at the concentration of 1 μM; cells were then incubated at 37 °C for 15 minutes, centrifuged and resuspended again in RPMI. The fluorescence was directly recorded with the flow cytometer (Coulter Cytomics FC500) using the 488 nm wavelength as excitation and the emission in FL3 channel.

6.2.8.5 <u>Analysis of cell cycle</u>

The analysis of cell cycle was performed through flow cytometry; this test is based on the fact that each cell cycle phase presents a different content of DNA.

For flow cytometric analysis of DNA content, 5×10^5 Jurkat cells in exponentially growth were treated with different concentrations of compounds; after the incubation period (24 hours), cells were centrifuged and fixed with ice-cold ethanol (70%), then treated with PBS buffer containing RNAse A (10 Kunit/ml) and propidium iodide (PI, 10 μg/ml). When intercalated in DNA, PI fluoresces in the red (620 nm, FL3), if it is excited at 488 nm [52]. Each experiment was repeated three times.
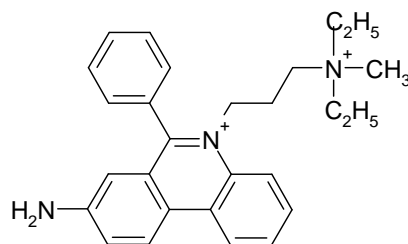
Fig. 6.7 Propidium iodide.

Samples were then analysed on a flow cytometer; for cell cycle analysis, results were examined with MultiCycle for Windows (Phoenix Flow Systems, San Diego, CA). Data were expressed as fractions of cells in the different cycle phases; diagrams of growing cultures display the characteristic x-axis distribution according to the DNA content, the first peak corresponding to cells in the G_1 phase, and the second peak to cells in G_2/M phase. Cells with an intermediate DNA content are in the S phase. When DNA is fragmented, as in apoptotic cells, the affinity with the intercalating PI dye is decreased and a so-called hypodiploid peak (or area) becomes apparent to the left of the G_1 peak: this is named sub-G_1 phase.
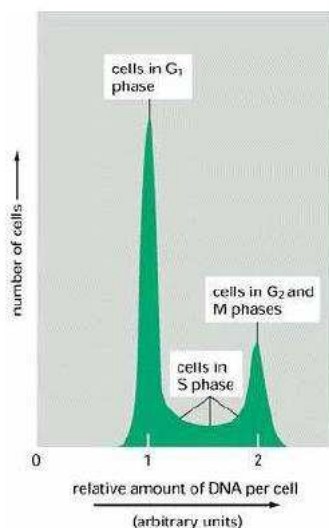
Fig. 6.8 Representation of cell cycle distribution

6.2.9 <u>Evaluation of EGFR inhibition</u>

For protein extraction and western blotting, 10^6 A-431 cells were seeded in 6 cm Petri dishes; after 24 hours, they were washed with PBS and starved overnight. Then, cells were incubated with or without 20 µM compounds for 3 hours and stimulated with EGF 100 ng/ml for 10 minutes.

Cell extracts were prepared after scraping in lysis buffer, incubating on ice for 15 minutes and clearing by centrifugation; 100 µg of proteins were then loaded in 12,5% SDS-PAGE and then blotted to a PVDF membrane (Bio-Rad). Membranes were washed with 0,2% casein, 0,1% Tween-20 in PBS (blocking buffer) for 1 hour and incubated with polyclonal anti-Phospho-EGFR (Tyr1173) (Santa Cruz), anti-Phospho-ERK1/2 (P-p42/p44) (Thr202/Tyr204) (Cell Signaling) overnight or with anti-EGFR (Santa Cruz) for 2 hours. After washing in blocking buffer, the membranes were incubated with the proper secondary antibody coupled to alkaline phosphatase (Jackson immunoresearch laboratories) for 1 hour.

Visualization was done with CDP-star (Tropix) according to the manufacturer's instructions.

6.2.10   <u>Determination of the mitotic index</u>

Exponentially growing Jurkat cells were incubated with test compounds for 24 hours prior to centrifugation at 400 rpm for 5 minutes; the resultant cell pellet was then resuspended in 75 mM

_____

KCl solution at 4 °C. After 20 minutes, the fixative methanol-acetic acid (3:l) was slowly added under constant mild agitation.

Slides were prepared after the cells were repelled, washed twice with fixative and resuspended in the fixative; after drying, samples were stained with Giemsa solution.

A total of 400 cells/treatment was scored for the presence of mitotic figures by optical microscopy, and the mitotic index was calculated as the proportion of cells with mitotic figures.

6.2.11   Evaluation of microtubule network perturbation

Microtubules are dynamic polymers made by the assembly of tubulin, a heterodimer consisting of α- and β-tubulin. Microtubule dynamics are involved in many microtubule dependent processes in cells, the most important being mitosis. During mitosis, the interphase microtubule network completely disassembles and a new assembly of microtubules occurs, leading to the mitotic spindle on which the chromosomes attach and segregate to the two spindle poles [47].

This feature was evaluated through two tests.

6.2.11.1 Immunofluorescence detection of microtubule perturbation

In this assay, A-431 cells were seeded on sterile microscope coverslips; after 24 hours, 20 μM test compounds and 1 μM vinblastine, used as reference compound, were added to the culture medium and cells were then incubated for 18 hours. Afterwards, cells were washed twice with PBS and treated with cold methanol for 10 minutes at –20 °C; then cell layer was rinsed twice for 10 seconds with cold acetone and, after two PBS washes, cells were let rehydrate in PBS for at least 30 minutes. Later, cells were incubated with monoclonal anti-β-tubulin-FITC antibody diluted in PBS containing 1% bovine serum albumin (BSA) for 1 hour at room temperature; slides were then washed repeatedly with PBS, mounted with mounting medium, and finally analysed by confocal microscopy under green light.

6.2.11.2 Tubulin polymerisation

The effects of test compounds on the polymerisation of microtubule protein isolated from porcine brain were analysed by using a microtubule polymerisation assay kit (Cytoskeleton) following the

recommended protocol; polymerisation was followed by fluorescent enhancement because of the incorporation of a fluorescent reporter into microtubules as polymerisation occurred.

The assay was performed in 96-well microtiter plates; the reaction was initiated by the addition of tubulin. The plate was incubated at 37 °C in a fluorescence microplate reader, and the fluorescence measurement (λ_{excit} = 355 nm and λ_{emiss} = 450 nm) was determined every minute for 1 hour. Vinblastine and Taxol were used as reference compounds.

6.2.12   Evaluation of antivascular activity in vitro

6.2.12.1 Motility assay

HUVEC cells (1×10^5) were seeded into twelve-well plates until a confluent monolayer was formed and cell monolayer was scratch wounded using a pipette tip; then, cells were treated with the test compounds and, at different times after the scratch, they were photographed under a light microscope with 10× magnification. Wound closure was finally evaluated by Optika pro-vision software.

HUVEC cells were purchased from Invitrogen and cultured in 0,3% collagen I-coated flasks in M200 medium supplemented with Low Serum Growth Supplement (Invitrogen).

6.2.12.2 Endothelial cell vessel formation on a Matrigel matrix

A Matrigel matrix was kept at 4 °C overnight and then 200 µl of Matrigel were added to each well of a 24-well plate. After gelling at 37 °C for 30 min, gels were overlaid with 500 µL of medium containing 6×10^4 HUVEC cells; cells were incubated over Matrigel for 6 hours to allow the formation of the capillary-like tubes. Then, compounds were added and continuously incubated for additional times, and the possible antivascular effect was monitored by optical microscope (at least five fields for each well; 10x magnification); pictures were taken using a digital camera and image analysis was carried out using the ImageJ image analysis software and evaluating both dimensional parameters (percent area covered by cells, total length of cell network per field and percent area inside meshes) and topological parameters (number of meshes and branching points per fields).

6.2.13   Lipid peroxidation

Lipid peroxidation was monitored by Morlière method or TBARS assay [55], which checks the formation of malondialdehyde, one of the final product of this oxidation process, as it reacts with thiobarbituric acid.

250000 Jurkat cells were irradiated (2,5 J/cm^2) in the presence of the most active compounds, dissolved in HBSS; then, the drug solution was replaced by RPMI medium and cells were incubated for 24 hours.

To verify lipids peroxidation, after cell centrifugation, 900 μl of surnatant were collected and put at 253 K after having added 90 μl of 2,6-di-tert-butyl-*p*cresol (BHT, 2% in absolute ethanol). Cells were washed, resuspended in 500 μl of water; 400 μl of cells were lysed with 400 μl of SDS (1% in water) and vortexed. This suspension was divided into two aliquots: in 500 μl were added 50 μl of BHT; 300 μl were used for protein quantification with Peterson method [56]. Lipid peroxidation was measured using a thiobarbituric acid assay as described by Morlière et al. [55]. A standard curve of 1,1,3,3 tetraethoxypropane was used to quantify the amount of produced malondialdehyde. Data were expressed in terms of nanomoles of TBARS normalized to the total protein content in an aliquot of the cell extract.

6.2.14   Photoreaction with model proteins

A possible photoreaction with some model proteins such as BSA and RNAse A was evaluated through Balasubramanian method [57]; BSA (Bovine Serum Albumine) is a fluorescent protein because of its Trp molecule (λ_{excit} = 280 nm, λ_{emiss} = 350 nm), RNAse A because of Tyr residual (λ_{excit} = 274 nm, λ_{emiss} = 300 nm).

A 0,5 μM protein solution in phosphate buffer was irradiated with incrementing UVA doses (0, 1,25, 2,5, 5, 7,5, 11,25 and 15 J/cm^2) in the presence of the most active compounds at the concentration of 10 μM; to detect the photoreaction, the fluorescence of the solution was observed after irradiation: a modification in the solution fluorescence reveals a photoreaction of the molecules with the model protein.

7. References

1. World Health Report, *Life in the 21st century. A vision for all.*, World Health Organisation, Geneva, Switzerland (1998).

2. Levi F., Lucchini F., Negri E., Zatonski W., Boyle P., La Vecchia C., *Trends in cancer mortality in the European Union and accession countries, 1980–2000*, Annals of Oncology, 15 (2004), pp. 1425-1431.

3. Workman P, Kaye S.B., *Translating basic cancer research into new cancer therapeutics*, Trends in Molecular Medicine, 8 (2002), pp. S1-S9.

4. Alberghina L, Gaglio D, Gelfi C., Moresco R.M., Mauri G., Bertolazzi P., Messa C., Gilardi M.C., Chiaradonna F., Vanoni M., *Cancer cell growth and survival as a system-level property sustained by enhanced glycolysis and mithocondrial metabolic remodeling*, Frontiers in Physiology, 3 (2012), art. 362.

5. Hanahan D., Weinberg R.A., *The hallmarks of cancer*, Cell, 100 (2000), pp. 57-70.

6. Mitscher L.A., *Antibiotics and antimicrobial agents*, in "Foye's principle of medicinal chemistry" (2002) Williams D.A., Lemke T.L., ed. Lippincott Williams & Wilkins, pp. 819-864.

7. Matsumoto Y., Takano H., Fojo T., *Cellular adaptation to drug exposure: evolution of the drug-resistant phenotype*, Cancer Research, 57 (1997), pp. 5086-5092.

8. Davey R.A., Su G.M., Hargrave R.M., Harvie R.M., Baguley B.C., Davey M.W., *The potential of N-[2-(dimethylamino)ethyl]acridine-4-carboxamide to circumvent three multidrug-resistance phenotypes in vitro*, Cancer Chemoter Pharmacol, 39 (1997), pp. 424-430.

References
───

9. Dorée M., Galas S, *The cyclin-dependent protein kinases and the control of cell division*, FASEB J., 8 (1994), pp. 1114-1121.

10. Gianni L., Sessa C., Capri G., Grasselli G., Bianchi G., Vitali G., *Farmaci chemioterapici in Medicina Oncologica*, Ed. Masson, Milano (2003), pp. 583-676.

11. Callery P., Gannet P., *Cancer and cancer chemotherapy*, in "*Foye's principles of medicinal chemistry*"(2002), D.A. Williams, T.L. Lemke, ed. Lippincott Williams & Wilkins, pp. 924-951.

12. Middleton M.R., Margison G.P., *Improvement of chemotherapy efficacy by inactivation of a DNA-repair pathway*, Lancet Oncol., 4 (2003), pp. 37-44.

13. Berger J.M., *Structure of DNA topoisomerases*, Biochim. Biophys. Acta, 1400 (1998), pp. 3-18.

14. McClendon A.K., Osheroff N., *DNA topoisomerase II, genotoxicity, and cancer*, Mut. Res., 623 (2007), pp. 83-97.

15. Galjard N., Perez F., *A plus-end raft to control microtubule dynamics and function*, Curr. Opin. Cell Biol., 15 (2003), pp. 48-53.

16. Jordan A., Hadfield J.A., Lawrence N.J., McGown A.T., *Tubulin as a target for anticancer drugs: agents which interact with the mitotic spindle*, Inc. Med. Res. Rev., 18 (1998), pp. 259-296.

17. Zhou J., Giannakakou P., *Targeting microtubules for cancer chemotherapy*, Curr. Med. Chem – Anti-Cancer Agents, 5 (2005), pp. 65-71.

18. Sawyers C., *Targeted cancer therapy*, Nature, 432 (2004), pp. 294-297.

19. Cohen P., *Protein kinases- the major drug target of the twenty-first century?*, Nat. Rev., 1 (2002), pp. 309-316.

20. Ziegler U., Groscurth P., *Morphological features of cell death*, News Physiol. Sci., 19 (2004), pp. 124-128.

21. Wang X., *The expanding role of mitochondria in apoptosis*, Genes and Development, 15 (2001), pp. 2922-2933.

22. Ricci J.E., Gottlieb R.A., Green D.R., *Caspase-mediate loss of mitochondrial function and generation of reactive oxygen species during apoptosis*, J. Cell Biol, 1 (2003), pp. 65-75.

23. Zhao M., Eaton J.W., Brunk U.T, *Protection against oxidant-mediated lysosomal rupture: a new anti-apoptotic activity of Bcl-2?*, FEBS Lett., 485 (2000), pp. 104-108.

24. Parrish J.A., Fitzpatrick T.B., Pathak M.A., Tanenbaum L., *Photochemotherapy of psoriasis with oral methoxsalen and longwave ultraviolet light*, N. Engl. J. Med., 291 (1974), pp. 1207-1211.

25. Walker D., Jacobe H., *Phototherapy in the age of biologics*, (2011), pp. 190-198.

26. Teiten M.H., Bezdetnaja L., Merlin J.L., Bour-Dill C., Pauly M.E., Dicato M, Guillemin F., *Effect of meta-tetra(hydroxyphenyl)chlorin (mTHPC)-mediated photodynamic therapy on sensitive and multidrug-resistant human breast cancer cells*, J. Photochem. Photobiol., 62 (2001), pp. 146-152.

27. Dolmans D.E.J.G.J., Fukumura D., Jain R.K., *Photodynamic therapy for cancer*, Nature, vol. 3 (2003), pp. 380-387.

28. Dalla Via L., Marciani Magno S., Rodighero P., Gia O., *Synthesis, photobiological activity and photoreactivity of methyl-thieno-8-azacoumarins, novel bioisosters of psoralens*, Bioorg. Medicin. Chem. Lett., 12 (2002), pp. 1253-1257.

29. Bethea D., Fullmer B., Syed S., Seltzer G., Tiano J., Rischko C., Gillespie L., Brown D., Gasparro F.P., *Psoralen photobiology and photochemotherapy: 50 years of science and medicine*, J. Dermatol. Sci., 19 (1999), pp. 78-88.

References

---

30. Bartošová J., Kuželová K., Pluskalová M., Marinov I., Halada P., Gašová Z., *UVA-activated 8-methoxypsoralen (PUVA) causes G2/M cell cycle arrest in Karpas 299 T-lymphoma cells*, J. Photochem. Photobiol., 85 (2006), pp. 39-48.

31. Bladon J, Taylor P.C., *Extracorporeal photopheresis: a focus on apoptosis and cytokines*, J. Dermatol. Sci., 43 (2006), pp. 85-94.

32. Marzano C., Chilin A., Bordin F., Baccichetti F., Guiotto A., *DNA damage and biological effects induced by photosensitization with new N_1-unsubstituted furo[2,3-h]quinolin-2(1H)-ones*, Bioorg. Medicin. Chem. Lett., 10 (2002), pp. 2835-2844.

33. Hennequin L.F., Thomas A.P., Johnstone C., Stokes E.S.E., Plé P.A., Lohman J.M., Ogilvie D.J., Dukes M., Wedge S.R., Curwen J.O., Kendrew J., Lamber-van der Brempt C., *Design and structure-activity relationship of a new class of potent VEGF receptor tyrosine kinase inhibitors*, J. Med. Chem., 42 (1999), pp. 5369-5389.

34. Palmer B.D., Trumpp-Kallmeyer S., Fry D.W., Nelson J.M., Showalter H.D.H., Denny W.A., *Tyrosine kinase inhibitors. 11. Soluble analogues of pyrrolo- and pyrazoloquinazolines as epidermal growth factor receptor inhibitors: synthesis, biological evaluation, and modeling of the mode of binding*, J. Med. Chem., 40 (1997), pp. 1519-1529.

35. Matsuno K., Nakajima T., Ichimura M., Giese N.A., Yu J., Lokker N.A., Ushiki J., Ide S., Oda S., Nomoto Y., *Potent and selective inhibitors of PDGF receptor phosphorilation. 2. Synthesis, structure activity relationship, improvement of aqueous solubility, and biological effect of 4-[4-(N-substituted (thio)carbamoyl)-1-piperazinyl]-6,7-dimethoxyquinazoline derivatives*, J. Med. Chem., 45 (2002), pp. 4513-4523.

36. Hunt J.T., Mitt T., Borzilleri R., Gullo-Brown J., Fargnoli J., Fink B., Han W., Mortillo S., Vite G., Wautlet B., Wong T., Yu C., Zheng X., Bhide R., *Discovery of the pyrrolo[2,1-f][1,2,4]triazine nucleus as new kinase inhibitor template*, J. Med. Chem., 47 (2004), pp. 4054-4059.

37. Wolf P., Nghiem D.X., Walterscheid J.P., Byrne S., Matsumura Y., Matsumura Y., Bucana C., Ananthaswamy H.N., Ullrich S.E., *Platelet-Activating Factor Is Crucial in Psoralen and Ultraviolet A-Induced Immune Suppression, Inflammation, and Apoptosis*, Am. J. Phatol., 3 (2006), pp. 795-805.

38. Song P.S., Tapley K.J., *Photochemistry and photobiology of psoralens*, Photochem. Photobiol., 29 (1979), pp. 1177-1197.

39. Moyer J.D., Barbacci E.G., Iwata K.K., Arnold L., Broman B., Cunningham A., Di Orio C., Doty J., Morin M.J., Moyer M.P., Neveu M., Pollack V.A., Pustilnik L.R., Reynolds M.M., Sloan D., Theleman A., Miller P., *Induction of apoptosis and cell cycle arrest by CP-358,774, an inhibitor of Epidermal Growth Factor Receptor Tyrosin Kinase,* Cancer Res., 57 (1997), pp. 4838-4848.

40. Wedge S.R., Ogilvie D.J., Dukes M., Kendrew J., Curwen J.O., Hennequin L.F., Thomas A.P., Sokes E.S.E., Curry B., Richmond G.H.P., Wadsworth P.F., *ZD4190: An orally active inhibitor of vascular endothelial growth factor signaling with broad-spectrum antitumor efficacy*, Cancer Res., 60 (2000), pp. 970-975.

41. Hennequin L.F., Stokes E.S.E., Thomas A.P., Johnstone C., Plé P.A., Ogilvie D.J., Dukes M., Wedge S.R., Kendrew J., Curwen J.O., *Novel 4-anilinoquinazolines with C-7 basic side chains: design and structure activity relationship of a series of potent, orally active, VEGF receptor tyrosine kinase inhibitors*, J. Med. Chem., 45 (2002), pp. 1300-1312.

42. Vermes I., Haanen C., Steffens-Nakken H., Reutelingsperger C., *A novel assay for apoptosis. Flow cytometric detection of phosphatidylserine expression on early apoptotic cells using fluorescein labelled Annexin V*, J. Immun. Methods, 184 (1995), pp. 39-51.

43. Kroemer G., Zamzani N., Susin S.A., *Mitochondrial control of apoptosis*, Immunol. Today, 18 (1997), pp. 44-51.

44. Cossarizza A., Baccarani Contri M., Kalashnikova G., Franceschi C., *A new method for the cytofluorimetric analysis of mitochondrial membrane potential using the J-aggregate*

References

forming lipophilic cation 5,5',6,6'-tetrachloro-1,1',3,3'-tetraethylbenzimidazolcarbocyanine iodide (JC-1), Biochem. Biophys Res. Commun., 197 (1993), pp. 40-45.

45. Reers M., Smith T.W., Chen L.B., _J-aggregate formation of a carbocyanine as a quantitative fluorescent indicator of membrane potential_, Biochemistry, 30 (1991), pp. 4480-4486.

46. Andreyev A.Y., Kushnareva Y.E., Starkov A.A., _Mitochondrial metabolism of reactive oxygen species_, Biochemistry (Mosc.), 70 (2005), pp. 200-214.

47. Zhai Y., Kronebusch P.J., Simon P.M., Borisy G.G., _Microtubule dynamics at the G2/M transition: Abrupt breakdown of cytoplasmic microtubules at nuclear envelope breakdown and implications for spindle morphogenesis_, J. Cell. Biol., 135 (1996), pp. 201–214.

48. Staton C.A., Reed M.W.R., Brown N.J., A critical analysis of current in vitro and in vivo angiogenesis assays, Int. J Exp. Path., 90 (2009), pp. 195-221.

49. Caffieri S., _Furocoumarin photolysis: chemical and biological aspects_, Photochem. Photobiol. Sci., 1 (2002), pp. 149-157.

50. Santini M.T., Romano R., Rainaldi G., Filippini P., Bravo E., Porcu L., Motta A., Calcabrini A., Mescini S., Indovina P.L., Arancia G., _The relationship between ^{1}H-NMR mobile lipid intensity and cholesterol in two human multidrug resistant cell lines (MCF-7 and LoVo)_, Biochim. Biophys. Acta, 1531 (2001), pp. 111-131.

51. Mosmann T., _Rapid colorimetric assay for cellular growth and survival: application to proliferation and citotoxic assay_, J. Immunol. Meth., 65 (1983), pp. 55-63.

52. Darzynkiewicz Z., Juan G., Li X., Gorczyca W., Muratami T., Traganos F., _Cytometry in cell necrobiology: analysis of apoptosis and accidental cell death (necrosis)_, Cytometry, 21 (1997), pp. 1-20.

53. Salvioli S., Ardizzoni A., Franceschi C., Cossarizza A., _JC-1 but not DiOC6(3) or rhodamine 123 is a reliable fluorescent probe to asses ΨΔ changes in intact cells:_

implications for studies on mitochondrial functionality during apoptosis, FEBS Lett., 411 (1997), pp. 77-82.

54. Rothe G., Valet G., *Flow cytometric analysis of respiratory burst activity in phagocytes with hydroethidine and 2',7'-dichlorofluorescin*, J. Leukoc. Biol., 47 (1990), pp. 440-448.

55. Morlière P., Moysan A., Santus R., Hüppe G., Mazière J., Dubertret L., *UVA-induced lipid peroxidation in cultured human fibroblasts*, Biochem. Biophys. Acta, 1084, (1991), pp. 261-268.

56. Peterson G.L., *A simplification of the protein assay method of Lowry et al. which is more generally applicable*, An. Biochem., 83 (1977), pp. 346-356.

57. Balasubramanian D., Du X., Zigler J.S., *The reaction of singlet oxygen with proteins, with special reference to crystalline*, Photochem. and photobiol., 52 (1990), pp. 761-776.

References

_____

UNIVERSITA' DEGLI STUDI DI PADOVA, DIPARTIMENTO DI SCIENZE DEL FARMACO

Professoressa Daniela Vedaldi, Professor Francesco Dall'Acqua, Dottoressa Alessia Salvador, Alice Ballan.

UNIVERSITA' DEGLI STUDI DI PADOVA, DIPARTIMENTO DI BIOLOGIA

Professoressa Luisa Dalla Valle.

UNIVERSITA' DEGLI STUDI DI PADOVA, DIPARTIMENTO DI MEDICINA MOLECOLARE

Professor Ignazio Castagliuolo, Dottoressa Paola Brun.

UNIVERSITA' DEGLI STUDI DI PALERMO, DIPARTIMENTO FARMACOCHIMICO, TOSSICOLOGICO E BIOLOGICO

Professor Girolamo Cirrincione, Assistant Professor Patrizia Diana, Assistant Professor Paola Barraja.